Innovative Permeable Reactive Barriers for the Elimination of Contaminants of Emerging Concern from Effluents of Wastewater Treatment Plants

Arthur Pietrobon Baldo

Thesis report submitted to

Escola Superior de Tecnologia e Gestão

Instituto Politécnico de Bragança

Master Degree in

Chemical Engineering

Supervisors:

Prof. Dr. Helder Teixeira Gomes

Prof. Dr. Pricila Marin

Bragança

2024

Innovative Permeable Reactive Barriers for the Elimination of Contaminants of Emerging Concern from Effluents of Wastewater Treatment Plants

Arthur Pietrobon Baldo

Thesis report submitted to **Escola Superior de Tecnologia e Gestão** of **Instituto Politécnico de Bragança** under the framework of the Master's Degree in Chemical Engineering, and the double diploma with the **Universidade Tecnológica Federal do Paraná - Campus Londrina**

Supervisors:

Prof. Dr. Helder Teixeira Gomes

Prof. Dr. Pricila Marin

Bragança

2024

ACKNOWLEDGEMENTS

This master's thesis is the result of many hours of work, collaboration, encouragement, and dedication from various individuals. I would like to express my deep gratitude for God and those who helped turn this dream into reality. I offer special thanks to my family, especially my parents, Rogério Artur Baldo and Vera Lúcia Pietrobon Baldo, my brother Heitor Pietrobon Baldo, and my life partner Larissa Camargo Ghirro, for their unconditional love, encouragement, patience, and endless support, which allowed me to be here. They are my daily inspiration, and I dedicate this work to them.

I am deeply thankful to my friends at UTFPR-LD, whom I met before and during my time there, and to the friends I made in Bragança, for their tireless support, companionship, and affection, which were essential in helping me stay motivated and persevere until the completion of this work. I am also grateful to my friend Bárbara Miqueletti de Oliveira, who has been by my side since the beginning of this journey, sharing every moment in another country during our master's studies.

I extend my gratitude to the entire research group for their teachings and immense support. Special thanks go to MSc. Ana Paula Ferreira da Silva for her wisdom, dedication, encouragement, patience, friendship and commitment throughout the years. I also thank MSc. Adriano Santos Silva, who consistently supported me with ideas and friendship, both inside and outside the laboratory.

I sincerely thank my supervisors, Professor Dr. Helder Teixeira Gomes from the Polytechnic Institute of Bragança (IPB), for trusting me with this research and providing essential support throughout the process. I am also grateful to Professor Dr. Pricila Marin from the Federal University of Technology of Paraná, Londrina (UTFPR-LD) for her guidance and assistance despite the distance.

Lastly, I would also like to thank all the professors and collaborators at UTFPR-LD and IPB for their teachings, opportunities, and trust throughout my academic journey. My gratitude extends to everyone who contributed, directly or indirectly, to the realization of this thesis, providing both intellectual and emotional support.

The authors acknowledge the Foundation for Science and Technology (FCT, Portugal) for financial support through national funds FCT/MCTES (PIDDAC) to CIMO (UIDB/00690/2020 and UIDP/00690/2020) and SusTEC (LA/P/0007/2020). This work was also financially supported by fundação La Caixa for the project INOVÁGUA.

ABSTRACT

Rapid industrialization and urbanization have led to significant environmental challenges, particularly the contamination of water bodies by contaminants of emerging concern (CECs) due to insufficient tertiary treatment in wastewater treatment plants (WWTPs). Pharmaceuticals like acetaminophen (ACT) and sulfamethoxazole (SMX), as well as phenolic compounds like gallic acid (GA), are persist and bioaccumulate, posing risks to water quality. This study explores the development of permeable reactive barriers (PRBs) using eco-friendly materials: geopolymers (GP), activated carbon (AC), and carbon nanotubes (CNT), sourced from waste. Integrating these materials into PRBs aligns with circular economy principles, providing a sustainable solution to reduce exposure to contaminated water. Elemental analysis revealed that AC contained 63.0% carbon, while CNT exhibited a higher carbon content of 92.5%. The GP analysis indicated substantial calcium and silicon content, and structural analysis via X-ray diffraction (XRD) identified key crystalline phases, predominantly calcite. Functional characterization using Fourier-transform infrared spectroscopy (FT-IR) confirmed the presence of hydroxyl and carbonyl groups in AC and notable C–O bonds in CNTs. Additionally, acid-base characterization demonstrated AC's high basicity (1250 μmol/g), enhancing its capacity to adsorb acidic compounds. Morphological studies using SEM and TEM illustrated the heterogeneous structure of GP and the arrangement of CNTs, including iron nanoparticles, from the synthesis process. BET analysis revealed AC's superior specific surface area (527 m^2/g) and pore volume (0.313 cm^3/g) compared to CNT (66 m^2/g) and GP (30 m^2/g), enhancing its adsorption capacity. Equilibrium analysis revealed that the Freundlich model effectively described the adsorption process, indicating favorable conditions and a strong affinity between adsorbates and adsorbents. The maximum adsorption capacities of AC were determined using the Langmuir model, with values of 112.19 mg/g for ACT, 40.25 mg/g for SMX, and 314.27 mg/g for GA. Kinetic studies confirmed that all materials followed a pseudo-second-order model, achieving equilibrium within approximately 50 minutes. Continuous flow experiments validated the batch adsorption results, showing the effective performance of AC and GP, with breakthrough capacities of 126.85 mg/g for ACT, 54.93 mg/g for SMX, and 151.53 mg/g for GA. Breakthrough times were recorded at 314 minutes for ACT, 66 minutes for SMX, and 68 minutes for GA. The multi-component system exhibited similar behavior, although saturation occurred earlier.

Keywords: Contaminants of emerging concern; Circular economy; Breakthrough curve; Permeable reactive barriers; Wastewater treatment.

RESUMO

A rápida industrialização e urbanização têm levado a desafios ambientais significativos, particularmente à contaminação dos corpos d'água por contaminantes de preocupação emergente (CECs) devido ao tratamento terciário insuficiente em estações de tratamento de águas residuais (ETARs). Fármacos como paracetamol (ACT) e sulfametoxazol (SMX), assim como compostos fenólicos como o ácido gálico (GA), persistem e bioacumulam, representando riscos à qualidade da água. Este estudo explora o desenvolvimento de barreiras reativas permeáveis (BRPs) utilizando materiais ecologicamente corretos: geopolímeros (GP), carvão ativado (AC) e nanotubos de carbono (CNT), oriundos de resíduos. A caracterização abrangente confirmou a eficácia dos materiais utilizados. A análise elementar revelou que o AC continha 63,0% de carbono, enquanto o CNT apresentou um conteúdo de carbono mais elevado, de 92,5%. A análise do GP indicou um conteúdo significativo de cálcio e silício, e a análise estrutural por meio de DRX identificou fases cristalinas-chave, principalmente calcita. A caracterização funcional por FT-IR confirmou a presença de grupos hidroxila e carbonila no AC, além de notáveis ligações C–O nos CNTs. Adicionalmente, a caracterização ácido-base demonstrou a alta basicidade do AC (1250 μmol/g), aprimorando sua capacidade de adsorver compostos ácidos. Estudos morfológicos utilizando SEM e TEM ilustraram a estrutura heterogénea do GP e o arranjo dos CNTs, incluindo nanopartículas de ferro. A análise BET revelou a maior área superficial (527 m^2/g) do AC em comparação ao CNT (66 m^2/g) e ao GP (30 m^2/g). A análise de equilíbrio revelou que o modelo de Freundlich descreveu efetivamente o processo de adsorção, indicando condições favoráveis e uma forte afinidade entre os adsorventes e os adsorvatos. As capacidades máximas de adsorção do AC foram determinadas utilizando o modelo de Langmuir, com valores de 112,19 mg/g para ACT, 40,25 mg/g para SMX e 314,27 mg/g para GA. Estudos cinéticos confirmaram que todos os materiais seguiram um modelo de pseudo-segunda ordem, atingindo o equilíbrio em aproximadamente 50 minutos. Experiências de fluxo contínuo validaram os resultados de adsorção em batelada, mostrando o desempenho eficaz do AC e do GP, com capacidades de ruptura de 126,85 mg/g para ACT, 54,93 mg/g para SMX e 151,53 mg/g para GA. Os tempos de ruptura foram registrados em 314 minutos para ACT, 66 minutos para SMX e 68 minutos para GA. O sistema multicomponente exibiu comportamento semelhante, embora a saturação tenha ocorrido mais cedo.

Palavras-chave: Contaminantes de preocupação emergente; Economia circular; Curva de ruptura; Barreiras reativas permeáveis; Tratamento de efluentes.

TABLE OF CONTENTS

LIST OF FIGURES

LIST OF FIGURES IN SUPPLEMENTARY MATERIAL

LIST OF TABLES

LIST OF ACRONYMS

AC	Activated Carbons
ACT	Acetaminophen
CEC	Contaminant of Emerging Concern
CNT	Carbon Nanotubes
CPCB	Central Pollution Control Board
C-PRB	Continuous Permeable Reactive Barrier
CVD	Chemical Vapor Deposition
DTG	Derivative Thermogravimetric
EOP	Exhausted Olive Pomace
FA	Fly Ash
FT-IR	Fourier Transform Infrared Spectroscopy
GA	Gallic Acid
GP	Geopolymers
HPLC	High Performance Liquid Chromatography
ICP-OES	Inductively Coupled Plasma Optical Emission Spectroscopy
IUPAC	International Union of Pure and Applied Chemistry
MWCNT	Multi-walled Carbon Nanotubes
OSPAR	Oslo and Paris Convention
PB	Permeable Barrier
PZC	Point of Zero Charge
PRB	Permeable Reactive Barriers
SEM	Scanning Electron Microscopy
SWCNT	Single-walled Carbon Nanotubes
SMX	Sulfamethoxazole
TEM	Transmission Electron Microscopy
TGA	Thermogravimetric Analysis
USEPA	United States Environmental Protection Agency
UWWTD	Urban Waste Water Treatment Directive
WWTP	Waste Water Treatment Plant
XRD	X-ray diffraction

1. INTRODUCTION

Environmental issues are being caused by rapid industrialization, the rising number of people, expanding urbanization and unrestrained excessive use of natural sources[1]. In 2022, the total domestic wastewater collected by downstream (composed of wastewater collection, drainage and elevation activities) services in Portugal achieved 650×10^6 m^3, equivalent to a production of 63 m^3 of wastewater per inhabitant, and 540 million m^3 was collected by upstream (composed of wastewater transportation, treatment and rejection activities) services[2]. Over the years, the increasing consumption and contamination of natural waters by thousands of chemical compounds, including organic compounds such as antibiotics, persistent organic pollutants, pharmaceuticals, personal care products and endocrine-disrupting chemicals[3], known as contaminants of emerging concern (CECs), has become a concern.

CECs in different aquatic environments mainly come from anthropogenic activities, and their extensive occurrence, persistence, bioaccumulation, constant circulation, migration and transformation in environmental media have generated a substantial global concern[4]. Among pharmaceutical compounds that are CECs and cause water pollution, paracetamol (acetaminophen, 4-acetylaminophene-nol) deserves particular attention since it has recently been identified as a potential pollutant of waters[5]. Another example of CECs that is a priority in the four study areas[6] (soil ecosystem, water ecosystem, humans, and terrestrial predators) is sulfamethoxazole, a widely used antibiotic.

In addition to the mentioned contaminants, phenolic compounds in wastewater, caused by pharmaceutical or dye industries, are persistent organic pollutants resistant to decomposition/degradation and cause harmful severe effects on the human health and the environmental ecosystem[1]. The phenolic pollutants and their metabolites in living cells cause mutagenicity and carcinogenicity[7]. Furthermore, some phenolic compounds, such as chlorophenols, nonylphenols and 4-tert-octylphenol, can block normal hormonal functions, mimic natural hormones, occupy their receptors in different organisms and cause severe hormone imbalance and health hazards[8].

Creating a new approach to environmental protection across different domains involves using strategies to minimize contaminants in wastewater treatment plants (WWTP), informed and enhanced by advancements in groundwater remediation techniques. Previous efforts to remediate polluted groundwater have culminated in the development of permeable reactive barriers (PRBs). They are subsurface filters filled with appropriate materials to treat through-

flowing polluted waters[9]. There is still a need to look for filler materials to use appropriately in permeable reactive barriers, with high efficiency, economy, effectiveness, and manufacturing with greenways without any adverse side effects on the environment[10].

Some materials with good adsorptive characteristics, such as geopolymers (GPs)[11], activated carbons (ACs)[12] and carbon nanotubes (CNTs)[13] can be obtained from waste sources. For example, GPs are attractive mainly because they are environmentally friendly, being possible to be produced using precursors that would otherwise be discarded, such as waste glass, municipal solid waste fly ash (FA), sugarcane bagasse ash, among many others[11]. Furthermore, ACs are materials with high porosity, which makes them remarkably suited for adsorption applications, with the main concern being to remove species from the liquid or gas phases so that the chemical substances are purified or recovered. Environmental questions are included, and agricultural wastes appear as significant precursors because they are cheap, renewable, safe and available in large quantities[12]. Due to their attractive characteristics, CNTs have been largely used as catalysts in many processes. Their attractiveness increases when obtained from carbon-containing wastes from a circular economy perspective. In this sense, plastic solid waste can be used as a carbon source[13].

There are numerous papers on PRBs, most of which focus on removing contaminants in groundwaters with multi-barrier systems so that high concentrations of contaminants are significantly reduced to a minimum[9,14–16]. Thus, by implementing the concept of PRBs in the effluents of WWTP and employing economically efficient reactive materials sourced from wastes, a connection can be established with the principles of circular economy and sustainable development. This approach aims to reduce the population's exposure to contaminated water and contributes to resource efficiency and environmental sustainability.

2. STATE OF ART

2.1. WASTEWATER TREATMENT PLANTS

In Portugal, households and specific industries in 453 urban areas generate 13.0 million population equivalent of wastewater every day, which is an amount equivalent to 2.59 million m^3. However, urban wastewater must be treated before discharge to avoid environmental pollution. In Portugal, urban wastewater is treated in 478 plants across the country before it is discharged[17].

Nowadays, it is recognized that many emerging contaminants can be correlated with the discharge of wastewater effluents, mainly from wastewater treatment plants located in highly industrialized and urban areas[18]. As previously reported[19], 52 CECs were detected in transnational river basins and coastal areas of the North of Portugal and Galicia, and in the WWTPs discharging on these environments. Indeed, conventional domestic wastewater treatment plants, often stabilization ponds and activated sludge systems, have not been designed to treat recalcitrant organic pollutants, including emerging substances[20].

Figure 1 shows the proportion of wastewater from households and the service industry safely treated at the source through centralized wastewater treatment plants before being discharged into the environment in different countries in 2022, according to the World Health Organization[21]. Furthermore, this does not imply the elimination of persistent contaminants from wastewater.

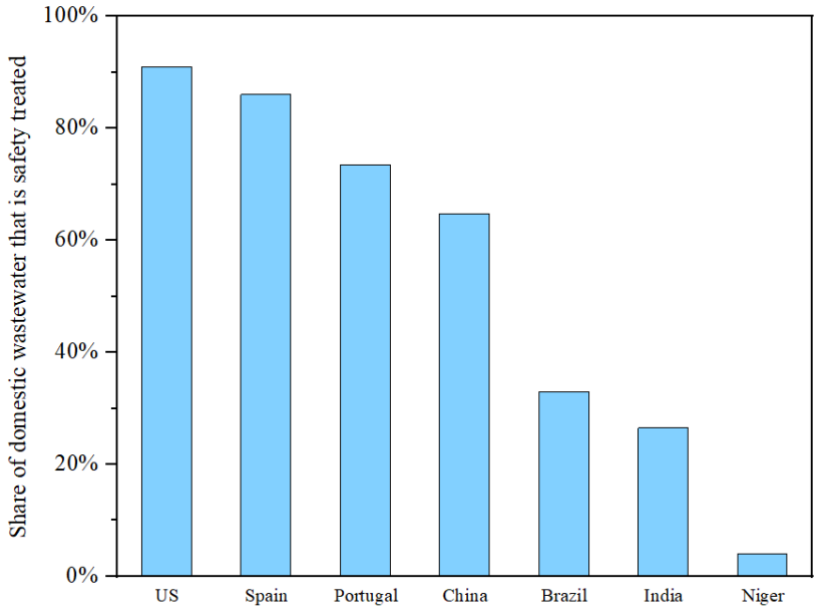

Figure 1: Share of domestic wastewater safely treated in some countries (adapted[21])

According to the Country Report Portugal 2019: Assessment of progress on structural reforms, prevention and correction of macroeconomic imbalances, and results of in-depth reviews[22], "Despite the progress achieved in recent years in water management, challenges remain, for instance with water governance and the need to close gaps in water investments, especially for wastewater and water body rehabilitation[23]".

Developing more efficient, cost-effective and environmentally friendly wastewater treatment processes is an urgent and essential step towards mitigating environmental pollution and meeting the ever-increasing water demand. With the increasing population growth and technological and industrial advancements, the amount of human-generated waste that finds its way to the environment through domestic and industrial wastewater increases[24]. The high concentrations of CECs in WWTP effluents led to an average increase of 50% in downstream water compared to upstream areas[25].

Table 1 shows the amounts of various pharmaceuticals detected in inlet and outlet waters of various WWTPs, confirming that many of these substances are not effectively removed by the treatments. A reduction in concentrations can be observed, however, WWTP may be potentially polluting the water bodies, as contaminants are still present.

Table 1: Pharmaceutical concentrations in wastewater of various WWTPs before and after treatment (adapted[26])

Type of pharmaceutical	**Substance detected**	**WWTP inlet (ng L^{-1})**	**WWTP outlet (ng L^{-1})**
Analgesics and anti-inflammatories	Acetaminophen	10194	2102
	Diclofenac	250	215
	Ibuprofen	516	266
	Ketoprofen	451	318
Lipid-lowering drugs	Bezafibrate	23	10
	Clofibrate	72	28
	Gemfibrozil	155	120
Antibiotics	Azithromycin	152	96
	Metronidazole	80	43
	Sulfamethoxazole	590	390
	Trimethoprim	1172	290

Generally, WWTPs contain two types of processes. Physical treatment processes comprise the preliminary and primary treatment, such as bar screening and sedimentation basins to remove most suspended solids. As the secondary treatment, biological treatment processes include the activated sludge, biological filter and rotating biological contactor processes. Some WWTPs include tertiary treatment, for example, disinfection, sand filtration,

constructed wetlands and soil aquifer treatment for deeper water purification[27]. Figure 2 shows the conventional sewage treatment flow.

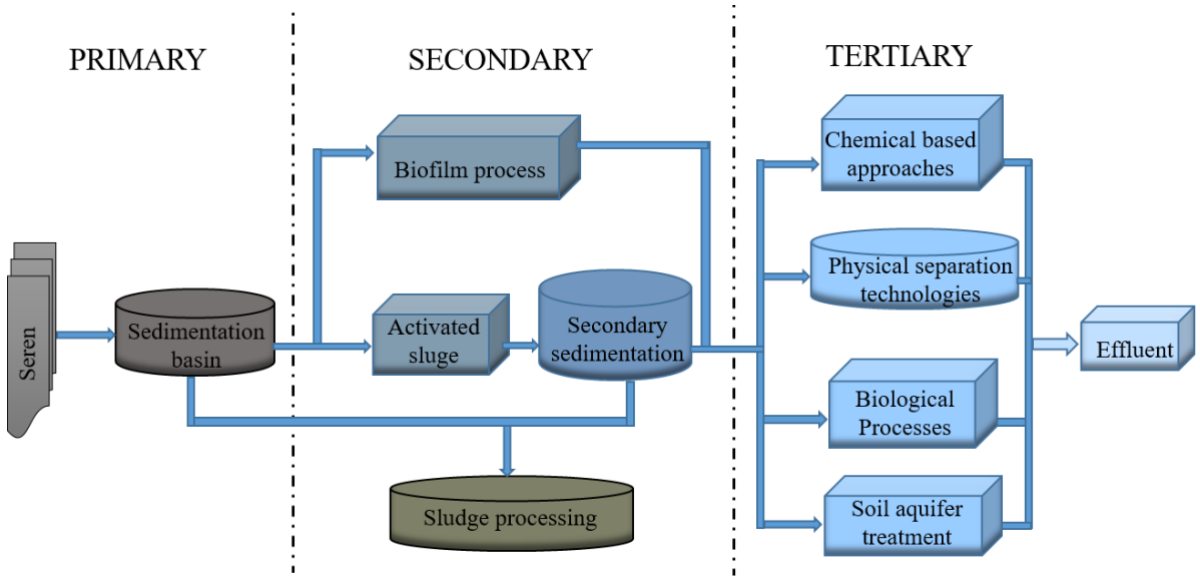

Figure 2: Flow of the traditional wastewater treatment crafts and some tertiary technologies (adapted[27])

The selection of the treatment method to remove solids, including colloids, organic matter, nutrients and soluble contaminants from the effluent depends on the characteristics and source of the water to be treated. Each treatment has its characteristics and is best suited for each type of situation in terms of cost, viability, efficiency, workability, reliability, environmental impact, sludge production, operational complexity, pre-treatment demands and production of potentially toxic by-products[28].

2.1.1. TERTIARY TREATMENTS

The activated sludge process is the most widespread sewage treatment method. It typically consists of a pre-treatment step, a primary settling tank, an aerobic degradation process and a secondary settling tank[29]. Tertiary treatment is a wastewater treatment process that can be applied after the secondary treatment. This step removes stubborn contaminants that secondary treatment could not clean up. Wastewater effluents become even cleaner, due to more robust and advanced treatment systems, making it easier to reuse[30].

Unfortunately, traditional tertiary treatments either did not show to be effective or demonstrated only moderate effectiveness in removing certain contaminants from wastewater [31]. Chlorination, typically used as a disinfection step before WWTP effluent disposal or reuse, is poorly effective in the removal of CECs and in controlling antibiotic resistance[32]. UV-C

disinfection is effective in the inactivation of pathogens when sand filtration is used as pre-treatment but is poor in removing CECs[33]. Treatment by ozonation can inactivate pathogens and remove CECs, but an additional posttreatment step can be necessary to remove ozonation by-products (i.e., nitrosodimetylamine and bromate)[34]. Therefore, removal of contaminants with a PRB is an alternative tertiary treatment.

The 10th biennial report on Member States' implementation of the Urban Wastewater Treatment Directive (UWWTD) shows that collection and treatment of urban wastewater have improved over the last decade in the EU (from 2010 to 2020), with compliance rates of 95% for collection, 88% for secondary (biological) treatment and 86% for more stringent treatment (removal of phosphorus and nitrogen)[35]. However, some member states still have ways to comply fully with the UWWTD. Table 2 shows the types and percentage of urban wastewater treatment in some Oslo and Paris Convention (OSPAR) countries in 2016[36]. It's notable to observe that among the countries mentioned, Portugal stands out with the lowest utilization rate of tertiary treatment.

Table 2: Urban wastewater collection and treatment in some OSPAR countries (adapted[36])

	Type of wastewater treatment (%)				
Country	**None**	**Primary**	**Secondary**	**Tertiary**	**Not specified**
Belgium	5	0	8.4	74.6	0
Denmark	0	0.2	1.4	90.4	0
Netherlands	0	0	0.8	98.7	0
Norway	1.9	21.3	3.9	58.9	0
France	0	0	11	69	2
Portugal	0.1	7	46.7	38	0.1
Spain	0.3	1.7	23.9	69	2.3

The distance to target remains significant in some Member States: an amount of urban wastewater corresponding to 6.6 million p.e. (1%) is not collected, and over 37 million p.e. (6%) of the wastewater collected are not sufficiently well treated to meet secondary treatment standards, while nearly 32 million p.e. (8%) do not meet more stringent treatment standards. This means there are agglomerations in the European Union where infrastructure needs to be built or improved[35].

2.1.2. CONTAMINANTS OF EMERGING CONCERN

Emerging contaminants are a group of natural and synthetic chemicals and biological agents that are not or are poorly regulated. These substances are currently of concern because

they are known or are suspected to have adverse impacts on the environment and human health. Indeed, emerging contaminants are not necessarily of new use but newly identified, and data on their presence and fate in the environment and their effects on organisms is not entirely understood[37]. According to research[38], 69,526 structures with CAS numbers were aggregated from various CECs data sources, and simulation of phase I metabolites resulted in 306,279 unique metabolites.

A long list of chemicals with adverse effects on human and environmental health, including antibiotics, pain relievers, hormones, antidepressants, anti-inflammatory drugs, disinfectants, sunscreens, fragrances, pesticides and industrial chemicals, are detected in natural water systems[39]. Pharmaceuticals and personal care products cover a good part of these chemicals; for example, acetaminophen, metformin, sulfamethoxazole, oxybenzone[19] and the pesticides acesulfame and diuron can be some examples.

The fate and occurrence of CECs in the water bodies, identifying hot spots and sources, and associated risks for the aquatic environment are of current interest[19]. Introduction routes into the aquatic environment for CECs consist of point and nonpoint sources. Primary point sources include WWTPs, industries and hospitals[40]. Regarding the level of persistence, some CECs pass unaltered through WWTPs and, therefore, they are released into different aquatic environments[41,19].

Despite their wide-ranging uses, CECs can harm human health and other animals due to their high resistance to degradation, a quality attributed to their complex structure and other factors[42]. For example, roxithromycin, used as an antibiotic, can affect the growth inhibition of algae (Pseudokirchneriellasubcapitata)[43] and sulfamethoxazole, a commonly used synthetic antibiotic from the sulfonamide class, frequently employed in the treatment of venereal, with yet some uncertainty over their toxic effects. The scientific community and regulatory authorities have recently become increasingly concerned about the widespread presence of CECs in surface and groundwater sources due to their extensive use[44].

Figure 3 shows the average concentration of two representative CECs, that will be explored in this work, acetaminophen and sulfamethoxazole, classified as pharmaceuticals and personal care products[45], with 17 samples collected from raw and treated wastewater from Spain and Portugal. In a previous report[19], acetaminophen was identified as having one of the highest concentrations of the 52 CECs presented but, after treatment, the concentration was reduced. Similarly, with sulfamethoxazole, it was still possible to detect the presence of these contaminants in the treated water.

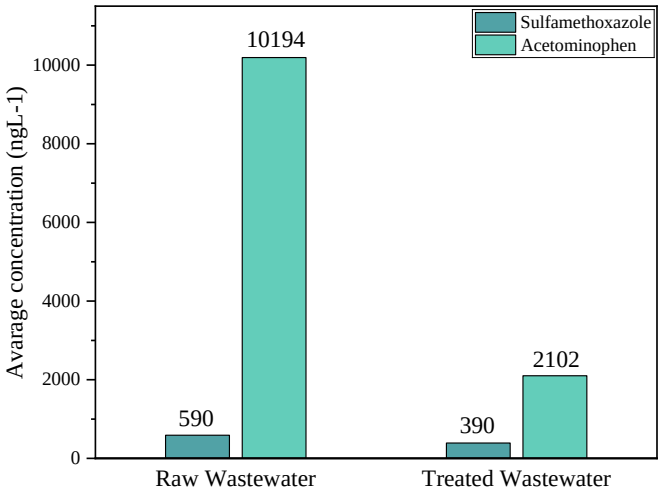

Figure 3: Average concentration (log scale) of pharmaceuticals in the analyzed samples of raw and treated wastewater (adapted[19])

2.1.3. ACETAMINOPHEN

Acetaminophen (ACT) or paracetamol ($C_8H_9NO_2$, MW 151.163, IUPAC N-4-hidroxifenil ethanamide) is one of the most popular painkillers used without a prescription for the relief of headache, backache and rheumatic pains[46]. Its molecule is presented in Figure 4. Continuous exposure to low concentrations of pharmaceutical compounds, such as paracetamol, and their metabolites, causes chronic diseases and antibiotic-resistant genes in aquatic organisms[47].

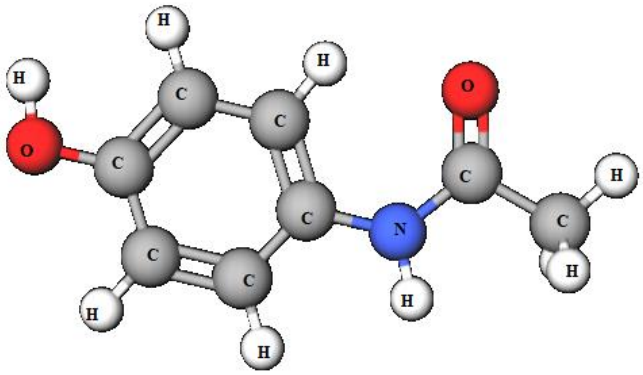

Figure 4: Acetaminophen molecule (adapted[46])

Researchers estimated the global production of ACT to be around 100 tons per year[48]. This mass production of ACT increases the leakage opportunity into the environment, which increases the threats of ACT and its by-products on the ecosystems[46].

During the chlorination of water contaminated with ACT, toxic by-products such as 1,4-benzoquinone and N-acetyl-benzoquinone imine are formed, which can damage the human liver and kidneys, considering the adverse effects of pharmaceuticals, including ACT on the environment, such as mortality in fish of the species *Orzias latipes* when the concentration is over 160 mg/L or inhibition of algae *Scenedesmus subspicatus* when the concentration is more significant than 134 mg/L[49]. Effectively eliminating these compounds from contaminated effluents is a principal environmental concern[48].

Conventional treatments cannot remove paracetamol from water[50], such as chlorination, which consists in the addition of chlorine for water treatment. In this process, a rapid reaction occurs for the pharmaceutical compounds containing amine, forming more compounds containing chlorine[26,51]. However, other compounds such as cimetidine, diltiazem and gemfibrozil, when chlorinated, degrade. In a previous work it was demonstrated that acetaminophen was either more chlorinated or remained unchanged[52]. Another way to treat wastewater is using activated carbons to improve the contaminant removal efficiency by using adsorption mechanisms; the main advantage of using activated carbons to remove pharmaceuticals is that it does not generate toxic or pharmacologically active products[26].

2.1.4. SULFAMETHOXAZOLE

Sulfamethoxazole (SMX), which molecule is shown in Figure 5, is an antibiotic inhibiting folic acid synthesis in bacteria with low solubility and permeability[53]. It is a commonly used synthetic antibiotic from the sulfonamide class, frequently employed in the treatment of venereal infections across various fields, including aquaculture, veterinary medicine, poultry farming, and human healthcare. Approximately 50% of ingested SMX is excreted to the aquatic environment without proper modification, resulting in the discharge of residual SMX into the sewage pipes[54].

The presence of such drugs that have significant environmental impact and high toxicity in WWTP effluents threatens the safety of water bodies[55]. The long-term effects of antibiotics, including bioaccumulation in the food chain and the promotion of resistant bacteria, pose a significant risk to the environment and human health[56].

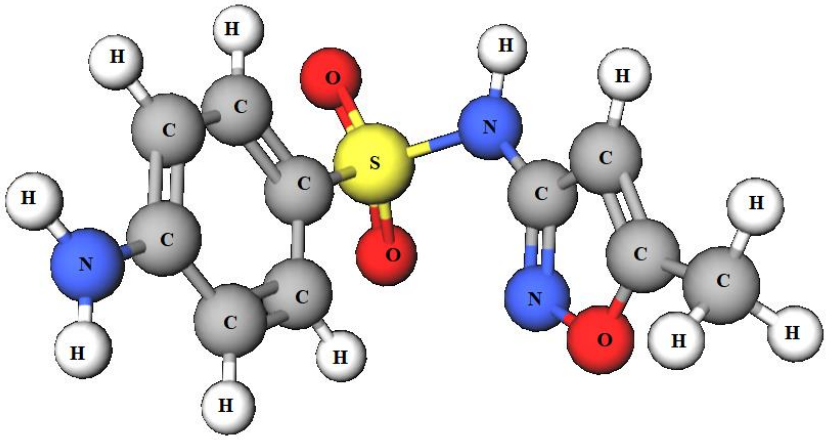

Figure 5: Sulfamethoxazole molecule (adapted [56])

SMX has seen to be present in high concentrations in water effluents in Europe, mainly in Baltic Sea. SMX is thought to be persistent in the environment due to its capability to avoid degradation by conventional biological treatments of wastewater. SMX is shown to promote antibiotic resistance in bacterial populations in river samples (dose 500 µg/L), emphasizing the importance of reducing the levels in water effluents[57].

2.1.5. PHENOLIC COMPOUNDS

Phenolic compounds have been reported as significant pollutants by various environmental protection agencies[58]: US Environmental Protection Agency (USEPA), Central Pollution Control Board (CPCB), among others; polyphenols commonly exist in agro-industrial wastewaters, such as soft drink wastewater, cork wastewater, oil mill wastewater, landfill leachate, pulp mill wastewater, winery wastewater and tannery wastewater. Polyphenols at high concentrations tend to suppress or even eliminate the efficiency of biological wastewater treatment processes[59]. These compounds are known for their high persistence in the environment for an extended period (low biodegradability), making them compounds among the chemicals of major environmental concern[11]. The phenolic micropollutants generally include chlorine, bromo, nitro and alkyl phenol. Because of their toxicity and persistence in the environment, these phenolic compounds are considered priority pollutants and appear on a list of dangerous substances of the USEPA[60].

Discharging these compounds without treatment may lead to serious health risks to animals (carcinogenicity, endocrine disruption and allergies) and aquatic systems. International regulatory bodies have set strict discharge limits for phenols for a sustainable environment. For example, the USEPA has set a water purity standard of less than 1 ppb for phenol in surface

water[61]. The toxicity levels usually are in the range of 9-25 mg/L for both humans and aquatic life[62]. Similarly, phenyl phenols and bisphenols are widely used in hospitals and households as disinfectants. Therefore, extensive research[7,61,63] has been conducted to find effective methods for their removal. Several treatment approaches have been explored, including chemical oxidation, membrane retention and adsorption[63].

Gallic acid (GA) is one polyphenolic compound most representative of wastewater. Moreover, it is one of the simplest models of natural organic compounds and is commonly used as a standard reference to quantify polyphenols[55,11].

This polyphenol, a naturally occurring low molecular weight tri phenolic compound, has emerged as a potent antioxidant and as an efficient apoptosis-inducing agent; gallic acid derivatives have also been found in several phytomedicines with diverse biological and pharmacological activities, including radical scavenging, interfering with the cell signaling pathways and apoptosis of cancer cells[64].

Figure 6 exhibits the molecule of GA, a well-known polyphenol. Though this compound is commonly considered safe for humans[59], other phenolic compounds are not. Adsorption processes have been identified as the leading technology for removing organic compounds from different wastewater. Their removal and recovery from wastewater are important from both environmental and economic points of view. Environmentally, it is a must for reducing the organic charge in wastewater. At the same time, the extraction and recovery of polyphenols with essential implications for human health are also attractive from the industrial and economic points of view.

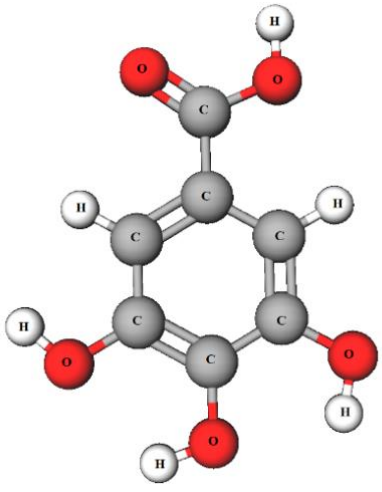

Figure 6: Gallic acid molecule (adapted[64]).

2.2. PERMEABLE REACTIVE BARRIERS

Remediating contaminated groundwater is essential to ensure the sustainability of this water source, and both active and passive groundwater remediation technologies have been implemented with this purpose. Specifically, passive remediation via PRBs has been applied since 1995[65]. Figure 7 is a representation of how PRBs are applied for groundwater remediation.

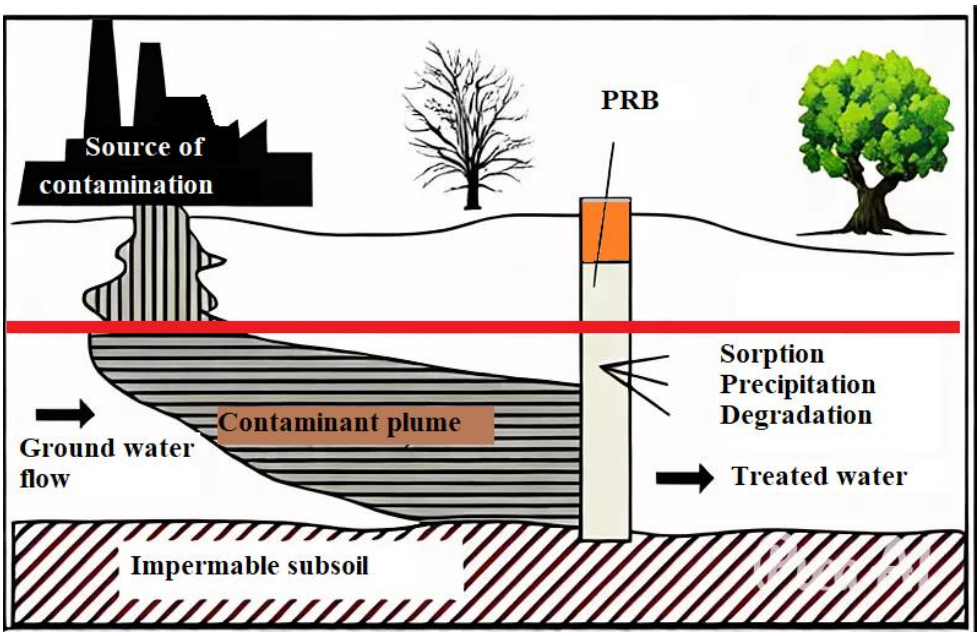

Figure 7: Principle of groundwater remediation by PRBs (adapted[66])

PRBs appear to be an exciting option since the contaminant plume with various groundwater pollutants, for example heavy metals and organic and inorganic pollutants[67], moves through the reactive zone by natural hydraulic gradient, allowing for a passive treatment with no external energy inputs. For this reason, complete remediation can take many years. This concept can be expanded for the application of PRBs in the treatment of persistent/priority pollutants[68], as will be focus on this work.

The benefits and significant limitations of this *in situ* technology are presented in Table 3. These limitations can be addressed using the efficient barrier design that addresses the plume and site characteristics[65].

Table 3: Benefits and limitations of Permeable Reactive Barriers (adapted[65])

Benefits	Limitations
Low energy consumption, which reduces the carbon footprint of the process and the operating costs	The depletion of the reactive chemical compounds over time due to their reaction with the contaminant
Requires monitoring of its activity with only minimum scheduled maintenance after a specified period of operation, if needed	Clogging of the barrier pores
Easy installation and removal procedures and low maintenance costs[67]	
Provides efficient and targeted remediation, where these barriers convert specified pollutants to fewer toxic species and/or retain them	

2.2.1. DESIGN AND CONFIGURATION

An appropriate PRB configuration is critical to the engineering design, which should be selected considering specific hydrogeologic conditions and characteristics of the contaminant plume. The most common PRB configuration is the continuous permeable reactive barrier (C-PRB)[67], placed perpendicularly to the groundwater flow[66], otherwise known as crossflow. Another configuration is the funnel and gate, a system consists of permeable gate (as a reactive media) located between 2 impermeable walls, which direct the polluted plume towards reactive media[69].

An accurate, adequate, optimized PRB design increases treatment efficiency and reduces maintenance costs. PRB treatment is more cost-effective than the traditional pump and treatment technology[68]. It is possible to compare the two widely used configurations, the continuous wall or trench and the funnel and gate, in Figure 8. The decision between the two configurations is depending on hydrogeological parameters of the site and on the reactive materials cost[69]. The funnel and gate configuration is recommended for designing PRB because this setup requires less reactive material in the treatment zone.

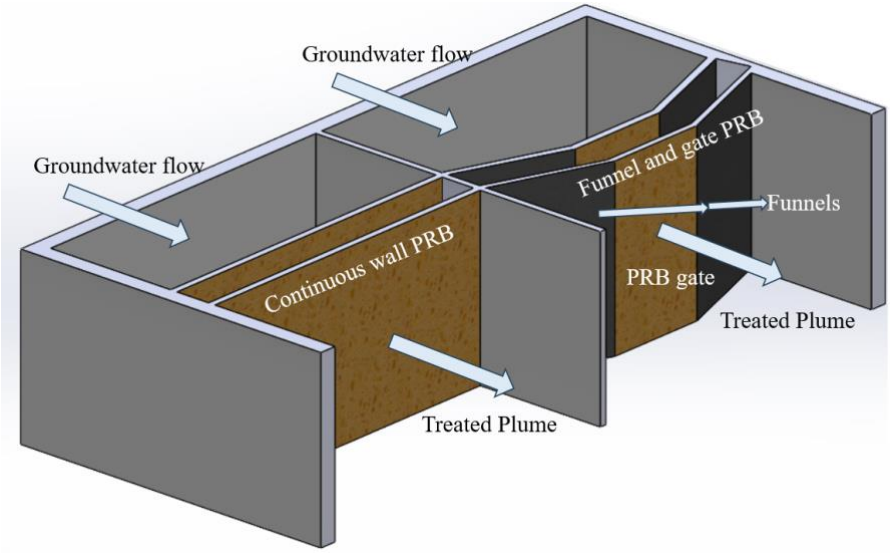

Figure 8: Configuration of the PRB designs (adapted[65])

An important condition of successful remediation is the requirement that the contaminant plume flows through the reactive gate of specified thickness b with a certain velocity v. That means the contaminant will contact a reactive medium in specified time t_{res} (residential time). Considering the safety factor SF, it is crucial to design a reactive gate with sufficient thickness. The thickness of the PRB wall can be estimated according to Eq. 1[70].

$$b = v \,.\, t_{res} \,.\, SF \qquad (1)$$

Another essential part is the composition of the barrier. Mixing with several solid materials such as solid industrial wastes, mineral materials, carbonaceous materials, (reductive) graphene oxide and biochar in permeable barrier applications is popular in the construction of reactive materials because of simplicity, cost, environmental benignity and scarce chemical agent use[15].

This process does not require any bonding formation among various partial materials; each partial material consisting of a mixed material can jointly achieve higher pollutant removal rates than a single material, for example via a mixing process with materials having excellent hydraulic conductivity. Simultaneously, mixed material can have access to the decontamination of multi-component pollution[16].

The selection and use of PRB materials are based on conditions such as the type of target contaminants (organic or inorganic), their concentration, mechanisms needed to remove them (biodegradation, adsorption, etc.), and the cost of materials[71]. In addition, the considerations influencing the choice of materials for permeable reactive barriers include[65]:

- Hydraulic conductivity: the barrier should have adequate permeability to allow the passage of the contaminated groundwater without considerable retardation in its velocity.
- Environmental compatibility: the used material should not have the potential to release toxic species into the host environment.
- Long-term physical and chemical stability: the material should have adequate long-term stability to eliminate the need of maintenance of the barrier during its service life.

The technology of PRBs can be extended to offer a versatile solution not only for the remediation of contaminated groundwater but also for the effluent polishing of wastewater treatment plants, approach envisaged in this work. Implementing PRBs in wastewater treatment ensures that the water discharged into the environment is treated and free from harmful contaminants. This proactive approach safeguards local water resources and mitigates the potential risks of releasing untreated wastewater. As a result, integrating PRBs into wastewater treatment strategies holds the promise of providing a comprehensive and sustainable solution to combat water contamination at its source, contributing to the preservation and protection of vital groundwater supplies.

2.2.2. LOW-COST FILLERS FOR PERMEABLE REACTIVE BARRIERS

Adsorption is a fundamental mass transfer process suitable for the removal of contaminants, particularly organic contaminants, from wastewater streams[72]. According to the different forces of attraction between substances, adsorption can be divided into chemisorption and physical adsorption.

In physical adsorption, contaminants accumulate on the adsorbent surface due to physical forces such as van der Waals forces, hydrogen bonding, hydrophobic interactions, polarity and space forces[73]. The dipole-induced dipole interactions and the chemistry of π–π interactions also produce adsorption effects[74]. The chemisorption of molecular and atomic species on solid-state material surfaces is a central concept in chemistry, physics, and material science[75]. The main difference is that chemisorption involves strong chemical interactions and often leads to irreversible binding, while physical adsorption involves weaker, non-chemical interactions and is usually reversible.

Moreover, adsorbent dosage, temperature, pH, adsorbate concentration and contact time, among others, constitute some of the factors directly influencing adsorption[76]. The

physical presence of a barrier reduces runoff velocities, which promotes the settling of solids, while the barrier's permeability allows solid particles to be filtered by the media as runoff passes through it[77].

PRBs are made of various materials and may be configured in various ways depending on the treated runoff's location, volume and nature. Some filter media may rely primarily on physical filtering processes to remove pollutants, while other media, such as compost or vegetation, may also enhance pollutant removal through chemical and biological reactions within the media[77]. Through a mass transfer process, the barrier will be positioned as a tertiary treatment stage at the end of the WWTP treatment processes to reach better-treated wastewater qualities, allowing their reuse in irrigation activities. In the present work it is aimed to explore the use of low-cost materials derived from waste sources as filler materials in the development of PRBs.

2.2.2.1. GEOPOLYMERS

Geopolymers (GP) are one of the green cementing materials whose research began in the 1970s. GP attracts extensive attention for its high-temperature resistance, low permeability, excellent durability, mechanical performance, among other characteristics[78]. GP is an inorganic aluminosilicate material dominantly composed of tetrahedral silica (SiO_4) and alumina (AlO_4), which are formed through polycondensation of a precursor rich in aluminosilicate and an alkali-activator, resulting in hardened 3-D molecule networks[79,80]. GP has a wide variety of applications depending on the Si/Al ratio[80] used in the synthesis process.

Considering these propositions, an improved structural model based on a previous model[81], was proposed by Rowles et al. (2007)[82], as shown in Figure 9, for polymerization and formation from a NaOH-activated metakaolinite precursor approach. This model is only valid for incompletely reacted geopolymer. It involves free Al-OH groups that will later, with time or temperature, perform polycondensation with opposed Si-O-Na, resulting into sialate bonds[83].

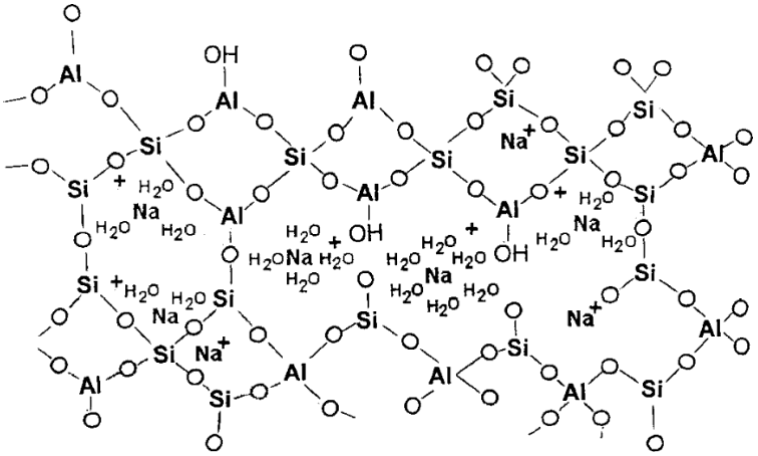

Figure 9: A proposed schematic model for GP structure based on a previous original model[81] (adapted[82])

The innovation of GPs relates to the possibility of hardening at room temperature without high treatment temperature and consequently reduced CO_2[84], representing an eco-friendly innovative material[85]. This process mainly involves dissolution, gelation and condensation reactions occurring in parallel to form the material of interest[11].

One source of alumina silicate material is fly ash (FA)[84], and it is the most used and suitable waste material in geopolymerization due to the considerable amount produced worldwide, estimated to be around 780 million tons annually, and its great workability[85,86]. FA is a by-product derived from the combustion of coal powders and collected by mechanical and electrostatic separators from the flue gases of the power plants[87].

As a result of its large production, there is a growing need to reduce its accumulation, improve the way it is disposed, and to focus mainly on how to reuse this material, enabling it to be put back into the economy and fostering a circular economy[88].

While most GP research focused on the cement and concrete industry, it has recently gained attention as an alternative material to solve environmental problems in water and wastewater pollution[80]. This implies the potential of this new material as an innovative media in wastewater treatment because these eco-friendly materials have attractive advantages, such as low cost, high efficiency, simple production and readily scalable characteristics[11,89].

GP has a three-dimensional mesh structure that provides the GP with high porosity and many mesopores that enhance the adsorption capacity by providing more exposed binding sites with pollutants and impurities on the surface[90,73].

Table 4 shows some examples reported in the literature on the application of GP as adsorbent, their contaminants as adsorbates, and some of the findings from the adsorption tests.

Table 4: Examples of geopolymer for wastewater treatment application

Author/year	Precursor	Contaminant	Findings
Onutai et al. (2019)[91]	Porous fly ash-based	Pb, Cu, Cd and Ni	The adsorption capacity of heavy metal ions on geopolymer composite fiber follows the order of Pb, Cu, Cd and Ni in removing heavy metal ions from wastewater.
Novais et al. (2016)[92]	Porous fly ash-based	Pb	More porous geopolymers presented better lead removal efficiency, while higher pH in the solution reduced their removal ability since metal precipitation is enhanced.
Wang et al. (2022)[93]	Metakaolin based GP microspheres	Tetracycline (pharmaceutical compound)	With oleic acid modification technique the fabricated modified geopolymer's surface area and pore volume was increased. Moreover, the obtained geopolymer exhibited a maximum Langmuir uptake capacity of 645.70 mg/g at 298 K.
Barbosa et al. (2018)[94]	Metakaolin and rice husk ash	Methyl violet 10B	Using soybean oil as a mesostructured directing agent was essential. The maximum adsorption capacity of mesoporous geopolymer was reported to be 276.90 mg/g.
Lee et al. (2017)[95]	Fly ash and slag	Cs^+	An investigation of the adsorption isotherms revealed that the adsorption of Cs^+ onto mesoporous geopolymers were favorable and followed multilayer adsorption.
Aprilina et al. (2021)[96]	Metakaolin and biomass ash	Cu (II)	Adsorption occurred on the geopolymer surface by forming a monolayer of adsorbate molecules with maximum adsorption capacity of 58.824 mg/g.

2.2.2.2. ACTIVATED CARBONS

Activated carbons (ACs) are non-polar and non-graphitic materials, structurally heterogenous, with very high surface area, mainly due to microporosity; hence, it offers a very high adsorption capacity and are widely used as adsorbents[97,98]. Due to these characteristics, from the materials used in adsorption, commercial activated carbons have greater prominence

since significantly remove several types of contaminants[99] and is an excellent adsorbent material for the isolation and recovery of trace materials in the food, beverage, cosmetic, pharmaceutical and chemical industries[97].

Several studies have sought alternative, highly available, renewable, cheap and efficient materials, some employing waste sources[100]. Using activated carbons in industrial processes implies constantly reducing production costs to maintain competitiveness with other technologies and materials[12].

There are two steps in the production of AC: carbonization and activation. The carbonization step is a pyrolysis procedure, but specifically for carbonaceous materials[101]. An essential advantage of ACs is the fact that they can be obtained practically from any carbon-containing raw material; some of the most often used raw materials to obtain activated carbons are bituminous coals, bones, coconut shells, wood and waste biomass from agriculture, wastes from cellulose industry and olive pomace[102]. In this work, olive pomace will be considered in the production of ACs as filer materials for PRBs.

Since the developed porosity is insufficient, an activation step is needed to enlarge the pores and modify their surface. Activation can be chemical or physical. In chemical activation processes, the precursor is first treated with a chemical activation agent, often phosphoric acid, then heated to a temperature of 450 – 700 °C in an activation kiln[103]. Although chemical activation produces larger surface areas, requires shorter time and allows for a more careful control of micro-porosity, it is more expensive and polluting than physical activation. Physical activation allows more environmentally friendly activations, conducted at elevated temperatures in an oxidizing agent (steam or CO_2) for a controlled time, which can be considered partial gasification[101].

The specific surface area of microporous ACs usually amounts to at least 90% of the total surface area. Microporous materials are important in water treatment because of their ability to adsorb a wide variety of contaminants in the aqueous phase[104].

For commercial-grade carbons, surface area values typically vary between 500 and 1500 m^2/g or even as high as 3000 m^2/g[105]. The surface area of AC obtained from wastes varies. For example, an AC based in olive pit with 883 m^2/g was obtained by thermal treatment[106] or an AC with 474 m^2/g with more conventional physical activation using steam/nitrogen[107].

The quality of AC depends on its structure, as most of these structures have micropores, macro pores and mesopores. As different pore sizes will adsorb different-sized molecules in their structure, only a few micropores will align directly toward the outer surface of the carbon particles[97]. Table 5 shows the pore types and their sizes, standardized worldwide by the

International Union of Pure and Applied Chemistry (IUPAC), and their respective adsorbable molecules.

Table 5: Pore classification according to the general classification by IUPAC

Pore types	Diameter	Adsorbable molecules
Micropores	< 2 nm	Small molecules such as gas, small organic and water molecules, and ions[108]
Mesopores	2-50 nm	Larger molecules such as organic compounds, surfactants, and polymers, large ions[109]
Macropores	> 50 nm	Transport of the molecules, allowing for the efficient flow of fluids, larger particles or even cells

2.2.2.3. CARBON NANOTUBES

Carbon nanotubes (CNTs) are a class of one-dimensional nanomaterials with a cylindrical structure composed of carbon atoms arranged in a honeycomb lattice[110]. Besides diamond, graphite and fullerene (C_{60}), quasi-one-dimensional nanotubes are another form of carbon first reported by Ijima in 1991 when he discovered multiwalled carbon nanotubes (MWCNTs) in carbon soot made by an arc-discharge method. About two years later, he observed single-walled carbon nanotubes (SWCNTs)[111]. The comparison between these two types is presented in Table 6.

Table 6: Comparison between SWCNT and MWCNT (adapted[112])

SWCNT	MWCNT
A single layer of graphene	Multiple layers of graphene
A catalyst is required for the synthesis	Can be produced without a catalyst
Bulk synthesis is difficult as it requires proper control overgrowth and atmospheric condition	Bulk synthesis is easy
Not fully dispersed, and form bundled structures	Homogeneously dispersed with no apparent bundled formation
Characterization and evaluation are easy	It has a very complex structure
It can be easily twisted and is more pliable	It cannot be easily twisted

These methods are commonly used to synthesize CNTs: arc discharge, laser ablation and chemical vapor deposition (CVD). The basic elements to form carbon nanotubes are a catalyst and a carbon source of sufficient energy[112]. CVD has proved to be a preferred route for large-scale production of carbon nanotubes[113], and it is a technique in which the vaporized reactants react chemically and form a nanomaterial product that is deposited on the catalyst[110].

Figure 10 shows the diagram of the CVD method to produce CTNs, with hydrocarbon gas as a precursor; however, research efforts are exploring the use of solid carbon sources, such as plastics[13,114]. The treatment of plastics to convert them into CNTs by sequential pyrolysis and CVD is viable at certain temperatures and flows[114].

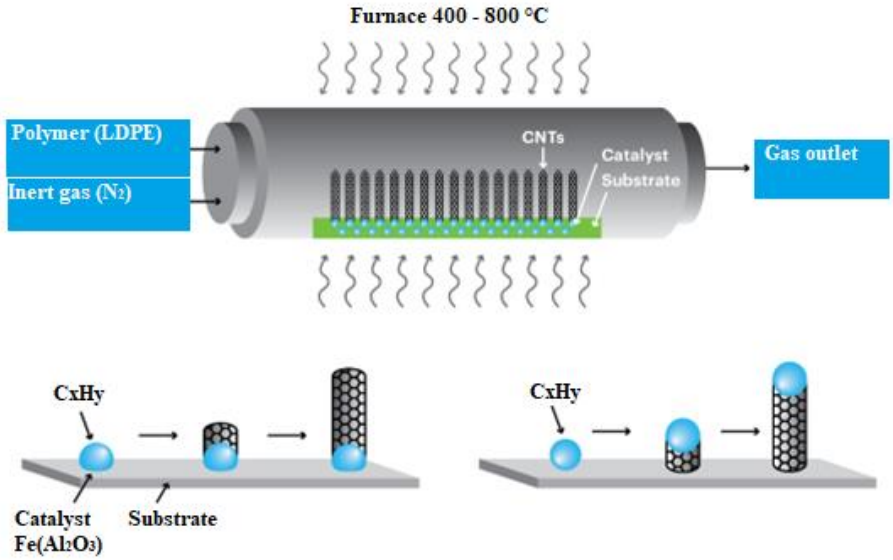

Figure 10: Diagram of the standard chemical vapor deposition (CVD) method for synthesizing CTNs (adapted[115])

The strength of the sp2 carbon-carbon bonds gives CNTs amazing mechanical properties. No previous material has displayed the combination of superlative mechanical, thermal and electronic properties attributed to them[112]. They can be used in several applications, including aerospace, the healthcare field and wearable devices[108], as catalysts or catalysts supporting renewable energy (storage and generation) and environmental technologies, such as oxidation or remediation[116].

Also, the properties of CNTs, such as high surface area, adsorption capacity and selectivity, make them potential adsorbents for organic solutes in aqueous solutions[13,117]. Their attractiveness increases when obtained from carbon-containing wastes from a circular economy perspective. In this sense, plastic solid waste (PSW) can be used as a carbon source[13].

3. OBJECTIVES

The principal aim of this dissertation is to design PRBs tailored for the purification of effluents from wastewater treatment plants, specifically targeting the removal of CECs and incorporating high-added value materials as fillers, including geopolymers derived from fly ash, activated carbons from exhausted olive pomace, and carbon nanotubes from residual plastic. The specific objectives envisaged include the following:

- Synthesis of GP from fly ash;
- Production of ACs using exhausted olive pomace;
- Synthesis of CNTs from plastic solid waste;
- Characterize various produced materials, including GP, AC, and CNTs, to understand their properties and performance.
- Manufacture of PRBs incorporating the developed materials;
- Conduct batch adsorption tests to understand the behavior of both adsorbents and adsorbates.
- Perform breakthrough curves in continuous systems with individual compounds and multicomponent systems.
- Apply the PRBs in a model wastewater treatment containing representative contaminants.

4. MATERIALS AND METHODS

4.1. REACTANTS

The reactants employed in this investigation are delineated below and classified according to their specific applications.

Contaminants used in the simulation of wastewater:

- Paracetamol ($C_8H_9NO_2$ - 98%), provided by Alfa Aesar;
- Sulfamethoxazole ($C_{10}H_{11}N_3O_3S$ - 98%), provided by Supelco®.
- Gallic Acid ($C_6H_2(OH)_3COOH$ - 98%), provided by EMD Millipore Corporation.

Production of geopolymers:

- Fly ash, provided by SOGAMA;
- Sodium Hydroxide pearls (NaOH - 98%), provided by Labkem;
- Sodium Silicate (Na_2SiO_3 - Na_2O = 10.6% and SiO_2 = 26.5%), provided by Fisher Chemical
- Hydrochloric acid (HCl - 37%), provided by VWR Chemicals.

Production of activated carbons:

- Dried olive pomace extract, provided by Mirabaga;
- Carbon dioxide (CO_2), provided by AirLiquide;
- Nitrogen (N_2), provided by Alphagaz™;
- Silica wool, provided by Elemental Microanalysis.

Production of carbon nanotubes:

- Low-density polyethylene (LDPE), molecular Weight Distribution 35000 g/mol, $[C_2H_4]_n$, provided by Sigma-Aldrich;
- Nitrogen (N_2), provided by Alphagaz™;
- Aluminum oxide (Al_2O_3), provided by BASF;
- Ethanol Absolute (C_2H_5OH - 99.99%), provided by Fisher Chemical;
- Ethylene glycol ($C_2H_6O_2$ - 99%), provided by Fisher Chemical;
- Iron (II) chloride tetrahydrate ($FeCl_2 \cdot 4H_2O$), provided by Acros Organics;
- Iron (III) chloride hexahydrate ($FeCl_3 \cdot 6H_2O$), provided by VWR Chemicals.

4.2. MATERIALS PREPARATION

4.2.1. GEOPOLYMERS

The geopolymerization reaction occurs from a source of aluminosilicates and an alkali-activating solution; in this case, 10g of FA was used as the basis for calculations. Initially, the solutions of Na_2SiO_3 (5.67g) and NaOH (2.27g) are mixed with magnetic stirring for 5 minutes. Subsequently, the mixture is manually combined with FA and cured for 24 hours at room temperature. GP was washed multiple times with distilled water and a 0.5 M hydrochloric acid solution until the pH reached neutrality.

4.2.2. ACTIVATED CARBONS

The process of producing AC is carried out in a slow pyrolysis furnace. This involves inserting 10g of exhausted olive pomace (EOP) into a quartz cell containing porous ceramic in the middle. The production occurs under a nitrogen flow of 100 NmL/min; during the initial two hours, only nitrogen is injected to condition the material, facilitating the gradual development of porosity in the subsequent hours.

From the third hour onwards, a heating ramp is initiated at a rate of 5°C per minute, transitioning from ambient to high carbonization temperatures. The process involves three different temperature stages: 400°C and 600°C for 1 hour each and 800°C for 4 hours, ensuring the entire production process is completed within 9 hours.

The methodology for producing AC-CO_2 involved a slow pyrolysis process. The production of both materials occurred under a nitrogen flow of 100 NmL/min, using a heating rate of 5 °C/min, transitioning from ambient temperature to high carbonization temperature. This process involved three different temperature stages: 400 ºC and 600 ºC for 1 h each and 800 ºC for 4 h. For the activation of AC-CO_2, N_2 injection was replaced by CO_2 injection at 800 ºC for 1 h. Following the CO_2 injection phase, N_2 is recirculated once more until the oven reaches a cooling temperature. A representative scheme of the programming operation, including heating ramps and residence time, and a drawing of the laboratory pyrolysis oven are available in Figure S1 of the supplementary materials.

After cooling the reactor under a nitrogen atmosphere, the materials were removed and sieved to obtain a particle size of less than 53 µm. Subsequently, the carbon materials were

stored in sealed bags for future use to remove phenolic compounds. Finally, the AC was washed multiple times with distilled water and a 0.5 M hydrochloric acid solution until the pH reached neutrality ($pH \leq 7$).

4.2.3. CARBON NANOTUBES

The synthesis method was chosen based on Diaz de Tuesta et al. (2023)[118]. CNTs were synthesized using CVD on an iron-oxide-based catalyst supported by alumina (IO/Al_2O_3).

The catalyst was prepared using a sol-gel method. Initially, 10 mmol of $FeCl_2$ was dissolved in 20 mL of ethanol and heated until boiling. Meanwhile, 20 mmol of $FeCl_3$ was dissolved in 80 mL of ethylene glycol and maintained at 60 °C for 5 minutes. Both solutions were then combined in an ice bath to reach thermal equilibrium. Subsequently, the solutions were mixed with 6.6 g of Al_2O_3 in a beaker and heated to 60 °C for 2 hours on a stirring hot plate. The temperature was then raised to 120 °C until a gel-like consistency was achieved. Further heating to 200 °C resulted in a powdery texture. The obtained powder underwent thermal treatment under nitrogen flow at 300 °C for 12 hours and 600 °C for 24 hours, yielding Fe/Al_2O_3.

The CVD process was conducted using a vertical oven (TH/TV, Termolab), as shown in Figure S2, in the supplementary material employing low-density polyethylene (LDPE) as the carbon source. This oven comprises upper and lower crucibles and has three temperature control zones (T1, T2, and T3).

To synthesize CNTs, 1 g of the catalyst was loaded into the lower crucible, while 5 g of LDPE was placed in the upper crucible. The synthesis took place at a temperature of T3 = 800 °C with a holding time of 1 hour upon reaching the desired temperature under a nitrogen atmosphere (flow rate of 40 $mNL.min^{-1}$).

After the synthesis, the CNT was subjected to acid washing to reduce the quantity of the metal catalyst attached to the structure (50% v/v H_2SO_4, 140 °C, 3 h, under reflux). After cooling down, the material was abundantly washed with distilled water to remove excess acid and then dried at 60 °C for over 12 h.

4.3. PROTOTYPE DESIGN FOR PRB

For continuous testing, a prototype support for the materials was designed using 3D printing. The prototypes were initially sized using AutoCAD 2023 software from AutoDesk, then designed in SOLIDWORKS 2022 from SolidWorks, and finally printed with polylactic acid (PLA) filament. The preliminary version is presented in Figure S3 in the supplementary materials.

The second prototype was created in a cylindrical shape, illustrated in its design in Figure 11, featuring a sealing system that uses the expansion of the geopolymer, to solve the problem of preferential pathways. From this perspective, the barriers were assembled using structured GP as the structural factor, CNTs as the catalytic medium, and AC as the adsorbent material functioning as a filler for the barrier. This prototype was used in continuous mode as a proof of concept.

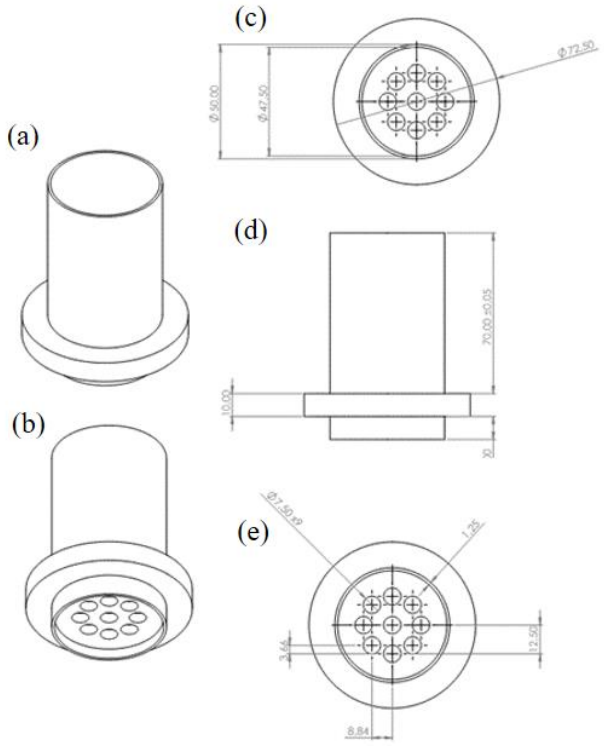

Figure 11: Cylindrical prototype design, the views are as follows: (a) upper isometric, (b) lower isometric, (c) top, (d) side, and (e) bottom.

4.4. CHARACTERIZATION TECHNIQUES

4.4.1. QUANTITATIVE AND QUALITATIVE ANALYSIS OF ELEMENTS

Inductively Coupled Plasma Optical Emission Spectroscopy (ICP-OES) is an analytical technique employed to quantify specific elements within a sample. In this context, it was utilized to analyze the chemical composition of FA. It is based on the excitation of the electron to a more active layer due to energy absorption from the atom. In ICP-OES, the energy source to move the electron is the heat of an argon plasma[119]. This technique is particularly adept at identifying and quantifying a diverse array of chemical elements from the sample of interest using a spectrometer Agilent 5800 with a measurement range from 167 to 758nm.

Elemental analysis of the AC and CNT was performed using a CHNS analyzer Flash 2000 (Thermo Fisher Scientific, Massachusetts, USA), equipped with a thermal conductivity detector to quantify the carbon, hydrogen, nitrogen, and sulfur contents. The analysis were done at Rey Juan Carlos University – Spain.

4.4.2. X-RAY DIFFRACTION

This technique involves directing X-rays onto the sample and analyzing the resulting diffraction patterns, which provide insights into the material's atomic arrangement and crystallographic properties. X-ray diffraction (XRD) measurements were performed on the material by depositing it on a glass sample holder and analyzing it using a diffractometer. The analyses were made at room temperature by a PANalytical X'Pert Pro diffractometer, equipped with an X'Celerator detector and secondary monochromator in θ/2θ Bragg-Brentano geometry. The measurements were carried out using 45 kV and 40 mA, a CuKα radiation (λα 1 =1.5406 Å), 0.017°/ step, 100 s/step, in a 10-80° 2θ angular range. Data processing was performed using the software X'Pert HighScore Plus with reference cards from the Crystallography Open Database.

4.4.3. FOURIER-TRANSFORM INFRARED SPECTROSCOPY

Infrared spectroscopy analysis is valuable for identifying the molecules present in a sample. The Fourier-transform infrared (FT-IR) spectra of four distinct samples were recorded using a Perkin Elmer FT-IR spectrophotometer UATR Two, with a resolution of 4 cm^{-1}. The wavenumber range used for analysis ranged from 450 to 4000 cm^{-1}. All measurements were

conducted on solid samples at room temperature. This analysis was carried out at the Analytical Chemistry Laboratory of the Bragança Polytechnic Institute.

4.4.4. ACID-BASE CHARACTERIZATION

Evaluating the acid-base characteristics of the material is a pivotal aspect that can greatly influence the efficacy of the tree materials as adsorbents. This assessment yields crucial insights into the adsorption mechanism and the interplay between the adsorbent and the adsorbate[11].

Analyzing the acid-base properties of the material offers insights into the adsorption mechanism and the interaction between the adsorbent and the adsorbate, allowing characterization of its basicity or acidity. The material's acidity was determined by adding 0.2g of the solid sample into 25 mL of a 0.02 mol/L NaOH solution and mixing on a magnetic stirrer at 300 rpm for 48 h. The resulting solution was then filtered, and a 20 mL aliquot of the recovered solution was titrated with 0.01 mol/L HCl solution using phenolphthalein as an indicator. For basicity, 0.2 g of the solid sample was added to 25 mL of 0.02 mol/L HCl solution and mixed on a magnetic stirrer at 300 rpm for 48 h. After filtration, 20 mL of the recovered solution was titrated with 0.01 mol/L NaOH solution, using phenolphthalein as an indicator.

To find the pH at the point of zero charge (pHpzc), six dilutions of 0.01 mol/L NaCl were prepared in Erlenmeyer flasks. The pH of each solution was adjusted to values 2, 4, 6, 8, 10, and 12 by adding 0.02 mol/L NaOH or HCl. To study the effect of pH on the material's performance as an adsorbent, 50mg of the solid sample was added to each solution, which was then stirred on a magnetic stirrer at 300 rpm and 20 ºC for 24 h. After filtering the solutions, their pH was measured. The final pH values were plotted on the y-axis, and the corresponding initial values on the x-axis. A correlation was established between these two values, and an identity curve was generated on the graph. The intersection point between the pH value and identity curves represents the pHpzc.

4.4.5. SCANNING ELECTRON MICROSCOPY AND TRANSMISSION ELECTRON MICROSCOPY

Scanning electron microscopy (SEM) stands out as one of the most adaptable tools for scrutinizing and dissecting the microstructural attributes of solid materials. Its notable utility stems from its capacity to achieve high resolutions, often on the order of 10 nm, particularly when analyzing bulk objects[5]. Another significant advantage of SEM imaging lies in its ability

to present specimens in three dimensions, a feature directly attributable to its considerable depth of focus; The samples were analyzed using a FEI Quanta 400 SEM with a resolution of 4 nm, equipped with an Everhart-Thornley detector for backscattered and secondary electron contrast. This analysis was done at the University of Trás-os-Montes and Alto Douro.

Transmission electron microscope (TEM) type of electron microscope has three essential systems: an electron gun, which produces the electron beam; the condenser system, which focuses the beam onto the object; the image-producing system, consisting of the objective lens, movable specimen stage, and intermediate and projector lenses, which focus the electrons passing through the specimen to form an accurate, highly magnified image, and the image-recording system, which converts the electron image into some form perceptible to the human eye. The image-recording system usually consists of a fluorescent screen for viewing and focusing the image and a digital camera for permanent records. A JEOL 2100 high-resolution transmission electron microscope (HRTEM) with LaB6 filament operating at 200 kV was used to obtain microphotographs of the CNTs. This analysis was done at the International Iberian Nanotechnology Laboratory.

4.4.6. TEXTURAL ANALYSIS

Textural analysis was performed by determination of N_2 adsorption isotherms at 77 K, using the BET (Brunauer-Emmett-Teller) method to quantitatively determine the surface area of porous materials, such as powders and porous solids. Before the analysis, the samples were degasified for 16 h at 120 °C, following IUPAC recommendation. Total pore volume (V_T), S_{BET}, and Langmuir-specific surface areas (S_{BET} and $S_{langmuir}$) were gathered using the Quantachrome TouchWinTM software, following the procedure used in previous works. The external surface area (S_{ext}) and the micropore volume (V_{mic}) were obtained by the t-method (thickness was calculated by employing ASTM standard D-6556-01). The microporous surface area (S_{mic}) was determined as the subtraction of S_{ext} from S_{BET} and the average pore width (W_{mic}) by approximation ($W_{mic} = 4\ V_{mic}.S_{mic}^{-1}$). The total pore volume (V_{Total}) was determined at p/p0 = 0.98. Calculations of those methods were all done by using TouchWinTM software v1.21. This analysis was conducted at the Analytical Chemistry Laboratory of the Bragança Polytechnic Institute (IPB).

The bed voidage, is defined as the fraction of the total volume which is free space available for the flow of fluids, and thus the fractional volume of the bed occupied by solid material is $(1-\varepsilon)$. Depending upon the nature of the porous medium, the voidage may range from near zero to almost unity. To conduct the test, we used:

- Two graduated cylinder;
- 26.90 grams of structured geopolymer in cubic shape;
- 100 ml of water.

Allowing us to calculate the void fraction using the Eq. 2:

$$\varepsilon = \frac{V_{void}}{V_{bed}}.100 \quad (2)$$

Where ε is the bed voidage, V_{void} is the volume of the voids, that can be calculated using the V_{final} (ml) final volume and $V_{initial}$ (ml) initial volume of the bed V_{bedl} before the addition of the GP.

4.4.7. THERMOGRAVIMETRIC ANALYSIS

Thermogravimetric Analysis (TGA) is a technique that measures the mass variation of a material as a function of temperature, aiming to assess its thermal stability and decomposition behavior. It determines the decomposition temperature, quantifies mass loss due to volatilization or chemical reactions, and analyzes the moisture and volatile content. The TGA of the materials was conducted under an air atmosphere in a Diamond TG/DTA (TG 209F3, NETZSCH) apparatus heating from 50 to 850 ºC at 10ºC min^{-1}. This analysis was done at Rey Juan Carlos University – Spain.

4.5. MASS TRANSFER

Understanding the dynamics of mass transfer processes is essential for designing efficient PRBs and predicting their behavior in wastewater treatment. In both batch tests, it was necessary to calculate the adsorption capacity q (mg/g), which was determined with Eq. 3.

$$q = \frac{(C_0 - C_e) \times V}{m} \quad (3)$$

Where C_0 (mg/L) is the initial concentration of the pollutant, C_e (mg/L) is the concentration in the liquid phase of the pollutant at the equilibrium time, V (L) is the volume of the pollutant solution, and m (g) is the mass of adsorbent.

4.5.1 ADSORPTION KINETICS

The study of kinetics in adsorption processes is essential for understanding the rate at which contaminants are removed from solutions by adsorbents. Adsorption kinetics describe the time-dependent interaction between the adsorbate and the adsorbent, providing insights into the mechanisms of adsorption, the efficiency of the process, and the factors affecting the rate of adsorption. For the adsorption kinetics tests, nine experiments were conducted, each relating a different adsorbent to a distinct adsorbate, as shown in Table 7.

Table 7: Compilation of the studied adsorbents and adsorbates

Adsorbents	**Adsorbates**		
	ACT	**SMX**	**GA**
GP	ACT with GP	SMX with GP	GA with GP
AC	ACT with AC	SMX with AC	GA with AC
CNT	ACT with CNT	SMX with CNT	GA with CNT

The following series of steps were carried out for each adsorbent-adsorbate pair:

- The solution containing 100 mg/L of each compound was prepared with a volume of 100 mL;
- An adsorbent mass of 0.25 g was added to the solution, resulting in a concentration of 2.5 $g_{adsorbent}/L_{solution}$;
- The mixture was agitated on a magnetic stirrer at 300 rpm at room temperature;
- At 13 different time intervals (0, 2, 5, 10, 15, 20, 30, 45, 60, 90, 120, 240, and 360 min) aliquots of 2 mL were withdrawn from the solution;
- At the final stage, all 2 mL aliquots were collected using a syringe with a solids filter and analyzed by HPLC.

This work used key models such as the pseudo-first-order, pseudo-second-order kinetic models, and intraparticle diffusion to analyze experimental data and determine the rate constants. Understanding these kinetic behaviors is crucial for optimizing adsorption systems, scaling up processes for industrial applications, and ensuring the effective removal of pollutants in environmental remediation. The pseudo-first-order model can be mathematically represented by Eq. 4[120]:

$$q_t = q_e(1 - e^{-k_1 t}) \quad (4)$$

Where q_t is the adsorption capacity (mg/g) at a time t (min), q_e is the adsorption capacity at equilibrium (mg/g), and k_1 is the adsorption rate kinetic constant of the pseudo-first-order model (min^{-1}).

Eq. 5[120] represents the mathematical formulation of the pseudo-second-order model.

$$q_t = \frac{q_e^2 k_2 t}{1 + q_e k_2 t} \quad (5)$$

Where k_2 is the adsorption rate kinetic constant of the pseudo-second-order model (g mg^{-1} min^{-1}). The intraparticle diffusion model is expressed mathematically in Eq. 6[120]

$$q_t = k_{id} t^{1/2} + I \quad (6)$$

Where k_{id} is the intraparticle diffusion rate constant (mg/(g·$min^{0.5}$)), and I (mg/g) is the intercept, which represents the initial adsorption stage (boundary layer effect) before intraparticle diffusion becomes the rate-limiting step.

4.5.2 EQUILIBRIUM ISOTHERMS

Equilibrium isotherms describe the relationship between the concentration of adsorbate in solution and its concentration on the surface of the adsorbent at equilibrium. These isotherms are essential to understand how adsorbents interact with pollutants in environmental and industrial processes, providing insights into adsorption capacity, affinity, and the effectiveness of adsorption systems.

The adsorbent that demonstrated the best performance in the adsorption kinetics tests, activated carbon, was selected to construct the equilibrium isotherms. The following steps were then carried out:

- Preparation of 10 mL solutions of each contaminant with 8 different concentrations: 15, 25, 50, 75, 100, 150, 200, 400 mg/L;
- A AC mass of 0.025 g was added to the solution, resulting in a concentration of 2.5 $g_{adsorbent}/L_{solution}$;
- The mixture was agitated on a magnetic stirrer at 300 rpm at room temperature for 24 hours;
- At the final stage, a 2 mL aliquot was withdrawn with a solids filter syringe for analysis by HPLC.

Similarly, adjustments were made using mathematical models for the equilibrium isotherms. In this study, the most used models in liquid-solid, such as Langmuir and Freundlich, were applied.

The Langmuir adsorption isotherm assumes that monolayer adsorption exists at all surface sites that are homogeneous, with the ability to have no interaction of adsorbed molecules with the neighboring adsorption sites[121]. The Langmuir equation is represented in Eq. 7[121]:

$$q_{eq} = \frac{q_{max} K_L C_{eq}}{1 + K_L C_{eq}} \tag{7}$$

Where q_{eq} is the adsorption capacity at equilibrium (mg/g), q_{max} is the maximum adsorption capacity of the adsorbent (mg/g), C_{eq} is the equilibrium concentration (mg/L), and K_L is the Langmuir adsorption constant (L/mg).

The Langmuir isotherm parameter (K_L) was used to calculate the affinity between the adsorbent and adsorbate via dimensionless separation factor, C_0 is the initial concentration, the R_L is the indicator of the affinity of the solute, determined using Eq. 8[121]:

$$R_L = \frac{1}{1 + K_L C_0} \tag{8}$$

When $R_L = 0$, the adsorption process is considered irreversible. If $0 < R_L < 1$, the process is considered favorable to adsorption. $R_L = 1$ signifies a linear process, while $R_L > 1$ indicates an unfavorable adsorption process.

The empirical Freundlich isotherm model describes adsorption on a non-uniform (heterogeneous) surface with the interaction between adsorbed molecules in the reversible and non-ideal adsorption process. The Freundlich model is expressed mathematically in Eq. 9[121]:

$$q_{eq} = K_F C_{eq}^{1/n_F} \tag{9}$$

The physical meanings of the constants in this model are as follows: $1/n_F$ represents the intensity of the adsorption process or the surface heterogeneity. A $1/n_F$ value less than 1 indicates that the adsorption is favorable; the adsorbate is preferentially adsorbed at higher concentrations, while a $1/n_F$ value greater than 1 suggests that adsorption is less favorable. The

physical meaning of K_F, the Freundlich constant (L/g), is an approximate measure of the adsorbent's adsorption capacity; the higher the K_F value, the greater the adsorption capacity[122].

4.5.3 BREAKTHROUGH CURVES

Breakthrough curves are important in adsorption processes because they provide quantitative data on adsorbents' performance, efficiency, and kinetics related to continuous processes. This information is essential for designing effective adsorption systems, optimizing process parameters, validating theoretical models, and ensuring environmental and economic sustainability in various applications.

Barros et al. [123] explains that at the beginning of the run, most of the mass transfer occurs near the inlet of the bed, where the fluid initially contacts the sorbent. If the solid initially contains no sorbate, the fluid concentration decreases exponentially to zero before reaching the end of the bed. This concentration profile and the breakthrough curve are illustrated in Figure 12.

As the run proceeds and the solid near the inlet becomes nearly saturated, most of the mass transfer shifts further down the bed, creating an S-shaped concentration gradient. The region where most concentration change occurs is known as the mass-transfer zone. This progression accurately represents the mass transfer process in fixed beds.

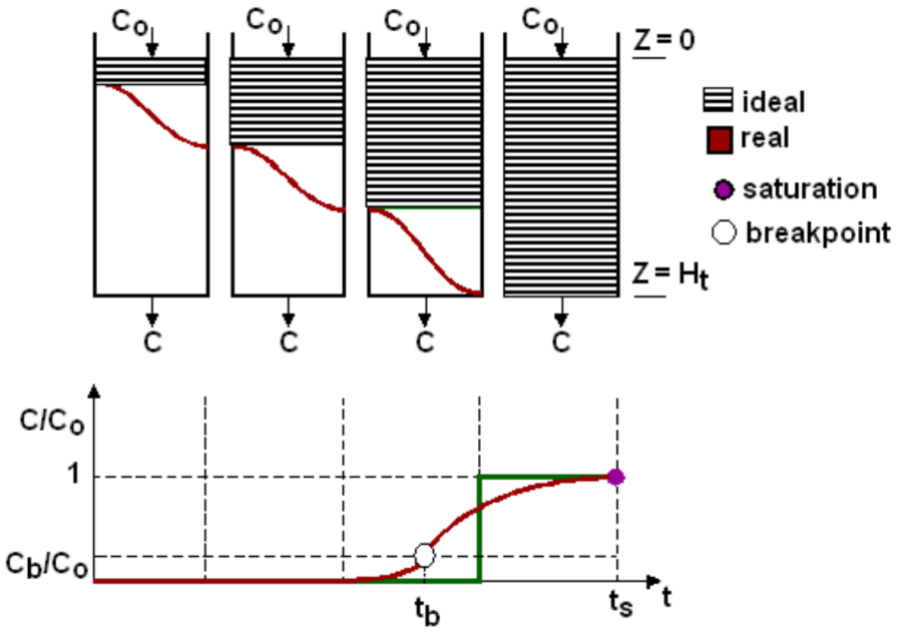

Figure 12: Concentration profile and breakthrough curve (adapted from[123])

Regarding design, PRB will not follow traditional designs as they overly emphasize certain factors such as: the suitability of a site for PRB application, site characteristics affecting barrier design, location, configuration, barrier dimensions, and monitoring strategy[124]. So, for a tertiary treatment application, the sizing can be approximated to that of a fixed-bed column.

These operations are conducted under non-steady-state conditions, where the adsorbate concentrations in both the fluid phase and the solid phase vary with time and position within the bed. The adsorption column was used to conduct this test, while the prototype was employed for comparison. The following steps were required:

- 3D printing of the prototype, which will serve as the skeleton of the barrier;
- Addition of the GP made with 20g of FA inside the prototype;
- Washing with 2M hydrochloric acid to neutralize the GP;
- Adsorption column, Labbox 150mm.
- Addition of 0,5 grams of AC powder;
- Addition of glass beads;
- Circulation of the contaminated solution using an HPLC pump Cole-Parmer at a flow rate of 1 mL/min;
- Analysis of contaminants using HPLC.

Based on the results obtained from the experiment, it is possible to theoretically calculate some parameters; these will be presented below. The time equivalent to the usable capacity of the bed (t_u) and the time equivalent to the total stoichiometric capacity of the packed-bed tower (t_t), if the entire bed reaches equilibrium, are provided by a mass balance in the column, and they are determined by Eq. 10 and Eq. 11[125]:

$$t_u = \int_0^{t_b} \left(1 - \frac{C_A}{C_{A0}}\right) dt \tag{10}$$

$$t_t = \int_0^{t_s} \left(1 - \frac{C_A}{C_{A0}}\right) dt \tag{11}$$

Where t_b is the breakpoint, defined as the time when C/C_0 exceeds the limit established by legislation, t_s is the time corresponding to the saturation of the bed, C_A is the concentration in the liquid phase at a given time, and C_{A0} is the initial concentration.

If total operation time (t_t) is assumed to be the time equivalent to the usable capacity of the bed (t_u) up to t_b, parameter τ may be simplified to t_u/t_t. This ratio is the fraction of the total

bed capacity or length used to the breakpoint[125,126]. Hence, the length of the unused bed (H_{UNB}) is the unused fraction times the total length (H_t), given by Eq. 12:

$$H_{UNB} = \left(1 - \frac{t_u}{t_t}\right) H_t \tag{12}$$

From the mass balance in the column, it is possible to determine the total adsorption capacity q_A (mg/g), as shown in Eq. 13, as well as the useful adsorption capacity q_b (mg/g), as exhibited in Eq. 14:

$$q_A = \frac{QC_{A0}}{m_{ads}} \int_0^{t_s} \left(1 - \frac{C_A}{C_{A0}}\right) dt \tag{13}$$

$$q_b = \frac{QC_{A0}}{m_{ads}} \int_0^{t_b} \left(1 - \frac{C_A}{C_{A0}}\right) dt \tag{14}$$

In which, Q is the volumetric flow rate (L/min) and m_{ads} is the mass of adsorbent to be used in the barrier. The efficiency of the column can be calculated with Eq. 15:

$$\text{n} = \frac{q_b}{q_A} \tag{15}$$

4.6. ANALYTICAL METHODS

The HPLC (High-Performance Liquid Chromatography) measurements encompassed two distinct analyses equipped with a UV-VIS detector (UV-2075 Plus) and a quaternary gradient pump (PU-2089 Plus). HPLC was employed to analyze the three contaminants under investigation (SMX, ACT, and GA). An Ultra BiPh 5 µm column (150 mm x 2.1 mm) was used for this analysis. The mobile phases consisted of 95% ultrapure water with 0.1% formic acid and 5% acetonitrile with 0.1% formic acid for SMX and PCM, which share a detection wavelength of 254 nm, in an isocratic system operating at a flow rate of 0.5 mL/min. For GA, the mobile phase consisted of 5% acetonitrile and 95% ultrapure water with 0.1% phosphoric acid. The isocratic system for GA operated at a flow rate of 0.3 mL/min, with the compounds' absorbance peaks measured at a wavelength of 277 nm.

However, to conduct the tests in the multi-component system, it was necessary to adjust other methodologies to separate the peaks of each contaminant. A new methodology was developed specifically for SMX, using a mobile phase of 75% ultrapure water with 0.1% formic acid and 25% acetonitrile with 0.1% formic acid at a flow rate of 0.5 mL/min and a wavelength

of 254 nm. For ACT and GA, a different methodology was applied, with a flow rate of 0.3 mL/min and mobile phases consisting of 95% ultrapure water with 0.1% formic acid and 5% acetonitrile with 0.1% formic acid, maintaining a wavelength of 277 nm.

Calibration curves must be constructed for each component to convert the areas of the integrals of electrochemical signal peaks into concentration units. These curves were generated and demonstrated high accuracy, with all curves exhibiting an R^2 value of 0.99. Figure S4 in the supplementary material presents the graphical representation of these calibration curves.

5. RESULTS AND DISCUSSION

5.1 PROTOTYPE DESIGN FOR PRB

The PRB was mainly produced with the materials obtained from wastes that have already proven their capacity to adsorb[11–13]. Following several design iterations and optimizations, the prototype for supporting the adsorbent layers was created and 3D printed. This prototype enabled continuous mode testing, as illustrated in Figure 13. A prototype was developed in which the GP structure is cured within the support. This approach takes advantage of the GP's ability to expand, thereby mitigating preferential pathways that do not contact the adsorbent materials.

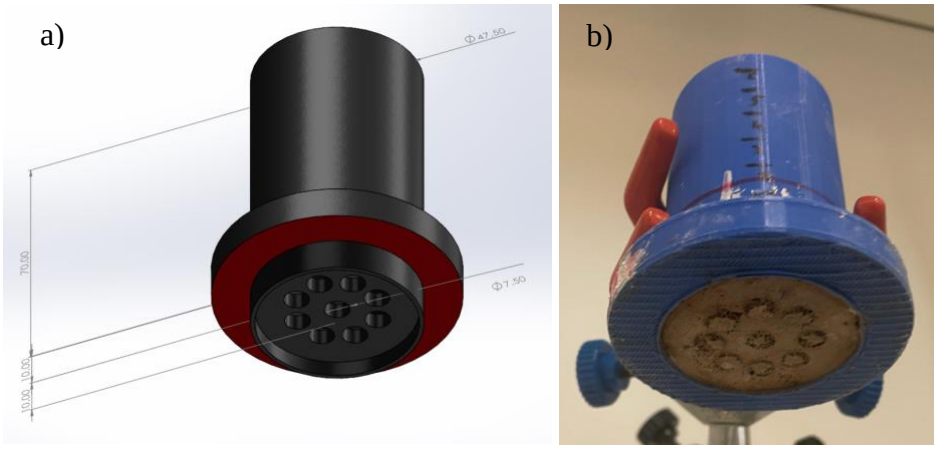

Figure 13: a) Prototype design modeled using SolidWorks software; b) Final prototype after 3D printing, filled with the target material.

5.2 CHARACTERIZATION OF MATERIALS

5.2.1 TEXTURAL PROPERTIES

The analysis results are summarized in Table 8, which compares the three materials based on surface area, average pore width, and total pore volume. The N_2 adsorption-desorption isotherms at 77 K for all the materials are available in Figure S5 in the supplementary material.

All materials exhibit noteworthy surface area values; however, AC stands out with significantly higher values than the other materials.

Table 8: Textural properties analysis for the materials

Sample	S_{BET} ($m^2 g^{-1}$)	$S_{Langmuir}$ ($m^2 g^{-1}$)	S_{ext} ($m^2 g^{-1}$)	S_{mic} ($m^2 g^{-1}$)	V_{mic} ($mm^3 g^{-1}$)	W_{mic} (nm)	V_{total} ($mm^3 g^{-1}$)
AC	527	782	33	494	269	2.2	313
CNT	66	68	66	0	0	0	212
GP	30	42	30	0	0	0	68

The detailed analysis of the surface area of AC demonstrated that CO_2 injection is an effective activation method, revealing noteworthy characteristics that emphasize its effectiveness as an adsorbent. A material with an area of 527 m²/g signifies the presence of numerous active sites available for chemical interactions. The surface area of the AC produced in this work can be compared to the AC found in the work of Labied et al.[127] in which a BET surface area of 608 m²/g was found.

The average pore width is approximately 2.2 nm, close to 2 nm, which indicates a high presence of micropores. According to Dubinin[108] microporous ACs offer enhanced adsorption capacity due to their high surface area and strong van der Waals forces within the confined pores. This structure selectively adsorbs small molecules, making it effective for gas separation, air purification, and water treatment.

The BET surface area of the CNT developed in this work was 66 m²/g. In Birch et al.'s work[128], the highly graphitized multi-walled CNT had a surface area of 74 m²/g, consistent with the decreased specific surface areas reported for such graphitized materials, which is related to the lower residual ash and total metal content.

Although the GP does not surpass the other two materials in this comparison, it remains interesting since its surface area triples compared to its precursor[11]. The surface area results for GP are comparable to those shown by Syial et al.[129], where a geopolymer was produced using the same precursor. The surface area obtained in that study was 31 m²/g, while in this study, it

was found to be 30 m²/g. In addition, by checking the SEM images, it is also possible to see that the material tends to have a more macroporous profile.

On the other hand, bed voidage is a critical parameter in PRBs because it directly influences the hydraulic conductivity, contaminant transport, and reaction kinetics within the barrier. Proper voidage optimizes the distribution of contaminants across the reactive surface, enhancing treatment efficiency. Since GP is the structuring material of the barrier, the empty bed test was performed exclusively with it.

In Table 9, the volumes of distilled water before and after contact and saturation with GP are represented as V_0 and V_{final}, respectively. The difference between these values corresponds to the volume of adsorbed water. Additionally, the bed was the structured GP itself, which has a defined volume (V_{bed}). Using this information, Eq. 2 was applied to calculate the bed voidage percentage, reaching 43%.

Table 9: Bed voidage for structured GP

Parameter	**GP structured**
V_0 (mL)	150.0
V_{final} (mL)	128.0
V_0- V_{final} (mL)	22.0
V_{bed} (mL)	38.5
Bed voidage	43.0%

According to the Eurokin[130] report, the typical value of the bed porosity or bulk void fraction is 0.38 - 0.40. Higher porosities occur if the particle size is less than one order of magnitude smaller than the bed diameter.

5.2.2. PROXIMATE AND ULTIMATE ANALYSIS

This section delves into two prominent techniques used for quantitative and qualitative analysis: Elemental analysis, also known as CHNS (carbon, hydrogen, nitrogen, sulfur) analysis, and ICP-OES.

CHNS analysis was used to determine the organic materials' composition and ash content, including biomass, specifically EOP for AC production, AC, and CNT. The obtained values are presented in Table 10 .

Table 10: Proximate and ultimate (CHNS-elemental analysis) analysis for AC and CNT

Sample	Proximate analysis				Ultimate analysis				
	M	V.M	F.C	Ashes	C	N	H	S	Remaining*
EOP	3.7	78.9	13.2	4.2	47	2	8	<0.1	39
AC	8.9	16.2	58.5	16.4	63	1.7	0.8	<0.1	18
CNT	-	-	-	6	92.5	*	0.2	*	1.3

*N and S-contents are negligible; *The remaining was determined as the difference: O (wt.%) = 100 – N (wt.%) - C (wt.%) - H (wt.%) - S (wt.%) – Ashes (wt.%).

As expected, the carbon percentage is predominant in all materials. In the work of Elmaguana et al.[131], optimal conditions to produce AC were developed, resultidng in a carbon content of 67% and oxygen content of 17%. These values are like those obtained in Table 10, where the activated carbon shows 63% carbon and 18% oxygen.

Furthermore, Tuesta et al.[131] demonstrated that the carbon content increased when using washed CNTs due to the significant removal of metals because of treatment with sulfuric acid for purification. Consequently, the ash content in the washed CNTs is substantially lower than in the non-washed CNTs.

In Table 11, the ICP-OES analysis of the inorganic material FA, which serves as precursor for the GP, is presented. This analysis is crucial for assessing the reactivity of the components, such as the Si/Al ratio, which in this case is 1.27. Additionally, it is useful to identify the crystalline phases present.

Table 11: Chemical composition of FA (dried basis)

Sample (%)	Ca	Si	Al	K	Fe	Mg	Zn	Cu	Mn
FA	27.47	12.17	9.60	2.92	2.10	1.87	0.43	0.15	0.08

5.2.3. X-RAY DIFFRACTION

In the context of the present study, XRD analysis was conducted on the metallic catalyst used in the synthesis of CNT and on the GP, both of which are inorganic in nature, these materials usually possess well-defined crystalline structures, which allow for precise identification of phases and characterization of crystallographic properties. The XRD analysis of the metallic catalyst was essential to determine the phases present, ensuring the catalytic process's effectiveness in synthesizing CNT. Similarly, XRD was used for the GP to identify the crystalline phases present within the matrix, providing critical insights into its structural composition and potential performance characteristics.

Figure 14 presents the XRD pattern of the GP. Several crystalline phases are discernible using the software X′ Pert HighScore Plus in the diffractogram, including calcite, silicate, and aluminum-based phases, based on reference cards 96-901-6707, 96-710-3015, and 96-901-1603 respectively (data obtained from Crystallography Open Database). The identification of these phases aligns with the elemental composition results obtained from the ICP-EOS analysis, as discussed earlier. This correlation between the XRD and ICP-EOS data reinforces the reliability of the structural and compositional characterization of the GP.

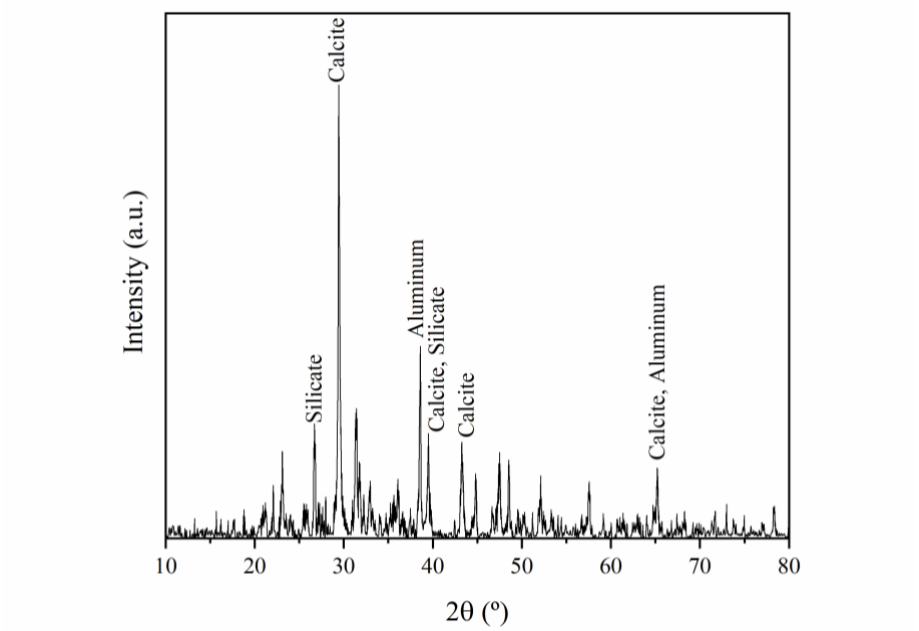

Figure 14: X-ray diffractogram of GP

Calcite, a key crystalline phase found in geopolymeric materials, comprises calcium carbonate. Known for its impressive adsorption properties, calcium carbonate has been the subject of extensive research, particularly for its effectiveness in the pharmaceutical[132] and heavy metals[133] removal process.

The presence of silicates is likely attributed to their precursor, sodium silicate, which may contain some unreacted molecules. In the work of Chao et al.[134], the results of the XRD analysis showed the presence of a quartz phase (crystalline mineral composed of silica) and mullite phase (an intermediate phase of the binary alumina-silica system) in the composite material, which has proven to be effective in the removal of lead from wastewater.

In the study conducted by Benavent et al.[135], it was observed that intentionally increasing the concentration of aluminum had notable effects on the geopolymeric system. Specifically, introducing $NaAlO_2$ as an additive reduced the average size of oligomers in solution, a shortened setting time for the geopolymer, and significant alterations in porosity. As

the concentration of sodium aluminate in the solution increased, there was a marked decrease in the porosity accessible to nitrogen, suggesting a transition towards either a more closed porous network or a more macroporous structure.

The analysis was also performed on the catalyst used for CNT synthesis to determine its crystalline composition, as shown in Figure 15. The analysis of IO/Al_2O_3 using the X'Pert HighScore Plus software enabled the identification of phases such as alumina, hematite, and magnetite, corresponding to reference cards 96-152-8248, 96-900-9783, and 96-900-6248, respectively (data sourced from the Crystallography Open Database).

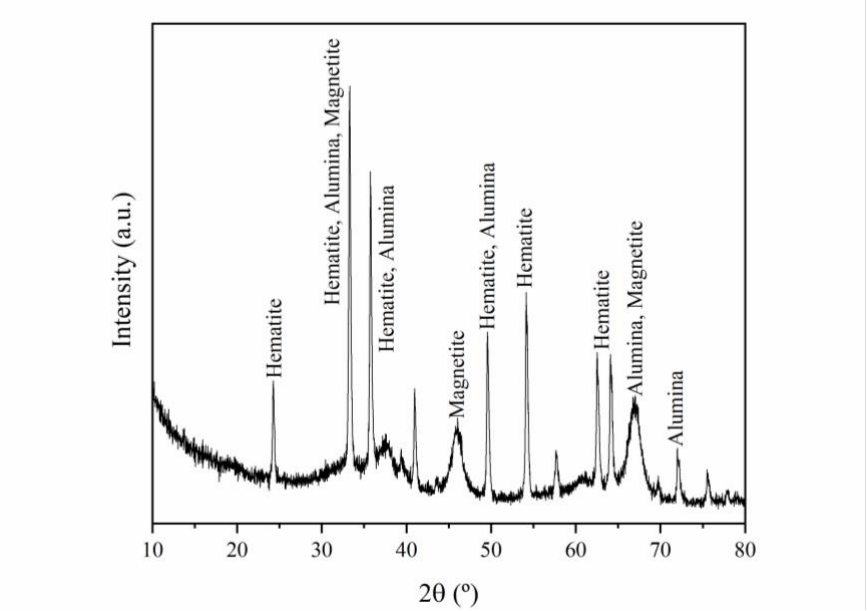

Figure 15: X-ray diffractogram of IO/Al_2O_3

The XRD peaks confirm that the material was synthesized correctly, with the presence of iron and alumina evident. The most prominent peak, occurring around 34°, likely represents the combination of these three phases. Confirming that the catalyst synthesis was performed efficiently.

On the other hand, XRD analysis was not performed on AC, due to the inherent challenges associated with their structural characterization using this technique. Carbon materials often exhibit a high degree of structural complexity and low crystallinity[136]. These characteristics result in diffuse and less well-defined diffraction patterns, making obtaining meaningful insights from XRD data difficult.

5.2.4. SURFACE CHEMISTRY

Functional groups in AC, CNT, and GP were analyzed using the FT-IR method. The spectra of AC in Figure 16 (a) shows the four main peaks. Bands at frequency values attributed to OH stretching in hydroxyl groups (in 3431 cm^{-1}), to the presence of carbonyl groups (C=O) at 1636 cm^{-1}, which indicates the presence of oxygen-containing functional groups on the surface of the materials, these groups acting as active sites for adsorption and reaction processes, participating in acid-base reactions and hydrogen bonding, as previously assigned in the work[127]. Hydroxyl groups can influence the adsorption behavior of AC by affecting its interaction with water and other molecules; they can increase the affinity of the adsorbent to water, which may impact the adsorption of target contaminants[137].

The C=O stretching vibration at 1636 cm^{-1} signifies chemical stability, bolsters the carbon material's overall robustness and longevity. The C-H deformation vibration at 1383 cm^{-1} reveals the presence of aliphatic hydrocarbons or other organic functional groups on the adsorbent surface. These functional groups may facilitate adsorption through interactions with adsorbates mediated by van der Waals or other intermolecular forces. Moreover, the C-O-C vibration at 1022 cm^{-1} attests to the incorporation of aromatic rings within the molecular framework.

In Figure 16 (b), the spectrum of the CNTs is depicted. This spectrum also displays a hydroxyl group band at 3433 cm^{-1}, as well as a C-O stretching vibration at 1636 cm^{-1} that typically signifies the presence of carbonyl groups and can also indicate the bending vibration of adsorbed water or arising from the absorption of atmospheric CO_2 on the surface of CNTs[138]. Like the AC spectrum, these results can be supported by the data obtained by elemental analysis.

In addition, the sharp band at 1380 cm^{-1} confirmed the existence of a C-O bond on raw CNTs, reinforcing the interaction with carboxylate groups[138]. Furthermore, a band at 780 cm^{-1} is attributed to graphitic sp^2 domains[139].

In Figure 16 (c), the FT-IR spectra for the GP are presented. The characteristic bands of GPs are commonly located at a wavelength range of 1300–900 cm^{-1}. The existing bands in this range are credited to asymmetric stretching vibrations of Al-O-T and Si-O-T, according to He et al.[140].

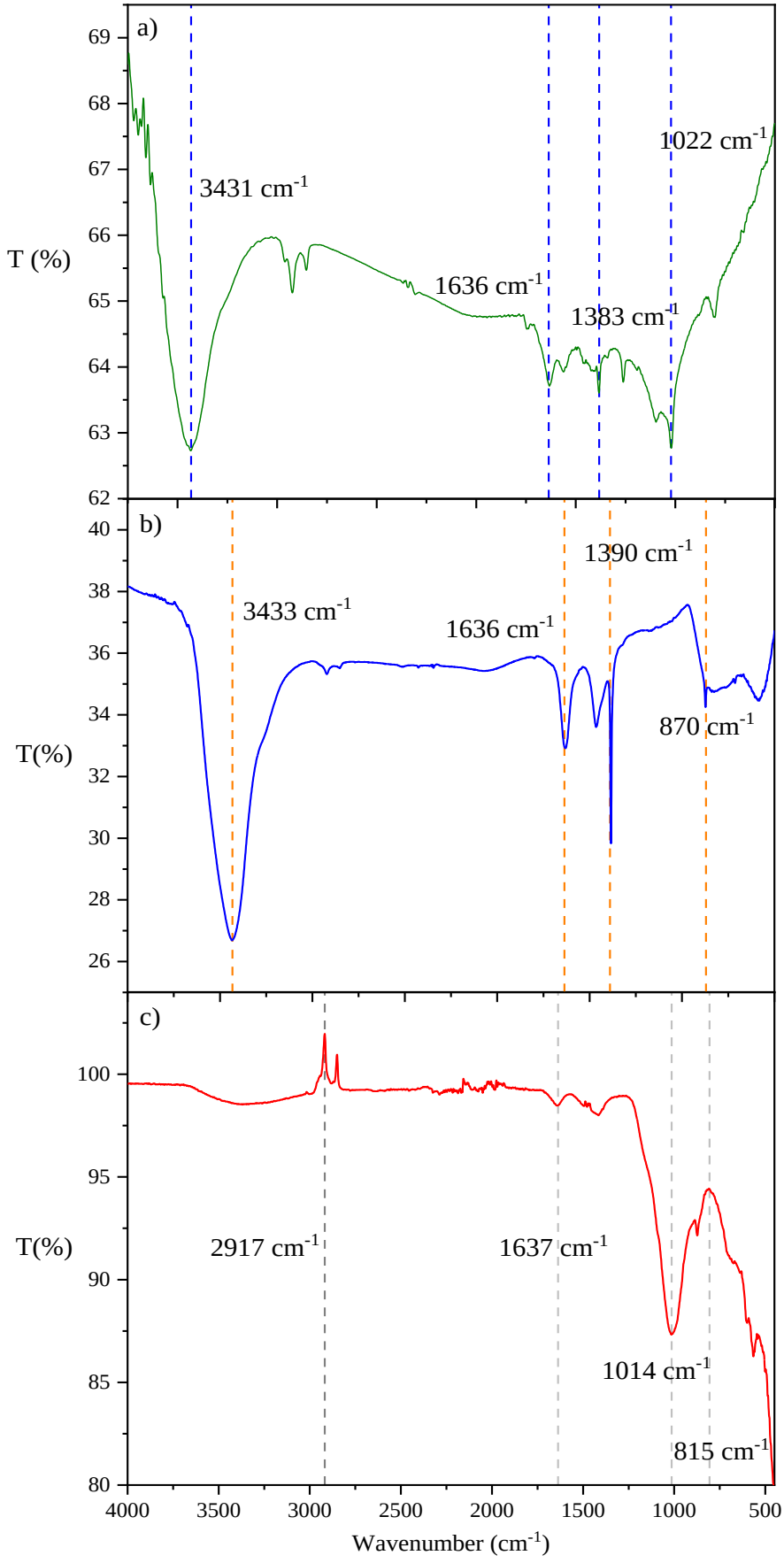

Figure 16: FT-IR spectra of a) AC; b) CNT, and c) GP.

The narrow band observed at 1637 cm^{-1} is attributed to the bending vibration of H-O-H, indicating the presence of hydroxyl groups from water molecules. A peak around 1600 cm^{-1} followed by a weaker band near 815 cm^{-1} suggests C-O bending vibrations, characteristic of the carbonate ion (CO_3^{2-}). These bands are likely the result of surface carbonation caused by atmospheric CO_2 interacting with the geopolymer.

The peak observed at 1014 cm^{-1} in the GP spectrum corresponds to the asymmetric stretching vibrations of Si-O-T (T-tetrahedral Al or Si); the reduction in the intensity of this band in the geopolymer spectrum suggests a characteristic change associated with geopolymerization. The other characteristic peaks for the calcite form of $CaCO_3$, which occurs with wave number 870 cm^{-1}, corresponding to the asymmetric CO_3 band (out-of-plane vibration), also found in the work of Zielinska et al.[132], confirming the XRD results.

Still, in surface chemistry, pH_{pzc}, acidity, and basicity are crucial parameters for understanding the surface properties of materials. These parameters dictate how a material interacts with its environment, particularly in adsorption and catalysis; the pH_{pzc} shows that the surface may be positively charged, negatively charged, or have no charge at specific pH values, the acidity and basicity of a material are quantified by the concentration of acidic and basic sites on its surface, usually expressed in micromoles per gram (µmol/g). These parameters are shown in Table 12 for each material studied, and they are crucial for understanding the material's ability to interact with acidic or basic species in its environment.

Table 12: Values of pHpzc, basicity, and acidity of the materials

GP	pH_{PZC}	Basicity (µmol/g)	Acidity (µmol/g)
AC	9.8	1250	0
CNT	6.9	820	1360
GP-6	7.6	1925	865

The AC exhibits a relatively high pH_{pzc} of 9.86, close to 9.0 found in Labied et. al[127] where the AC was obtained from lignocellulosic material, indicative of a predominantly basic surface character and AC has a basicity of 1250 µmol/g and an acidity of 0 µmol/g, indicating a surface that is entirely basic with no detectable acidic sites. This lack of acidic sites, combined with its high basicity, reinforces AC's strong preference for interacting with acidic substances[105].

At a pH below 9.86, the surface would attract anions, while above this pH, the surface would be negatively charged and more likely to interact with cations. The high basicity and the

pHpzc of 9.86 suggest that AC is particularly effective in adsorbing acidic pollutants and can be used in applications where strong basic interactions are required.

CNTs exhibit a pHpzc of 6.9, which is slightly acidic. In the study by Abdel-Ghani et al.[138], the pHpzc of MWCNTs was reported as 6.0, further supporting that the observed value is consistent with the literature. This value indicates a surface generally less basic than AC and GP, with a higher tendency to acquire a positive charge at neutral to mildly acidic pH levels. The acidity of CNTs is notably higher, at 1360 µmol/g, while the basicity is lower, at 820 µmol/g, reinforcing the characterization of a surface with a predominantly acidic nature. The slightly acidic and balanced nature of CNTs enhances their effectiveness in catalytic processes and environments where interaction with basic species is essential.

The pHpzc of 7.6 for GP indicates a surface near neutral to slightly basic. This value suggests that at pH above 7.6, the GP surface will predominantly carry a negative charge, enhancing its effectiveness in adsorbing cationic species. For instance, in the study by Chao et al.[134], an FA-based GP was used successfully as an adsorbent for Pb^{2+} ions, while Lee et al. [95] made adsorption of Cs^{+}. Conversely, at pH below 7.6, the surface becomes positively charged, favoring the adsorption of anionic species. Ali Siyal et al.[141] demonstrated this effect using an FA-based GP to adsorb anionic surfactants from aqueous solutions.

The intermediate pHpzc value of GP reflects its balanced surface chemistry, allowing interaction with a broad range of ionic species. The GP exhibits an acidity of 865 µmol/g and a basicity of 1925 µmol/g, with a predominance of basic sites. This balance between acidic and basic functionalities enables the GP surface to effectively interact with both acidic and basic species, making it versatile for various adsorption applications[129,142–144].

Consequently, based on previous characterizations, such as the presence of functional groups and the affinity for acidic molecules, along with the high surface area, the AC will serve as the primary adsorbent in the barrier.

5.2.5. SCANNING ELECTRON MICROSCOPY AND TRANSMISSION ELECTRON MICROSCOPY

A SEM analysis was conducted to visualize the morphology and surface structure of the GP. A TEM analysis was performed to examine the internal structure and distribution of the CNTs.

Figure 17 displays the SEM analysis of GP which has a Si/Al ratio of 2. The image reveals a heterogeneous appearance with unreacted FA particles and relatively larger formed structures. The geopolymerization process results in the transformation of the surface material,

rendering it more gel-like and porous. This change can be attributed to the alkaline activation process, which transforms the FA spherical particles into a geopolymer with an amorphous and porous structure[145].

The synthesized GPs exhibit an amorphous structure, meaning they have a random arrangement of molecules. These characteristic benefits adsorbent materials by providing large active sites, which can enhance adsorption. According to Zhu et al. [146] the amorphous structure of GPs allows for increased accessibility and availability of active sites, contributing to their effectiveness as adsorbents.

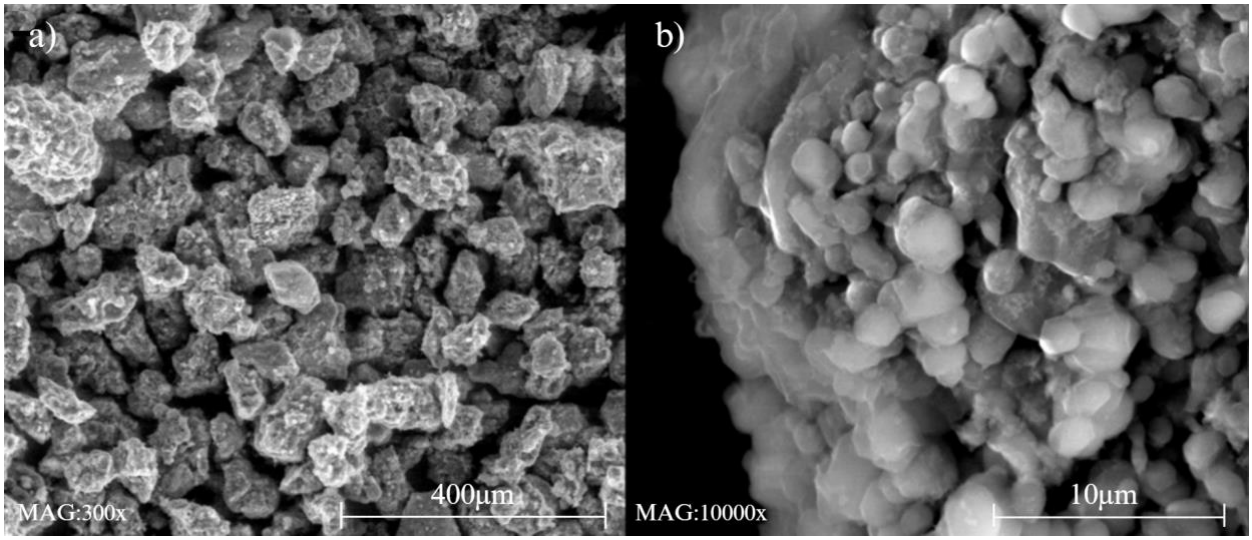

Figure 17: GP SEM images at a) 300x and b) 10000x

The morphology of the CNTs, which is presented in Figure 18 belong to a type of multi-walled fibrous structures with hollow cavities, allowing us to conclude the feasibility of employing the magnetic substrate as a catalyst for the growth of CNTs from LDPE[131]. The outer diameters observed among all the micrographs taken were determined as 37 ± 12 nm. In the same order, the thickness of the CNT was found to be 28 ± 3 nm.

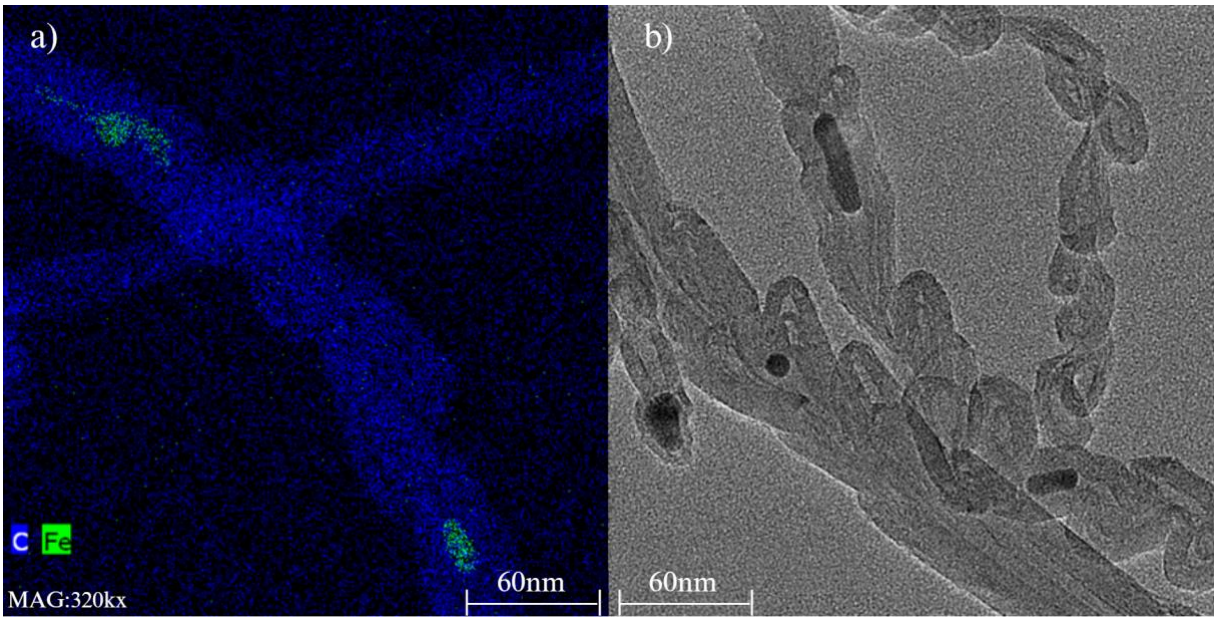

Figure 18: TEM micrographs of the CNTs at 320kx: a) elemental mapping and b) bright field

Elemental mapping shows that the CNTs are composed of carbon, while the dots in the image represent iron nanoparticles trapped within the nanotubes. This occurs because, in the CVD method, the tubes grow from the catalyst particles on the substrate. Notably, these iron nanoparticles remain even after the purification step with H_2SO_4, which was meant to remove metal residues from the CVD process. In the work of Wulan and Wijardono[147] it was also observed that the CNT possesses a buckling growth structure due to the interaction between CNT with CNT and CNT with catalyst during the agglomeration process.

5.2.6. THERMOGRAVIMETRIC ANALYSIS

TGA was conducted in air atmosphere for the three materials under investigation. All samples exhibited expected thermal behavior. AC demonstrated moderate thermal stability among the carbon-based materials, while CNT displayed high thermal stability. The GP, being inorganic, remained thermally stable even at elevated temperatures. Figure 19 (a) shows the TGA results and the first-order derivative thermogravimetric analysis (DTG) for AC.

The AC showed an initial mass reduction of 13% compared to its original state due to water evaporation. However, a more rapid mass loss occurs within the 300 to 450°C temperature range, where the highest DTG peaks are observed. In this range, the oxidation of

organic matter begins, but complete combustion only takes place after 500°C, resulting in a residual mass of 17% in the form of ash.

Similarly, Salgado et al.[148] found that activated carbons produced at 800°C experienced a mass reduction at approximately 100°C (due to water loss), with thermal decomposition starting around 340°C and stabilizing at 600°C. Therefore, it can be assumed that the activated carbon produced exhibits similar thermal stability. Figure 19 (b) displays the TGA and DTG curves of CNT, another carbon-based material; however, this one contains graphitic carbon.

DTG analysis shows that the primary mass loss occurs solely around 650°C, signifying a strong resistance to oxidation due to the material's robust architecture. This oxidation resistance aligns with the proposed structural models of these nanoscale materials characterized by dominant aromatic bonds and a minimal presence of dangling bonds. The CNTs experience oxidation at this point, leading to a substantial mass decrease.

Complete combustion is achieved only beyond 700°C, leaving behind 7.9% residual ash, which can be attributed to iron nanoparticles, as confirmed by the TEM images in Figure 18. The TGA and DTG for the GP, the only inorganic material, are present in Figure 19 (c).

The DTG analysis reveals a significant mass loss at around 100°C, attributed to water evaporation, which is expected and consistent with the findings in the literature[149,150]. The rapid decrease in mass before 150°C is indicative of the evaporation of both chemically bound water within the geopolymer structure and free water. Following this, there is a gradual but minor mass loss due to the elimination of hydroxyl groups (-OH) and chemically bonded water.

However, around 655°C, another peak in mass loss is observed. According to He et al.[149], this second weight loss, typically occurring between 300 and 650°C, is related to the dehydroxylation of Si-OH, Al-OH, and Ca-OH groups. The final stage of mass loss, often appearing above 750°C and associated with the decomposition of carbonate species, was not observed in this GP. Ultimately, the residual mass stands at 86.3%, which is close to the 79.8% found in fly ash-based geopolymers in the study by Abdulkareem et al.[150].

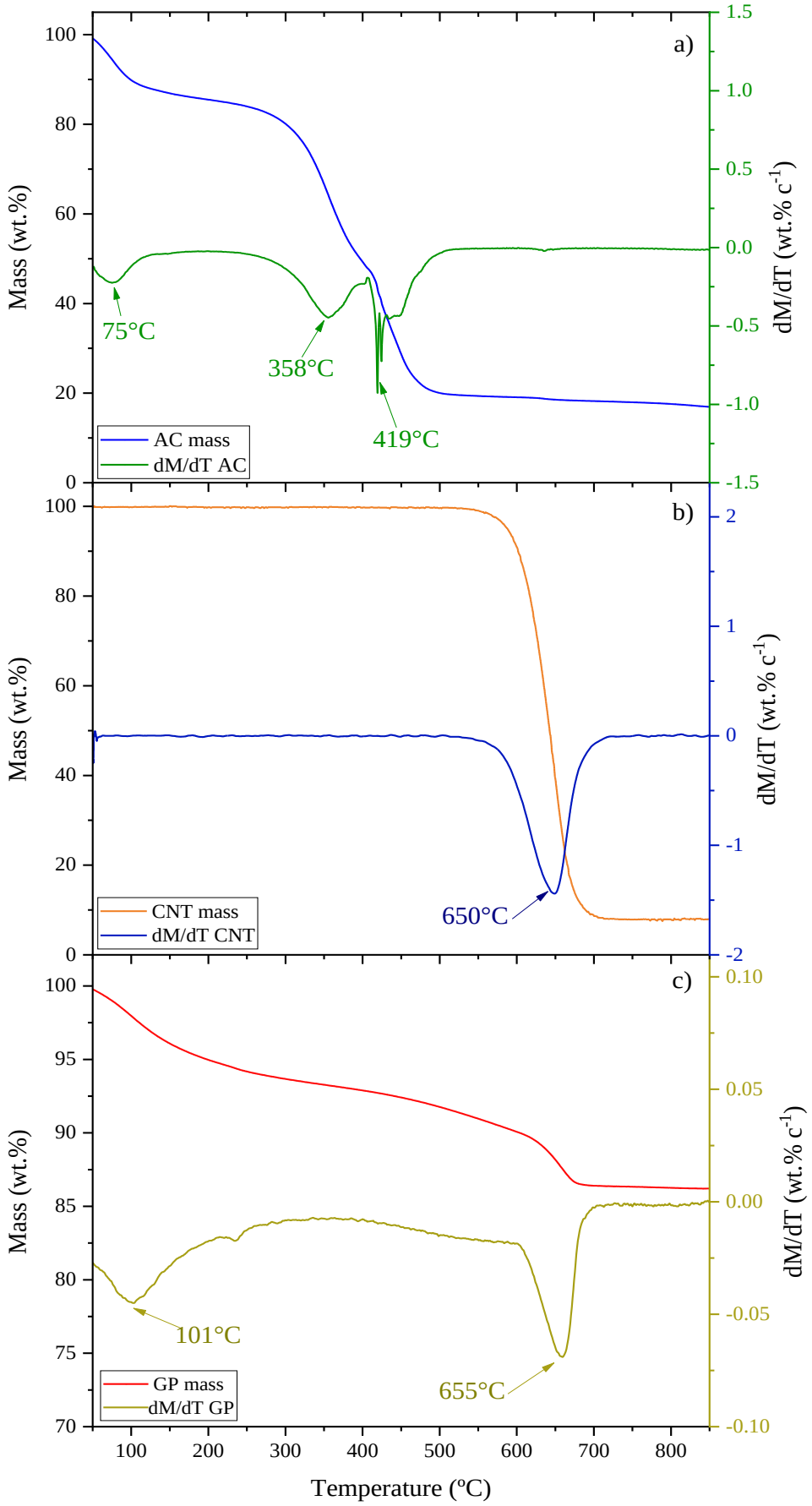

Figure 19: TGA/DTG of a) AC; b) CNT, and c) GP.

5.3 MASS TRANSFER

5.3.1 ADSORPTION KINETICS

This study conducted nine kinetic experiments, for each contaminant, the three different materials were tested to evaluate the rate and efficiency of the adsorption process.

The mathematical adjustments presented are important because they enable a deeper understanding of the adsorption process, optimization of processes, performance prediction, and comparison of different adsorbents, making the modeling more accurate and useful for practical applications. To achieve this, Eq. 4, 5, and 6, corresponding to the pseudo-first order, pseudo-second order, and intraparticle diffusion adjustments, respectively, were used, with the resulting kinetic fitting data presented in Table 13.

Table 13: Parameters of kinetic models.

			Pseudo-first order			**Pseudo-second order**			**Intraparticle diffusion**		
Compd.	Mater.	q_{exp} (mg/g)	q_e (mg/g)	K_1 (min^{-1})	R_1^2	q_e (mg/g)	K_2 (g/mg.min)	R_2^2	I (mg/g)	K_{id} ($mg/g.min^{1/2}$)	R_3^2
	AC	40.429	37.720	0.234	0.966	39.766	0.009	0.997	20.065	1.497	0.530
ACT	CNT	12.005	9.364	0.358	0.829	9.859	0.055	0.885	5.163	0.388	0.552
	GP	0.663	0.592	0.138	0.944	0.633	0.325	0.973	0.263	0.026	0.608
	AC	36.229	29.598	0.030	0.835	33.326	0.0012	0.912	6.251	1.659	0.829
SMX	CNT	25.514	24.547	0.375	0.945	25.497	0.025	0.923	16.650	0.662	0.285
	GP	4.078	4.912	1.382	0.489	4.886	0.005	0.487	3.373	0.155	0.239
	AC	35.895	34.847	0.558	0.977	36.013	0.029	0.997	24.467	0.964	0.296
GA	CNT	28.608	25.641	0.508	0.864	27.028	0.026	0.992	16.206	0.955	0.474
	GP	17.566	17.435	0.259	0.990	18.355	0.023	0.971	10.837	0.569	0.341

Upon analysis of Table 13, interesting observations can be made, including the absence of intraparticle diffusion and the predominance of the pseudo-second-order model. As described by Wang and Guo[151], internal diffusion models assume that the diffusion of the adsorbate within the adsorbent is the rate-limiting step. In this context, the diffusion of the adsorbate in the liquid film surrounding the adsorbent and the adsorption onto active sites are not instantaneous. Furthermore, while the pseudo-first order and pseudo-second order models yielded high R^2 values in the fitting process, the pseudo-second-order model provided the best fit, suggesting an abundance of active sites on the adsorbent.

Considering the parameter q_e, which represents the equilibrium adsorption amount, and comparing it with q_{exp}, the experimental adsorption capacity, it is evident that the values are closely aligned, thereby validating its applicability in describing the adsorption kinetics data. Furthermore, when assessing the adsorption capacity of the materials across the three different contaminants, AC performed the best in pseudo-second order and achieved values of 39.76 mg/g, 33.32 mg/g, and 36.01 mg/g for ACT, SMX, and GA, respectively.

Parameters K_1 and K_2 are frequently used to describe how fast the adsorption equilibrium is achieved, and higher values indicate a quicker attainment of equilibrium[151]. It is noteworthy that the highest value of K_1 was obtained for GP with SMX; however, the low R^2 value renders this result invalid.

Consequently, adsorption equilibrium is reached more quickly for AC and GA in the pseudo-first-order model, with a K_1 of 0.558, and for GP with ACT in the pseudo-second-order model, with a K_2 of 0.325. In the work of Pérez et al.[152], where the adsorption of GA onto AC was studied, the adsorption kinetics were also fitted to the pseudo-first-order equation, with a K_1 of 1.19.

Further on, Figure 20 presents the experimental points for each kinetic study across the different adsorbent/adsorbate groups and the previously mentioned fittings. As indicated by the R^2 values, the intraparticle diffusion fitting is unsuitable for this analysis and, therefore, will not be included in the graphs to avoid visual clutter.

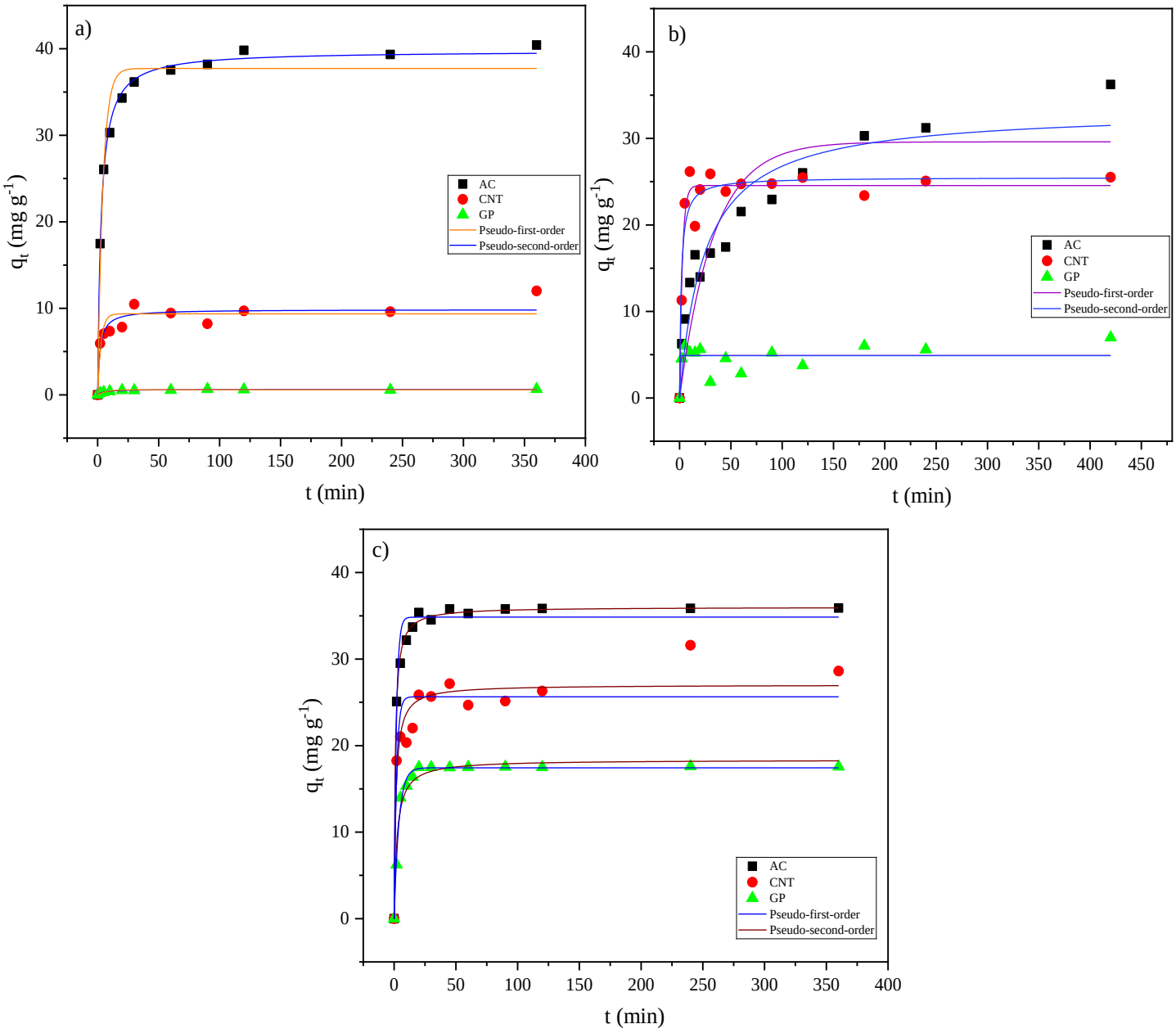

Figure 21: Fitting the kinetic models to the experimental data for a) ACT; b) SMX; c) GA.

In Figure 20 (a), AC demonstrated the best kinetics, reaching 64% of its adsorption capacity within 5 minutes, a value comparable to that found in the work of Nguyen et al.[153], where approximately 52% of ACT in solution was removed within the first 5 minutes of contact with their AC, and the Elovich model provided the best fit for their experimental data. The best fit for this study was achieved using the pseudo-second order model. Additionally, it is possible to notice that GP is not an effective material, whereas CNT exhibits some adsorption capacity.

In the work of Gómez-Avilés et al.[154], the best fit for the AC with ACT was also the pseudo-second-order model, with a K_2 value of 0.009. Additionally, the study observed that

changing the water matrix from distilled to tap water significantly reduced the amount adsorbed. This is likely due to the competitive adsorption of substances present in tap water with ACT molecules, leading to a slight decrease in the ACT adsorption capacity of the AC.

A similar behavior is observed for GA in Figure 20 (c); however, GP was more efficient in this case, fitting pseudo-first order better, possibly due to its reaction with basic sites and proven performance in Natal's et al.[11] work. CNT remains an intermediate material, while AC exhibits the highest capacity, with the pseudo-second order adjustment being the most suitable for this case. It is also noticeable that the rate at which all three materials reach equilibrium is quite similar; in the initial minutes, all materials can achieve maximum adsorption.

Regarding SMX, GP remains the least effective among the materials, while CNT is the quickest reaching equilibrium. However, once again, AC demonstrated the best results regarding adsorption capacity; once again, the pseudo-second-order model was the best fit.

Gutiérres et al.[155] investigated the adsorption of three pharmaceuticals, including SMX, onto powdered AC, in various water and wastewater matrices. The adsorption kinetics also followed a pseudo-second-order model, indicating that the number of available active sites primarily controls the sorption rate. Furthermore, the boundary layer effect appears to slow the adsorption rate as the compounds gradually reach the active sites at equilibrium.

5.3.2 EQUILIBRIUM ISOTHERMS

An equilibrium condition is attained when the solute concentration remains constant because of zero net transfer of solute adsorbed and desorbed from the adsorbent surface. The equilibrium adsorption isotherms describe these relationships between the equilibrium concentration of the adsorbate in the solid and liquid phases at constant temperature. Experimental data may provide different isotherm shapes, such as linear, favorable, strongly favorable, irreversible, and unfavorable[123], as shown in Figure 22.

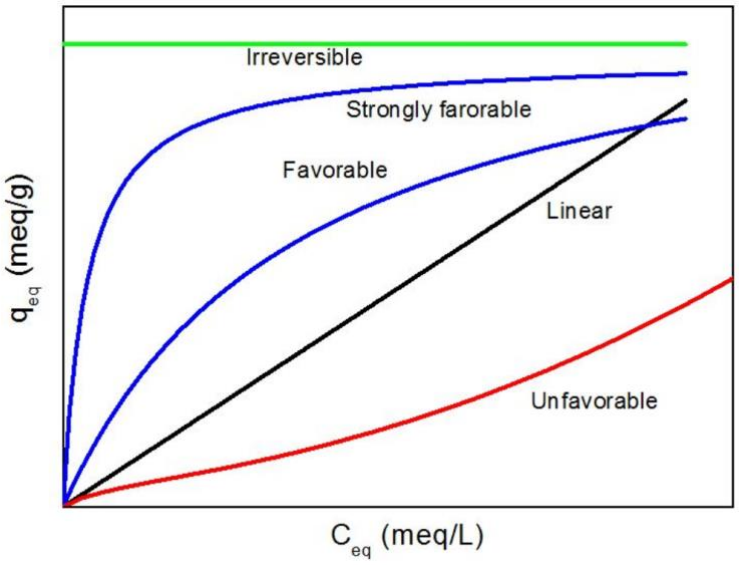

Figure 22: Adsorption Isotherms (adapted from[123])

The equilibrium isotherms were studied by fitting the Langmuir and Freundlich's models described by Eq. 7 and 9, respectively, to the experimental data. Table 14 presents the parameters obtained from the equilibrium fits for AC, which demonstrated the best performance among the other materials in the kinetic tests with three different compounds.

Table 14: Parameters of equilibrium models.

Material	**Compound**	**Langmuir**			**Freundlich**		
		q_{max} (mg/g)	**K_L (L/mg)**	**R^2**	**K_F (L/g)**	**n_F**	**R^2**
AC	ACT	112.198	5.141	0,903	62.965	4.654	0.967
	SMX	40.257	0.2450	0.924	14.823	4.322	0.989
	GA	314.277	0.0304	0.997	12.660	1.365	0.993

Analyzing the R^2 values for the systems, it is evident that the Freundlich model provides a better fit for the compounds ACT and SMX, while for GA, both models show nearly identical R^2 values. In the work of Nguyen et al.[153], the Freundlich model also provided a better fit than the Langmuir model for the adsorption of ACT onto AC.

The adsorbent/adsorbate interactions likely follow the description of Freundlich adsorption on a non-uniform (heterogeneous) surface, with interactions between adsorbed molecules in a reversible and non-ideal adsorption process rather than adsorption on a

monolayer surface. All the values of $1/n_f$ were less than 1, indicating that the adsorption is favorable and that the adsorbate is preferentially adsorbed at higher concentrations.

The Langmuir isotherm parameter (K_L) was used to calculate R_L, with Eq. 8, which indicates the affinity of the solute presented in Table 15. When $R_L = 0$, the adsorption process is considered irreversible. If $0 < R_L < 1$, the process is considered favorable to adsorption. The value of $R_L = 1$ signifies a linear process, while $R_L > 1$ indicates an unfavorable adsorption process.

Table 15: R_L calculated values.

C_0 (mg/L)	R_L		
	AC-ACT	**AC-SMX**	**AC-GA**
100	0.002	0.039	0.248
75	0.003	0.052	0.305
50	0.004	0.075	0.397
30	0.006	0.120	0.523
10	0.019	0.290	0.767

All calculated values fall between 0 and 1, indicating that the adsorption process is favorable. However, for the AC-ACT system, the values were notably low, which may suggest an irreversible process at higher concentrations.

Figure 23 displays the plots describing the fits of the two equilibrium models for the three tests. These graphs visually represent how the models fit with the experimental data.

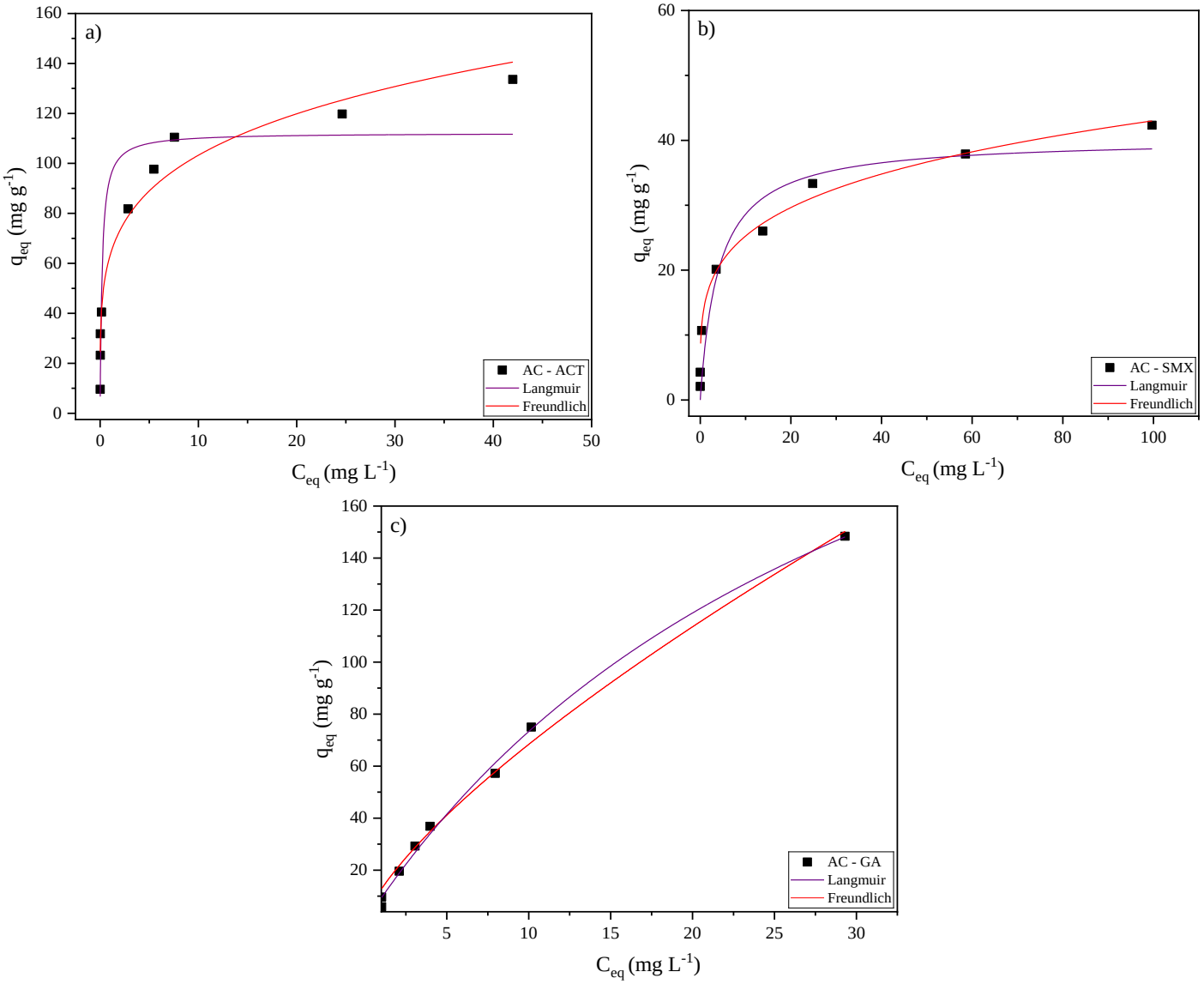

Figure 23: AC adsorption isotherms using Langmuir and Freundlich for a) ACT; b) SMX; c) GA.

It is interesting to relate the shape of the graphs to Figure 22, which shows that adsorption is strongly favorable for ACT and SMX, and favorable for GA. The results from the Langmuir model should not be disregarded but used with caution, as the R^2 values were greater than 0.90 for all three compounds, although the ideal value is above 0.95. This model's maximum adsorption capacities were 112.19 mg/g, 40.25 mg/g, and 314.27 mg/g for ACT, SMX, and GA, respectively.

In this sense, Kerkhoff et al.[156] reported a potential ACT removal capacity of 100 mg/g using zinc chloride AC derived from the endocarp of *Butia capitata*. In the work of Liu et al.[157], after applying the Langmuir model, the maximum adsorption capacity of SMX with AC was found to be 3.07 mg/g. However, after modification with $FeCl_3$, the maximum capacity

increased to 17.24 mg/g, which is still lower than the maximum adsorption value found for the activated carbon in this study.

These results may be linked to the basic characteristics of the AC, as observed in the acidity and basicity tests. The contaminants have a more acidic nature, with GA being the most acidic, which likely explains the higher adsorption capacity.

Another explanation for this behavior is found in the work of Chang et al.[158], who described that the difference in maximum adsorption capacity between ACT and SMX with AC decreases with the molecular weight of the adsorbate. Specifically, the smaller compound, ACT, demonstrated the highest adsorption density, while SMX exhibited the lowest.

5.3.3 BREAKTHROUGH CURVE

The breakthrough curve evaluates adsorption performance in continuous processes, representing the concentration profile of a solute as it exits over time. This analysis enables the determination of operational time, and the efficiency and adsorption capacity of the materials used in the present study. It is important to highlight that the time corresponding to C_{exit}/C_{in} = 5% is the breakthrough time, a percentage commonly used by several authors[159,160].

Table 16 presents the parameters obtained from the breakthrough curve analysis for each compound separately, where Eqs. 10 and 11 were used to determine the times for the usable capacity of the bed (t_u) and the time equivalent to the total stoichiometric capacity of the bed (t_t). Eqs. 13 and 14 were employed to calculate the total adsorption capacity, q_A (mg/g), and the useful adsorption capacity, q_b (mg/g). Additionally, Eq. 12 was used to demonstrate the length of the unused bed (H_{UNB}), where H_U represents the length of the bed used, and finally, Eq. 15 shows column efficiency.

Table 16: Breakthrough curve parameters for individual compounds.

Compound	t_u (min)	t_t (min)	q_A (mg/g)	q_b (mg/g)	H_U (cm)	H_{UNB} (cm)	n (%)
ACT	314.245	634.289	126.858	62.849	1.536	1.564	49.543
SMX	66.167	274.672	54.934	13.233	0.747	2.353	24.090
GA	68.250	758.171	151.634	13.650	0.279	2.821	9.002

For instance, the breakthrough curve demonstrates that the system, composed of only 0.5 g of AC and 1 g of GP — with no CNTs included, as batch tests revealed that CNTs would be more efficiently applied as catalysts — required 314 minutes to reach breakthrough for ACT, 66 minutes for SMX, and 68 minutes for GA, as shown in Figure 20. These results were

obtained using concentrations of 100 mg/L for each compound, a flow rate of 1 mL/min, and a room temperature of 20°C. The breakthrough time was determined when the effluent concentration reached 5% of the initial concentration, suggesting that the breakthrough time would be considerably longer for more diluted systems.

In the study carried out by Young et al.[161], the breakthrough times for the continuous adsorption system of sevoflurane using granular AC were varied depending on operational conditions, such as initial concentration and flow rate. The study observed that t_b was significantly influenced by changes in initial concentrations, with AC exhibiting a longer breakthrough time at lower sevoflurane concentrations. For instance, t_b occurred after approximately 55 minutes for one kind of AC and 45 minutes for another AC under specific conditions.

Moreover, the useful adsorption capacity of the compounds in continuous mode showed that ACT achieved a value of 62.85 mg/g, while the other two compounds reached values around 13 mg/g. These capacities were calculated based on the bed's usable capacity time, but if the bed is used until complete stoichiometric exhaustion, the values increase to 126.85 mg/g, 54.93 mg/g, and 151.63 mg/g for ACT, SMX, and GA, respectively.

According to Gómez-Avilés et al.[154], their breakthrough with AC derived from microwave-assisted $FeCl_3$ activation of lignin for PCM adsorption achieved a total bed adsorption capacity of 213 mg/g at a flow rate of 1 mL/min, like the conditions applied in this work. Additionally, the authors demonstrated that increasing the inlet concentration of acetaminophen decreases the breakthrough time and increases the total bed adsorption capacity, which agrees with the equilibrium uptakes observed at those concentrations.

The mass-transfer zone is represented by H_{UNB}. Small values of this parameter mean that the breakthrough curve is close to an ideal step with negligible mass-transfer resistance. Moreover, in the ideal condition, no axial dispersion would occur[126]. The total bed height is 3.1 cm, and based on the calculations, there was a significant portion of unused height. This is likely related to the GP height, where lower adsorption efficiency was expected, as indicated by the results of batch tests. Figure 24 shows the breakthrough curve for each contaminant in a separate system.

In the study by Samarghandi et al.[162], the results indicate that bed height and flow rate directly influence the breakthrough time and the amount of dye that can be removed before column saturation. For example, the column was tested with varying bed depths, and the breakthrough curves demonstrated that greater bed depth can increase adsorption capacity and extend the operational time before saturation.

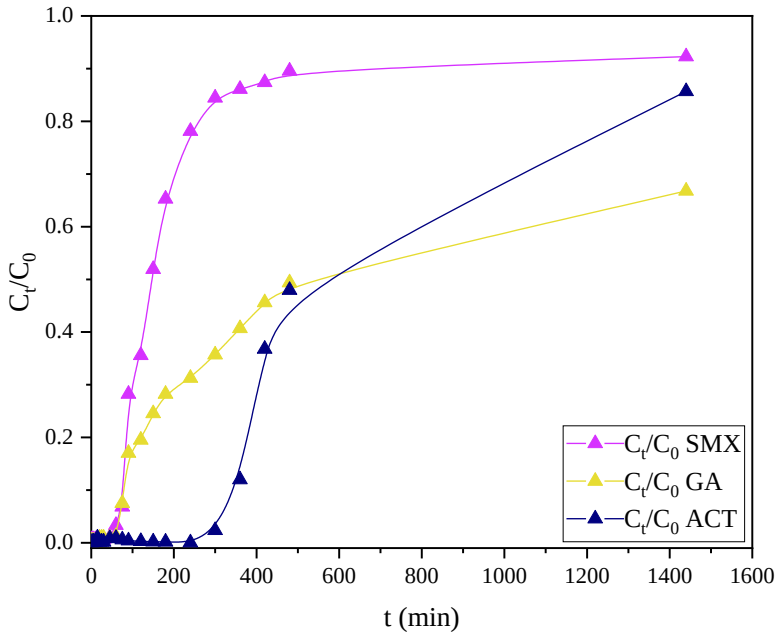

Figure 24: Breakthrough curve for single-component system

The lines connecting the experimental points serve only to guide the eye. In breakthrough curves, the areas above the curve correspond to the adsorption capacity, while the areas below the curve refer to the concentration in the effluent stream. It is important to note that these experiments lasted for 24 hours.

The column efficiency is also calculated based on the valuable adsorption capacity and total adsorption capacity. As a result, systems that reached 5% of the effluent concentration earlier exhibited lower efficiency, even though total breakthroughs did not occur as quickly as in the case of GA. On the other hand, the system for ACT and SMX removal showed an efficiency of 49.54% and 24.09%, respectively.

To assess the operational behavior and interactions between the contaminants and active sites in a multicomponent system, a breakthrough curve test was conducted with the three contaminants, as presented in Figure 25, each at a concentration of 100 mg/L. As a result, it was necessary to adjust parameters in the HPLC methodologies to prevent overlapping certain peaks and redo the calibration curves since the previous curves were generated using the pure spectra of the components.

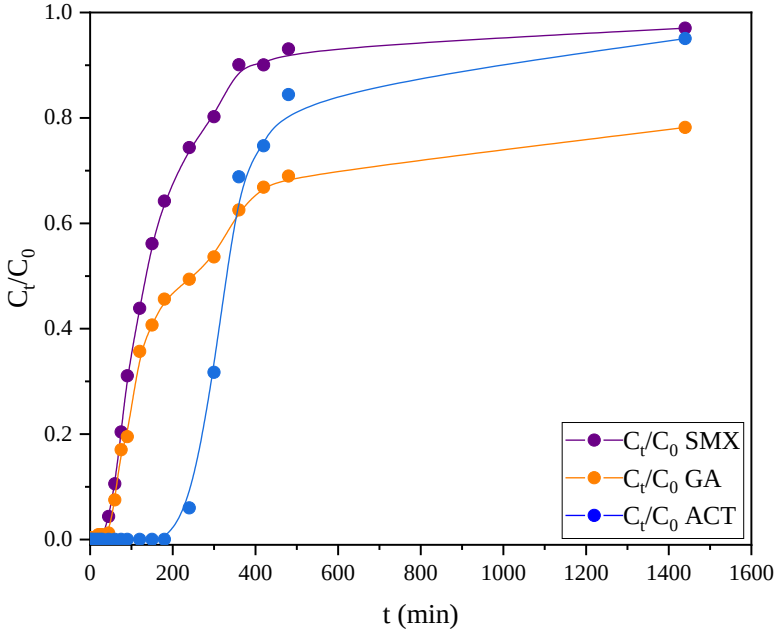

Figure 25: Breakthrough curve for multi-component system

The behavior of the three contaminants was similar to their performance in the individual system; however, it is evident that the barrier reached saturation much earlier, as the active sites of the adsorbent materials were consumed more rapidly. This can be observed in Table 17, which presents the parameters from the analysis of this breakthrough curve.

Table 17: Breakthrough curve parameters for a multicomponent system

Compound	**t_u (min)**	**t_t (min)**	**q_A (mg/g)**	**q_b (mg/g)**	**H_U (cm)**	**H_{UNB} (cm)**	**n (%)**
MIX-ACT	228.619	444.343	88.869	45.724	1.595	1.505	51.451
MIX-SMX	46.039	227.475	45.495	9.208	0.627	2.473	20.239
MIX-GA	53.580	521.610	104.332	10.716	0.317	2.783	10.224

The molar fractions of each compound are identical. Comparing the values of the usable capacity of the bed with the tests conducted for each compound individually, there is an average reduction of 26% in time for the multicomponent system. As expected, the adsorption capacity was also altered in the same proportion. However, the efficiency remained consistent with previous standards.

This aligns with the findings of Chang et al.[158], who observed that in multicomponent systems, with ACT and SMX, where adsorbates possess varying affinities and sizes, competitive adsorption can significantly influence adsorption in macropores. At the same time, its effect is less pronounced in mesopores and micropores. These results can be attributed to

either the limitations imposed by pore size or successive adsorption events that lead to the formation of multilayers by these pharmaceuticals.

The PRB design was also evaluated, with Figure 26 displaying the breakthrough curve for the multi-component system in the prototype. As it remains in the prototype stage, further improvements are needed. Consequently, the results from the column proved more favorable due to its uniform axial diffusion. In comparison, the prototype's low flow rate of 0.1 mL/min may lead droplets to follow preferential pathways.

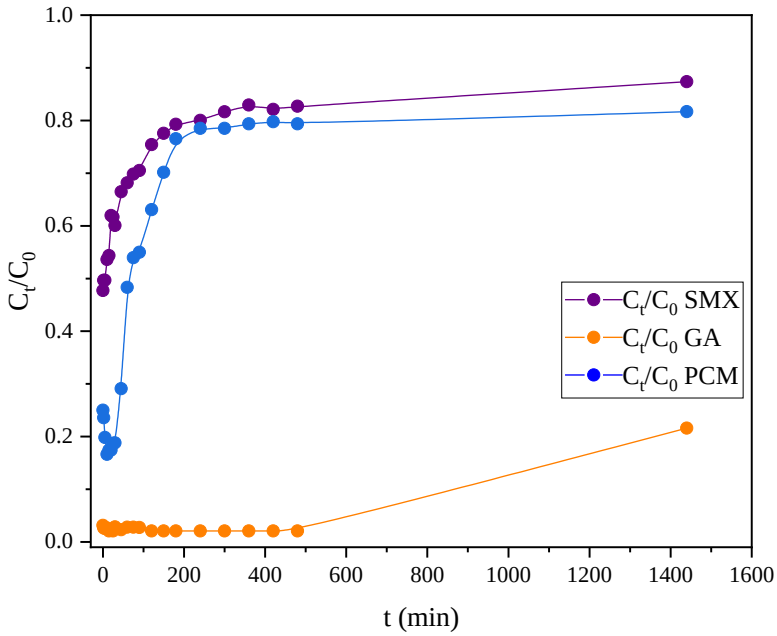

Figure 26: Breakthrough curve for the multi-component system in the prototype

The graph provides qualitative insights, such as the similar adsorption behavior of the column for SMX and PCM despite the system initially showing a higher outlet concentration. However, its concentration peaks were not observable for GA. The most likely hypothesis is that the large mass of structured GP in the prototype caused a nearly complete reaction of the GA.

6. CONCLUSIONS AND FUTURE RESEARCH

This research successfully explored the application of innovative PRBs for the elimination of CECs from wastewater. The integration of geopolymers, activated carbons, and carbon nanotubes as filler materials, all derived from waste, aligns with principles of sustainability and circular economy. Each material demonstrated unique characteristics that contributed to the overall efficiency of the PRB system in removing pollutants such as acetaminophen, sulfamethoxazole, and gallic acid.

The equilibrium study additionally revealed that the Freundlich model best described the adsorption behavior, indicating favorable conditions and strong affinity between adsorbate and adsorbent, but it is possible to use the maximum adsorption capacity of AC by Langmuir with values of 112.19 mg/g for ACT, 40.25 mg/g for SMX, and 314.27 mg/g for GA. Kinetic studies confirmed that all materials followed a pseudo-second-order model, with equilibrium achieved in approximately 50 minutes. The intraparticle diffusion model was disregarded as none of the materials fit this model. AC exhibited the highest adsorption rates, followed by CNT and GP, and all three contaminants.

Continuous flow experiments validated these batch results, with AC and GP performing well. Breakthrough capacities shown an adsorption capacity of 126.85 mg/g for ACT, 54.93 mg/g for SMX, and 151.53 mg/g for GA, with breakthrough times of 314 minutes for ACT, 66 minutes for SMX, and 68 minutes for GA. The system tested in multicomponent shows the same behavior but with earlier saturation of the barrier. The PRB prototype showed effectiveness, though further optimization is needed.

Overall, this study highlights the feasibility of using waste-derived materials in advanced water treatment systems, contributing not only to environmental protection but also to resource efficiency. Future work will focus on scaling up the process and exploring additional contaminants to further validate the versatility of this system in various wastewater treatment applications.

Future research should focus on:

- Pilot-Scale Implementation: Transitioning from laboratory-scale experiments to pilot-scale studies will provide valuable insights into the practical application of PRBs in real-world settings.
- Life Cycle Assessment (LCA): Conducting a comprehensive life cycle assessment of the PRB system will provide insights into its environmental impact and economic viability compared to conventional wastewater treatment methods.

- Integration with Other Technologies: Exploring the integration of PRBs with other treatment technologies, such as membrane filtration or advanced oxidation processes, aiming to enhance overall treatment efficacy.

7. REFERENCES

1. Karimi-Maleh H, Darabi R, Karimi F, Karaman C, Shahidi S, Zare N. State-of-art advances on removal, degradation and electrochemical monitoring of 4-aminophenol pollutants in real samples: A review. *Enviromental Research*. 2023;222:1-14. doi:10.1016/j.envres.2023.115338
2. Alves O, Garcia B, Rijo B, Lourinho G, Nobre C. Market Opportunities in Portugal for the Water-and-Waste Sector Using Sludge Gasification. *Energies 2022, Vol 15, 6600*. 2022;15(18):1-16. doi:10.3390/EN15186600
3. Blaise R, Lekene N, Matemb T, Strothman T. The efficient removal of ibuprofen, caffeine, and bisphenol A using engineered egusi seed shells biochar: adsorption kinetics, equilibrium, thermodynamics, and mechanism. *Environmental Science and Pollution Research*. 2023;30:100095-100113. doi:10.1007/s11356-023-29377-w
4. Ayaliew Werkneh A, Berhe Gebru S, Redae GH, Gashaw Tsige A. Removal of endocrine disrupters from the contaminated environment: public health concerns, treatment strategies and future perspectives-A review. *Heliyon*. 2022;8:1-12. doi:10.1016/j.heliyon.2022.e09206
5. Ferreira da Silva AP, Gomes H, Bineli A, Triviño J. *Production of Catalysts For The Valorization Of Plastic Waste, And For The Wet Peroxide Oxidation Of Paracetamol*. 2019. Master Dissertation.
6. Verlicchi P, Lacasa E, Grillini V. Quantitative and qualitative approaches for CEC prioritization when reusing reclaimed water for irrigation needs – A critical review. *Science of The Total Environment*. 2023;900:165735. doi:10.1016/J.SCITOTENV.2023.165735.
7. Panigrahy N, Priyadarshini A, Sahoo MM, Verma AK, Daverey A, Sahoo NK. A comprehensive review on eco-toxicity and biodegradation of phenolics: Recent progress and future outlook. *Environ Technol Innov*. 2022;27:1-16. doi:10.1016/J.ETI.2022.102423
8. Darbre PD. The history of endocrine-disrupting chemicals. *Curr Opin Endocr Metab Res*. 2019;7:26-33. doi:10.1016/J.COEMR.2019.06.007
9. Cao V, Yang H, Ndé-Tchoupé AI, Hu R, Gwenzi W, Noubactep C. Processes Tracing the Scientific History of Fe 0-Based Environmental Remediation Prior to the Advent of Permeable Reactive Barriers. *MDPI*. 2020;8:977. doi:10.3390/pr8080977

10. Alaa Abdulhusain N, Tark Abd Ali Z. Green approach for fabrication of sand-bimetallic (Fe/Pb) nanocomposite as reactive material for remediation of contaminated groundwater using permeable reactive barrier. *Alexandria Engineering Journal*. 2023;72:511-530. doi:10.1016/J.AEJ.2023.04.028
11. Silva Natal AP, Gomes H, Marin P. *Production of Geopolymers from Fly Ash for Wastewater Treatment*. 2023. Master Dissertation.
12. Martins Masso C, Gomes H, Pietrobelli J, Tuesta J. *Valorization of Compost in the Production of Carbon-Based Materials for the Treatment of Contaminated Wastewater*. 2018. Master Dissertation.
13. Piccinin de Grande L, Gomes H, Vieira A. *Catalytic Application of Carbon Nanotubes Obtained from Plastic Solid Waste in the Removal of Quinoline from Isooctane by Selective Oxidation with Hydrogen Peroxide*. 2022. Master Dissertation.
14. Naghikhani A, Karbassi A, Sarang A, Baghdadi M. Water Infrastructure. *Ecosystems and Society*. 2023;72:540. doi:10.2166/aqua.2023.006
15. Kong X, Huang G, Han Z, Xu Y, Zhu M, Zhang Z. Evaluation of zeolite-supported microscale zero-valent iron as a potential adsorbent for Cd2+ and Pb2+ removal in permeable reactive barriers. *Environmental Science and Pollution Research*. 2017;24(15):13837-13844. doi:10.1007/S11356-017-8974-9/TABLES/2.
16. Song J, Huang G, Han D, Hou Q, Gan L, Zhang M. A review of reactive media within permeable reactive barriers for the removal of heavy metal(loid)s in groundwater: Current status and future prospects. *J Clean Prod*. 2021;319:128644. doi:10.1016/j.jclepro.2021.128644.
17. European Enviroment Agency. Freshwater information system for europe. 2020. Accessed December 19, 2023. https://water.europa.eu/freshwater/countries/uwwt/portugal
18. Morin-Crini N, Crini G. Environmental applications of water-insoluble β-cyclodextrin–epichlorohydrin polymers. *Prog Polym Sci*. 2013;38(2):344-368. doi:10.1016/J.PROGPOLYMSCI.2012.06.005.
19. Montes R, Méndez S, Cobas J. Occurrence of persistent and mobile chemicals and other contaminants of emerging concern in Spanish and Portuguese wastewater treatment plants, transnational river basins and coastal water. *Science of The Total Environment*. 2023;8:1-16. doi:10.1016/J.SCITOTENV.2023.163737
20. Botero-Coy AM, Martínez-Pachón D, Boix C. "An investigation into the occurrence and removal of pharmaceuticals in Colombian wastewater." *Science of the Total Environment*. 2018;642:842-853. doi:10.1016/j.scitotenv.2018.06.088

21. World Health Organization. Share of domestic wastewater that is safely treated, 2022. 2022. Accessed December 6, 2023. https://ourworldindata.org/grapher/wastewater-safely-treated
22. Publications Office of the European Union. Country Report Portugal 2019 Including an In-Depth Review on the prevention and correction of macroeconomic imbalances Accompanying the document. Published online February 27, 2019. Accessed December 19, 2023. https://op.europa.eu/en/publication-detail/-/publication/e9fecc85-3b6b-11e9-8d04-01aa75ed71a1/language-en
23. Association of Portuguese companies in the environmental sector. Mandate of the Special Rapporteur on the human rights to safe drinking water and sanitation Report to the 75th session of the UN General Assembly in 2020 AEPSA Association of Portuguese companies in the environmental sector. 2020. Accessed December 19, 2023. www.aepsa.pt
24. Kahkeci J, Gamal El-Din M. Biochar-supported photocatalysts: Performance optimization and applications in emerging contaminant removal from wastewater. *Chemical Engineering Journal*. 2023;476:1-17. doi:10.1016/J.CEJ.2023.146530
25. Golovko O, Örn S, Sörengård M. Occurrence and removal of chemicals of emerging concern in wastewater treatment plants and their impact on receiving water systems. *Science of The Total Environment*. 2021;754:142122. doi:10.1016/J.SCITOTENV.2020.142122
26. Rivera-Utrilla J, Sánchez-Polo M, Ferro-García MÁ, Prados-Joya G, Ocampo-Pérez R. Pharmaceuticals as emerging contaminants and their removal from water. A review. *Chemosphere*. 2013;93(7):1268-1287. doi:10.1016/J.CHEMOSPHERE.2013.07.059
27. Pei M, Zhang B, He Y. State of the art of tertiary treatment technologies for controlling antibiotic resistance in wastewater treatment plants. *Environ Int*. 2019;131:1-20. doi:10.1016/J.ENVINT.2019.105026
28. Crini G, Lichtfouse E. Advantages and disadvantages of techniques used for wastewater treatment. *Environ Chem Lett*. 2019;17:145-155. doi:10.1007/s10311-018-0785-9
29. Zagklis DP, Bampos G. Tertiary Wastewater Treatment Technologies: A Review of Technical, Economic, and Life Cycle Aspects. *Processes*. 2022;10(11):2304. doi:10.3390/pr10112304
30. Mareddy AR. *Environmental Impact Assessment*. Butterworth-Heinemann; 2017. doi:10.1016/B978-0-12-811139-0.00012-8
31. Rizzo L, Agovino T, Nahim-Granados S, Castro-Alférez M, Fernández-Ibáñez P, Polo-López MI. Tertiary treatment of urban wastewater by solar and UV-C driven advanced

oxidation with peracetic acid: Effect on contaminants of emerging concern and antibiotic resistance. *Water Res*. 2019;149:272-281. doi:10.1016/J.WATRES.2018.11.031

32. Fu W, Li B, Yang J, Yi H, Chai L, Li X. New insights into the chlorination of sulfonamide: Smiles-type rearrangement, desulfation, and product toxicity. *Chemical Engineering Journal*. 2018;331:785-793. doi:10.1016/J.CEJ.2017.09.024
33. Lian J, Qiang Z, Li M, Bolton JR, Qu J. UV photolysis kinetics of sulfonamides in aqueous solution based on optimized fluence quantification. *Water Res*. 2015;75:43-50. doi:10.1016/J.WATRES.2015.02.026
34. Hollender J, Zimmermann SG, Koepke S. Elimination of organic micropollutants in a municipal wastewater treatment plant upgraded with a full-scale post-ozonation followed by sand filtration. *Environ Sci Technol*. 2009;43(20):7862-7869. doi:10.1021/ES9014629/SUPPL_FILE/ES9014629_SI_002
35. European Comission. *Report from the Commission to the European Parliament, the Council, the European Economic and Social Committee and the Committee of the Regions*.; 2023. Accessed November 24, 2023. https://ec.europa.eu/environment/water/waterframework/economics/OECD_study_en.
36. OSPAR Assessment Portal. Feeder Report - Waste water. 2021. Accessed November 24, 2023. https://oap.ospar.org/en/ospar-assessments/quality-status-reports/qsr-2023/other-assessments/waste-water/
37. Morin-Crini N, Lichtfouse E, Fourmentin M. Removal of emerging contaminants from wastewater using advanced treatments. A review. *Enviromental Chemestry Letters*. 2022;20:1333-1375. doi:10.1007/s10311-021-01379-5
38. Meijer J, Lamoree M, Hamers T. An annotation database for chemicals of emerging concern in exposome research. *Environ Int*. 2021;152:1-10. doi:10.1016/J.ENVINT.2021.106511
39. Samal K, Mahapatra S, Ali H. Pharmaceutical wastewater as Emerging Contaminants (EC): Treatment technologies, impact on environment and human health. *Energy Nexus*. 2022;6:100076. doi:10.1016/j.nexus.2022.100076
40. Sörengård M, Campos-Pereira H, Ullberg M, Lai FY, Golovko O, Ahrens L. Mass loads, source apportionment, and risk estimation of organic micropollutants from hospital and municipal wastewater in recipient catchments. *Chemosphere*. 2019;234:931-941. doi:10.1016/J.CHEMOSPHERE.2019.06.041
41. Pastorino P, Ginebreda A. Contaminants of Emerging Concern (CECs): Occurrence and Fate in Aquatic Ecosystems. *Int J Environ Res Public Health*. 2021;18(24):13401. doi:10.3390/IJERPH182413401

42. Yadav D, Rangabhashiyam S, Verma P, et al. Environmental and health impacts of contaminants of emerging concerns: Recent treatment challenges and approaches. *Chemosphere*. 2021;272:129492. doi:10.1016/J.CHEMOSPHERE.2020.129492
43. Long S, Yang Y, Pavlostathis SG, et al. Toxicity of tetracycline and its transformation products to a phosphorus removing Shewanella strain. *Chemosphere*. 2020;246:2-20. doi:10.1016/J.CHEMOSPHERE.2019.125681
44. Hajalifard Z, Mousazadeh M, Khademi S, Khademi N, Jamadi MH, Sillanpää M. The efficacious of AOP-based processes in concert with electrocoagulation in abatement of CECs from water/wastewater. *Clean Water*. 2023;6(1):30. doi:10.1038/s41545-023-00239-9
45. Miserli K, Athanasiou V, Boti V, Hela D, Konstantinou I. Determination of PFAS in wastewaters and natural waters by solid phase extraction and UHPLC LTQ/Orbitrap MS for assessing occurrence and removals. *Case Studies in Chemical and Enviromental Enginnering*. 2023;8:1-16. doi:10.1016/j.cscee.2023.100505
46. Qutob M, Hussein MA, Alamry KA, Rafatullah M. A review on the degradation of acetaminophen by advanced oxidation process: pathway, by-products, biotoxicity, and density functional theory calculation †. *RSC Adv*. 2022;12:18373-18396. doi:10.1039/d2ra02469a
47. Deng W, Li N, Zheng H, Lin H. Occurrence and risk assessment of antibiotics in river water in Hong Kong. *Ecotoxicol Environ Saf*. 2016;125:121-127. doi:10.1016/J.ECOENV.2015.12.002
48. Moussavi G, Momeninejad H, Shekoohiyan S, Baratpour P. Oxidation of acetaminophen in the contaminated water using UVC/S2O82− process in a cylindrical photoreactor: Efficiency and kinetics of degradation and mineralization. *Sep Purif Technol*. 2017;181:132-138. doi:10.1016/J.SEPPUR.2017.03.022
49. Fortunato A, Pena A, Lino C. *Ocorrência de Diclofenac, Ibuprofeno e Paracetamol Em Águas Residuais Em Portugal*. 2014.
50. Santos Silva A, Gomes H, Sgorlon J, Triviño JL. *Treatment of Wastewater Containing Pharmaceutical Compounds by Catalytic Wet Peroxide Oxidation Using Clay-Based Materials as Catalysts*. 2019. Master Dissertation.
51. Pinkston KE, Sedlak DL. Transformation of Aromatic Ether- and Amine-Containing Pharmaceuticals during Chlorine Disinfection. *Environ Sci Technol*. 2004;38(14):4019-4025. doi:10.1021/ES035368L

52. Gulamhussein MA, Saini B, Dey A. Removal of pharmaceutical contaminants through membrane bioreactor. *Mater Today Proc*. 2023;77:260-268. doi:10.1016/J.MATPR.2022.11.299
53. Patyk-Kaźmierczak E, Kaźmierczak M. Hydrate vs Anhydrate under a Pressure-(De)stabilizing Effect of the Presence of Water in Solid Forms of Sulfamethoxazole. *Cite This: Cryst Growth Des*. 2021;21:6879-6888. doi:10.1021/acs.cgd.1c00784
54. Zhang H, Gong W, Xue Y. Municipal wastewater contains antibiotic treatment using O 2 transfer membrane based biofilm reactor: Interaction between regular pollutants metabolism and sulfamethoxazole degradation. *Science of the Total Environment*. 2023;879:163060. doi:10.1016/j.scitotenv.2023.163060
55. Jiang B, Li A, Cui D, Cai R, Ma F, Wang Y. ENVIRONMENTAL BIOTECHNOLOGY Biodegradation and metabolic pathway of sulfamethoxazole by Pseudomonas psychrophila HA-4, a newly isolated cold-adapted sulfamethoxazole-degrading bacterium. doi:10.1007/s00253-013-5488-3
56. Hassan M, Zhu G, Yang Z, Lu Y. Simultaneous removal of sulfamethoxazole and enhanced denitrification process from simulated municipal wastewater by a novel 3D-BER system. Published online 2021. doi:10.1007/s40201-020-00562-0/Published
57. Patrolecco L, Rauseo J, Ademollo N. Persistence of the antibiotic sulfamethoxazole in river water alone or in the co-presence of ciprofloxacin. *Sci Total Environ*. 2018;640-641:1438-1446. doi:10.1016/J.SCITOTENV.2018.06.025
58. Kadia A, Urvish Chhaya ·, Kadia A, Chhaya U. Aerobic Granulation Technology as an Emerging Strategy to Mitigate Cresol Pollution in Wastewater: A Review. *Springer Nature Switzerland*. 2023;10:58. doi:10.1007/s40710-023-00670-7
59. Pan Y, Zhang Y, Hou M. Properties of polyphenols and polyphenol-containing wastewaters and their treatment by Fenton/Fenton-like reactions. *Sep Purif Technol*. 2023;317:1383-1390. doi:10.1016/j.seppur.2023.123905
60. Mainali K. Phenolic Compounds Contaminants in Water: A Glance. *Current Trends in Civil & Structural Engineering*. 2020;4(4):1-20. doi:10.33552/CTCSE.2020.04.000593
61. Kazemi P, Peydayesh M, Bandegi A, Mohammadi T, Bakhtiari O. Stability and extraction study of phenolic wastewater treatment by supported liquid membrane using tributyl phosphate and sesame oil as liquid membrane. *Chemical Engineering Research and Design*. 2014;92(2):375-383. doi:10.1016/J.CHERD.2013.07.023
62. Sharma S, Bhattacharya A. Drinking water contamination and treatment techniques. *Applied Water Science 2016 7:3*. 2016;7(3):1043-1067. doi:10.1007/S13201-016-0455-7

63. Arsuaga JM, López-Muñoz MJ, Aguado J, Sotto A. Temperature, pH and concentration effects on retention and transport of organic pollutants across thin-film composite nanofiltration membranes. *Desalination*. 2008;221(1-3):253-258. doi:10.1016/J.DESAL.2007.01.081
64. Badhani B, Sharma N, Kakkar R. Gallic acid: a versatile antioxidant with promising therapeutic and industrial applications. *RSC Adv*. 2015;5(35):27540-27557. doi:10.1039/C5RA01911G
65. Abdel Rahman RO, El-Kamash AM, Hung YT. Permeable Concrete Barriers to Control Water Pollution: A Review. *Water (Switzerland)*. 2023;15(21):3867. doi:10.3390/w15213867
66. Jirásko D., Vanícek I. *Permeable Reactive Barrier (PRB) and Its Influence on groundwater Regime*.; 2015.
67. Zheng K, Luo X, Tan Y. Passive convergence-permeable reactive barrier (PC-PRB): An effective configuration to enhance hydraulic performance. *Front Environ Sci Eng*. 2022;16(12):156. doi:10.1007/s11783-022-1591-y
68. Bortone I, Di Nardo A, Di Natale M, Erto A, Musmarra D, Santonastaso GF. Remediation of an aquifer polluted with dissolved tetrachloroethylene by an array of wells filled with activated carbon. *J Hazard Mater*. 2013;260:914-920. doi:10.1016/J.JHAZMAT.2013.06.050
69. Mokif LA, Faisal AAH. Funnel and Gate Permeable Reactive Barrier Permeable Reactive Barrier Configuration for Contaminated Groundwater Remediation – Designing, Installation, and Modeling: A Review. *Ecological Engineering and Environmental Technology*. 2023;24(9):15-33. doi:10.12912/27197050/173047
70. Carey MA, Fretwell BA, Mosley NG, Smith JWN. Guidance on the use of permeable reactive barriers for remediating contaminated groundwater. *Enviromental* . Published online 2002:10.
71. Rad PR, Fazlali A. Optimization of permeable reactive barrier dimensions and location in groundwater remediation contaminated by landfill pollution. *Journal of Water Process Engineering*. 2020;35:101196. doi:10.1016/J.JWPE.2020.101196
72. Cooney DO. *Adsorption Design for Wastewater Treatment*. Vol 1. Lewis Publishers, Boca Raton, FL (United States); 1998.
73. Xu J, Li M, Zhao D. Research and Application Progress of Geopolymers in Adsorption: A Review. *Nanomaterials*. 2022;12(17):3002. doi:10.3390/nano12173002

74. Saleh TA. Protocols for synthesis of nanomaterials, polymers, and green materials as adsorbents for water treatment technologies. *Environ Technol Innov*. 2021;24:101821. doi:10.1016/J.ETI.2021.101821
75. Saini S, Halldin Stenlid J, Abild-Pedersen F. Electronic structure factors and the importance of adsorbate effects in chemisorption on surface alloys. *Computational Materials*. 2022;8(1):163. doi:10.1038/s41524-022-00846-z
76. Micheletti DH, da Silva Andrade JG, Porto CE, et al. A review of adsorbents for removal of yellow tartrazine dye from water and wastewater. *Bioresour Technol Rep*. 2023;24:1-16. doi:10.1016/j.biteb.2023.101598
77. Rocha L, Van T, Manager S, Macmillan G. Erosion and Sediment Control Guide for Urban Construction Toronto and Region Conservation Authority - THE SUSTAINABLE TECHNOLOGIES EVALUATION PROGRAM. 2019. Accessed December 11, 2023. www.sustainabletechnologies.ca.
78. Wu Y, Chai K, Li X. Preparation and properties of metakaolin based porous geopolymer modified by potassium titanate whisker. *Constr Build Mater*. 2022;314:125580. doi:10.1016/J.CONBUILDMAT.2021.125580
79. Xie J, Kayali O. *Effect of Water Content on the Development of Fly Ash-Based Geopolymers in Heat and Ambient Curing Conditions*.; 2015. Accessed December 11, 2023. http://www.claisse.info/Proceedings.htm
80. Tigue AAS, Roy &, Malenab AJ, Angelo M, Promentilla B. A Systematic Mapping and Scoping Review on Geopolymer and Permeable Reactive Barrier for Acid Mine Drainage Treatment Research. doi:10.1007/s41660-020-00105-y
81. Barbosa VFF, MacKenzie KJD, Thaumaturgo C. Synthesis and characterisation of materials based on inorganic polymers of alumina and silica: sodium polysialate polymers. *International Journal of Inorganic Materials*. 2000;2(4):309-317. doi:10.1016/S1466-6049(00)00041-6
82. Mas Nmr N, Rowles MR, Hanna J V, Pike KJ, Smith ME. Applied Magnetic Resonance Study of the Bonding Character in Aluminosilicate Inorganic Polymers. *Appl Magn Reson*. 2007;32:663-689. doi:10.1007/s00723-007-0043-y
83. Geopolymer Institute. Examples of geopolymer frameworks. 2022. Accessed December 11, 2023. https://www.geopolymer.org/science/examples-geopolymer-frameworks/
84. Singh NB, Middendorf B. Geopolymers as an alternative to Portland cement: An overview. *Constr Build Mater*. 2020;237:117455. doi:10.1016/J.CONBUILDMAT.2019.117455

85. Toniolo N, Boccaccini AR. Fly ash-based geopolymers containing added silicate waste. A review. *Ceram Int*. 2017;43(17):14545-14551. doi:10.1016/j.ceramint.2017.07.221
86. Duan P, Yan C, Zhou W. Influence of partial replacement of fly ash by metakaolin on mechanical properties and microstructure of fly ash geopolymer paste exposed to sulfate attack. *Ceram Int*. 2016;42(2):3504-3517. doi:10.1016/J.CERAMINT.2015.10.154
87. Kupaei RH, Alengaram UJ, Jumaat MZ. The effect of different parameters on the development of compressive strength of oil palm shell geopolymer concrete. *Scientific World Journal*. 2014;2014. doi:10.1155/2014/898536
88. Soni R, Bhardwaj S, Shukla DP. Various water-treatment technologies for inorganic contaminants: current status and future aspects. *Inorganic Pollutants in Water*. Published online January 1, 2020:273-295. doi:10.1016/B978-0-12-818965-8.00014-7
89. Nasiri Azad F, Ghaedi M, Dashtian K, Montazerozohori M, Hajati S, Alipanahpour E. Preparation and characterization of MWCNTs functionalized by N-(3-nitrobenzylidene)-N′-trimethoxysilylpropyl-ethane-1,2-diamine for the removal of aluminum(III) ions via complexation with eriochrome cyanine R: spectrophotometric detection and optimization. *RSC Adv*. 2015;5(75):61060-61069. doi:10.1039/C5RA08746E
90. Glad BE, Kriven WM. Highly Porous Geopolymers Through Templating and Surface Interactions. *American Ceramic Society*. 2015;37. doi:10.1111/jace.13584
91. Onutai S, Kobayashi T, Thavorniti P, Jiemsirilers S. Porous fly ash-based geopolymer composite fiber as an adsorbent for removal of heavy metal ions from wastewater. *Mater Lett*. 2019;236:30-33. doi:10.1016/J.MATLET.2018.10.035
92. Novais RM, Buruberri LH, Seabra MP, Bajare D, Labrincha JA. Novel porous fly ash-containing geopolymers for pH buffering applications. *J Clean Prod*. 2016;124:395-404. doi:10.1016/J.JCLEPRO.2016.02.114
93. Wang X, Zhang Z, Ge Y. Oleic Acid-Tailored Geopolymer Microspheres with Tunable Porous Structure for Enhanced Removal from Tetracycline in Saline Water. *Sustainability (Switzerland)*. 2022;14(11):6705. doi:10.3390/SU14116705/S1
94. Barbosa TR, Foletto EL, Dotto GL, Jahn SL. Preparation of mesoporous geopolymer using metakaolin and rice husk ash as synthesis precursors and its use as potential adsorbent to remove organic dye from aqueous solutions. *Ceram Int*. 2018;44(1):416-423. doi:10.1016/J.CERAMINT.2017.09.193
95. Lee NK, Khalid HR, Lee HK. Adsorption characteristics of cesium onto mesoporous geopolymers containing nano-crystalline zeolites. *Microporous and Mesoporous Materials*. 2017;24:238-244. doi:10.1016/J.MICROMESO.2017.01.030

96. Purbasari A, Istadi I, Kumoro AC, Sumantri I, Silviana S. GEOPOLYMER FROM METAKAOLIN AND BIOMASS ASH FOR Cu(II) IONS ADSORPTION FROM AQUEOUS SOLUTIONS: KINETICS AND ISOTHERM STUDIES. *Journal of Chemical Technology and Metallurgy*. 2021;56(6):1225-1233.
97. Muttil N, Jagadeesan S, Chanda A, Duke M, Singh SK. Production, Types, and Applications of Activated Carbon Derived from Waste Tyres: An Overview. *Applied Sciences (Switzerland)*. 2023;13(1):257. doi:10.3390/app13010257
98. Bhatt AS, Sakaria PL, Vasudevan M, et al. Adsorption of an anionic dye from aqueous medium by organoclays: equilibrium modeling, kinetic and thermodynamic exploration. *RSC Adv*. 2012;2:8663-8671. doi:10.1039/c2ra20347b
99. Ferreira LM, de Melo RR. USE OF ACTIVATED CHARCOAL AS BIO-ADSORBENT FOR TREAMENT OF RESIDUAL WATERS: A REVIEW. *Nativa*. 2021;9(2):215-221. doi:10.31413/NATIVA.V9I2.11387
100. Bushra R, Mohamad S, Alias Y, Jin Y, Ahmad M. Current approaches and methodologies to explore the perceptive adsorption mechanism of dyes on low-cost agricultural waste: A review. *Microporous and Mesoporous Materials*. 2021;319:111040. doi:10.1016/J.MICROMESO.2021.111040
101. Pena J, Villot A, Gerente C. Pyrolysis chars and physically activated carbons prepared from buckwheat husks for catalytic purification of syngas. *Biomass Bioenergy*. 2020;132:26. doi:10.1016/J.BIOMBIOE.2019.105435
102. Eng Liliya Manoilova A, Eng Kamelia Ruskova A. ACTIVATED CARBON OBTAINING FROM VARIOUS RAW MATERIAL / VIA CHEMICAL ACTIVATION FOR THE PURPOSE OF ENVIRONMENTAL PURIFICATION-OVERVEW. *MECHANIZATION IN AGRICULTURE & CONSERVING OF THE RESOURCES*. 2019;LXV(6):204-206. Accessed December 20, 2023. www.chemicalsafetyconsulting.com,
103. Johnson P, Setsuda D, Williams R. Activated Carbon for Automotive Applications. *Carbon Materials for Advanced Technologies*. Published online January 1, 1999:235-268. doi:10.1016/B978-008042683-9/50010-8
104. Belaid KD, Kacha S, Kameche M, Derriche Z. Adsorption kinetics of some textile dyes onto granular activated carbon. *J Environ Chem Eng*. 2013;1(3):496-503. doi:10.1016/J.JECE.2013.05.003
105. Saleem J, Bin Shahid U, Hijab M, Mackey H, McKay G. Production and applications of activated carbons as adsorbents from olive stones. *Biomass Convers Biorefin*. 2019;9:775-802. doi:10.1007/s13399-019-00473-7/Published

106. Alslaibi TM, Abustan I, Ahmad MA, Foul AA. Application of response surface methodology (RSM) for optimization of Cu2+, Cd2+, Ni2+, Pb2+, Fe2+, and Zn2+ removal from aqueous solution using microwaved olive stone activated carbon. *Journal of Chemical Technology & Biotechnology*. 2013;88(12):2141-2151. doi:10.1002/JCTB.4073
107. Galiatsatou P, Metaxas M, Kasselouri-Rigopoulou V. Adsorption of zinc by activated carbons prepared from solvent extracted olive pulp. *J Hazard Mater*. 2002;91(1-3):187-203. doi:10.1016/S0304-3894(02)00008-0
108. Dubinin MM. Fundamentals of the theory of adsorption in micropores of carbon adsorbents: Characteristics of their adsorption properties and microporous structures. *Carbon N Y*. 1989;27(3):457-467. doi:10.1016/0008-6223(89)90078-X
109. Strangfeld C, Wiehle P, Munsch SM. About the Dominance of Mesopores in Physisorption in Amorphous Materials. *Molecules*. 2021;26(23):7190. doi:10.3390/MOLECULES26237190
110. Jagadeesan AK, Thangavelu K, Dhananjeyan V, Jagadeesan AK, Thangavelu K, Dhananjeyan V. Carbon Nanotubes: Synthesis, Properties and Applications. *21st Century Surface Science - a Handbook*. Published online July 31, 2020:1-22. doi:10.5772/INTECHOPEN.92995
111. Iijima S, Ichihashi T. Single-shell carbon nanotubes of 1-nm diameter. *Nature 1993 363:6430*. 1993;363:603-605. doi:10.1038/363603a0
112. Saifuddin N, Raziah AZ, Junizah AR. Carbon nanotubes: A review on structure and their interaction with proteins. *J Chem*. 2012;2013:1-18. doi:10.1155/2013/676815
113. Cassell AM, Raymakers JA, Kong J, Dai H. Large Scale CVD Synthesis of Single-Walled Carbon Nanotubes. *Journal of Physical Chemistry B*. 1999;103(31):6484-6492. doi:10.1021/JP990957S/ASSET/IMAGES/LARGE/JP990957SF00011.JPEG
114. Freitas I, Gomes H, Lenzi G, Triviño J. *Conversion of Plastic Solid Wastes into Carbon Nanotubes: Effect of Operating Conditions*. 2021.
115. Tuball. Single-walled Carbon Nanotubes: Structure, Properties, Applications. May 13, 2021. Accessed December 12, 2023. https://tuball.com/articles/single-walled-carbon-nanotubes
116. Rocha RP, Soares OSGP, Figueiredo JL, Fernando M, Pereira R, Thakur VK. Tuning CNT Properties for Metal-Free Environmental Catalytic Applications. *C 2016, Vol 2, Page 17*. 2016;2(3):17. doi:10.3390/C2030017
117. Bethi B, Sonawane SH, Bhanvase BA, Gumfekar SP. Nanomaterials-based advanced oxidation processes for wastewater treatment: A review. *Chemical Engineering and*

Processing - Process Intensification. 2016;109:178-189. doi:10.1016/J.CEP.2016.08.016

118. Diaz de Tuesta JL, Silva AS, Roman FF, et al. Polyolefin-derived carbon nanotubes as magnetic catalysts for wet peroxide oxidation of paracetamol in aqueous solutions. *Catal Today*. 2023;419:114162. doi:10.1016/J.CATTOD.2023.114162
119. Thakur SN. Atomic Emission Spectroscopy. *Laser-Induced Breakdown Spectroscopy*. Published online 2007:23-48. doi:10.1016/B978-044451734-0.50005-3
120. Surela AK, Chhachhia LK, Surela VK, Meena PL. Polypyrrole-Based Composites for Dyes Removal From Contaminated Water. *Reference Module in Materials Science and Materials Engineering*. Published online January 1, 2024. doi:10.1016/B978-0-323-95486-0.00019-3
121. Mustapha S, Shuaib DT, Ndamitso MM, et al. Adsorption isotherm, kinetic and thermodynamic studies for the removal of Pb(II), Cd(II), Zn(II) and Cu(II) ions from aqueous solutions using Albizia lebbeck pods. *Appl Water Sci*. 2019;9(6):1-11. doi:10.1007/S13201-019-1021-X/FIGURES/15
122. Neto HA da S, Garcia HL, Araujo RGO, Garcia CAB. Adsorção em coluna de leito fixo aplicada para a pré-concentração de cádmio em amostras de água. *Scientia Plena*. 2018;14(6). doi:10.14808/SCI.PLENA.2018.064208
123. Barros MASD, Arroyo PA, Silva EA, Barros MASD, Arroyo PA, Silva EA. General Aspects of Aqueous Sorption Process in Fixed Beds. *Mass Transfer - Advances in Sustainable Energy and Environment Oriented Numerical Modeling*. Published online July 24, 2013. doi:10.5772/51954
124. Gavaskar AR. Design and construction techniques for permeable reactive barriers. *J Hazard Mater*. 1999;68(1-2):41-71. doi:10.1016/S0304-3894(99)00031-X
125. Salim M. Geankoplis, Christie J. 1993 Transport processes and unit operations. Accessed July 2, 2024. https://www.academia.edu/36001183/Geankoplis_Christie_J_1993_Transport_processes_and_unit_operations
126. Chaplina TO, Chashechkin YD, Stepanova E V. Flows induced by sorption on fibrous material in a two-layer oil−water system. *Doklady Physics*. 2016;61(9):444-448. doi:10.1134/S1028335816090019
127. Labied R, Benturki O, Eddine Hamitouche AY, Donnot A. Adsorption of hexavalent chromium by activated carbon obtained from a waste lignocellulosic material (Ziziphus jujuba cores): Kinetic, equilibrium, and thermodynamic study. *Adsorption Science and Technology*. 2018;36(3-4):1066-1099.

doi:10.1177/0263617417750739/ASSET/IMAGES/LARGE/10.1177_0263617417750739-FIG13.JPEG

128. Birch ME, Ruda-Eberenz TA, Chai M, Andrews R, Hatfield RL. Properties that Influence the Specific Surface Areas of Carbon Nanotubes and Nanofibers. *Ann Occup Hyg*. 2013;57(9):1148. doi:10.1093/ANNHYG/MET042
129. Siyal AA, Shamsuddin MR, Rabat NE, Zulfiqar M, Man Z, Low A. Fly ash based geopolymer for the adsorption of anionic surfactant from aqueous solution. *J Clean Prod*. 2019;229:232-243. doi:10.1016/J.JCLEPRO.2019.04.384
130. EUROKIN spreadsheet on requirements for measurement of intrinsic kinetics in the gas-solid fixed-bed reactor. Published online 2012.
131. Diaz de Tuesta JL, Silva AS, Roman FF, et al. Polyolefin-derived carbon nanotubes as magnetic catalysts for wet peroxide oxidation of paracetamol in aqueous solutions. *Catal Today*. 2023;419:114162. doi:10.1016/J.CATTOD.2023.114162
132. Zielińska I, Polak D, Jurkiewicz A, et al. Application of Calcium Carbonate in the Pharmaceutical Removal Process. *Sustainability 2024, Vol 16, Page 3794*. 2024;16(9):3794. doi:10.3390/SU16093794
133. Fiorito E, Porcedda GE, Brundu L, et al. Calcium carbonate as sorbent for lead removal from wastewaters. *Chemosphere*. 2022;296:133897. doi:10.1016/J.CHEMOSPHERE.2022.133897
134. Chao Y, Zhao M, Ma X, Chen D, Guo H, Liao Y. Novel organic–inorganic geopolymer composite materials for removing Pb2+ from wastewater. *Mater Lett*. 2023;330. doi:10.1016/j.matlet.2022.133401
135. Benavent V, Steins P, Sobrados I, et al. Impact of aluminum on the structure of geopolymers from the early stages to consolidated material. *Cem Concr Res*. 2016;90:27-35. doi:10.1016/J.CEMCONRES.2016.09.009
136. Cheng R, He X, Li K, et al. Rational Design of Organic Electrocatalysts for Hydrogen and Oxygen Electrocatalytic Applications. *Advanced Materials*. 2024;36(25):2402184. doi:10.1002/ADMA.202402184
137. Petrovic B, Gorbounov M, Masoudi Soltani S. Impact of Surface Functional Groups and Their Introduction Methods on the Mechanisms of CO2 Adsorption on Porous Carbonaceous Adsorbents. *Carbon Capture Science & Technology*. 2022;3:100045. doi:10.1016/J.CCST.2022.100045
138. Abdel-Ghani NT, El-Chaghaby GA, Helal FS. Individual and competitive adsorption of phenol and nickel onto multiwalled carbon nanotubes. *J Adv Res*. 2015;6(3):405-415. doi:10.1016/J.JARE.2014.06.001

139. Maiyalagan T, Viswanathan B. Template synthesis and characterization of well-aligned nitrogen containing carbon nanotubes. *Mater Chem Phys*. 2005;93(2-3):291-295. doi:10.1016/J.MATCHEMPHYS.2005.03.039
140. He P, Xin K, Zhang X, Guo Z, Zheng W. Development of an activated carbon-geopolymer composite for treatment of Pb(II) polluted water and soil. *Int J Appl Ceram Technol*. 2023;20(5):3027-3040. doi:10.1111/ijac.14393
141. Siyal AA, Shamsuddin MR, Rabat NE, Zulfiqar M, Man Z, Low A. Fly ash based geopolymer for the adsorption of anionic surfactant from aqueous solution. *J Clean Prod*. 2019;229:232-243. doi:10.1016/J.JCLEPRO.2019.04.384
142. Dong D, Wang K, Yi M, et al. Preparation of TiO2 photocatalyst microspheres by geopolymer technology for the degradation of tetracycline. *J Clean Prod*. 2022;339. doi:10.1016/j.jclepro.2022.130734
143. Qiu J, Zhao Y, Xing J, Sun X. Fly ash-based geopolymer as a potential adsorbent for Cr(VI) removal. *Desalination Water Treat*. 2017;70:201-209. doi:10.5004/DWT.2017.20493
144. Sitarz-Palczak E, Kalembkiewicz J. APPLICATION OF HALLOYSITE GEOPOLYMERS TO REMOVAL OF METHYL BLUE FROM AQUEOUS SOLUTION. *International Journal of GEOMATE*. 2021;21(87):87-94. doi:10.21660/2021.87.j2330
145. Tian Q, Sasaki K. Application of fly ash-based geopolymer for removal of cesium, strontium and arsenate from aqueous solutions: kinetic, equilibrium and mechanism analysis. *Water Science and Technology*. 2019;79(11):2116-2125. doi:10.2166/WST.2019.209
146. Zhu C, Xu Q. Amorphous Materials for Enhanced Localized Surface Plasmon Resonances. *Chem Asian J*. 2018;13(7):730-739. doi:10.1002/ASIA.201701722
147. Wulan PPDK, Wijardono SB. Finding an optimum period of oxidative heat treatment on SS 316 catalyst for nanocarbon production from LDPE plastic waste. *Int J Adv Sci Eng Inf Technol*. 2017;7(2):552-558. doi:10.18517/ijaseit.7.2.2097
148. Salgado MDF, Abioye AM, Junoh MM, Santos JAP, Ani FN. Preparation of activated carbon from babassu endocarpunder microwave radiation by physical activation. *IOP Conf Ser Earth Environ Sci*. 2018;105(1). doi:10.1088/1755-1315/105/1/012116
149. He R, Dai N, Wang Z. Thermal and Mechanical Properties of Geopolymers Exposed to High Temperature: A Literature Review. *Advances in Civil Engineering*. 2020;2020(1):7532703. doi:10.1155/2020/7532703

150. Abdulkareem OA, Mustafa Al Bakri AM, Kamarudin H, Khairul Nizar I, Saif AA. Effects of elevated temperatures on the thermal behavior and mechanical performance of fly ash geopolymer paste, mortar and lightweight concrete. *Constr Build Mater*. 2014;50:377-387. doi:10.1016/J.CONBUILDMAT.2013.09.047
151. Wang J, Guo X. Adsorption kinetic models: Physical meanings, applications, and solving methods. *J Hazard Mater*. 2020;390. doi:10.1016/J.JHAZMAT.2020.122156
152. García-Pérez P, Losada-Barreiro S, Gallego PP, Bravo-Díaz C. Adsorption of gallic acid, propyl gallate and polyphenols from Bryophyllum extracts on activated carbon. *Sci Rep*. 2019;9(1). doi:10.1038/S41598-019-51322-6
153. Nguyen DT, Tran HN, Juang RS, et al. Adsorption process and mechanism of acetaminophen onto commercial activated carbon. *J Environ Chem Eng*. 2020;8(6):104408. doi:10.1016/J.JECE.2020.104408
154. Gómez-Avilés A, Peñas-Garzón M, Belver C, Rodriguez JJ, Bedia J. Equilibrium, kinetics and breakthrough curves of acetaminophen adsorption onto activated carbons from microwave-assisted FeCl3-activation of lignin. *Sep Purif Technol*. 2021;278:119654. doi:10.1016/J.SEPPUR.2021.119654
155. Gutiérrez M, Verlicchi P, Mutavdžić Pavlović D. Study of the Influence of the Wastewater Matrix in the Adsorption of Three Pharmaceuticals by Powdered Activated Carbon. *Molecules 2023, Vol 28, Page 2098*. 2023;28(5):2098. doi:10.3390/MOLECULES28052098
156. Kerkhoff CM, Boit Martinello K da, Franco DSP, et al. Adsorption of ketoprofen and paracetamol and treatment of a synthetic mixture by novel porous carbon derived from Butia capitata endocarp. *J Mol Liq*. 2021;339:117184. doi:10.1016/J.MOLLIQ.2021.117184
157. Liu Y, Liu X, Dong W, Zhang L, Kong Q, Wang W. Efficient Adsorption of Sulfamethazine onto Modified Activated Carbon: A Plausible Adsorption Mechanism. *Sci Rep*. 2017;7(1). doi:10.1038/S41598-017-12805-6
158. Chang EE, Wan JC, Kim H, Liang CH, Dai YD, Chiang PC. Adsorption of Selected Pharmaceutical Compounds onto Activated Carbon in Dilute Aqueous Solutions Exemplified by Acetaminophen, Diclofenac, and Sulfamethoxazole. *The Scientific World Journal*. 2015;2015. doi:10.1155/2015/186501
159. Patel H. Fixed-bed column adsorption study: a comprehensive review. *Appl Water Sci*. 2019;9(3):1-17. doi:10.1007/S13201-019-0927-7/METRICS
160. Fernandez RMD, Estrada RJR, Tomon TRB, et al. Experimental Design and Breakthrough Curve Modeling of Fixed-Bed Columns Utilizing a Novel 3D Coconut-

Based Polyurethane-Activated Carbon Composite Adsorbent for Lead Sequestration. *Sustainability 2023, Vol 15, Page 14344*. 2023;15(19):14344. doi:10.3390/SU151914344

161. Ang TN, Young BR, Taylor M, Burrell R, Aroua MK, Baroutian S. Breakthrough analysis of continuous fixed-bed adsorption of sevoflurane using activated carbons. *Chemosphere*. 2020;239:124839. doi:10.1016/J.CHEMOSPHERE.2019.124839
162. Samarghandi MR, Hadi M, McKay G. Breakthrough curve analysis for fixed-bed adsorption of azo dyes using novel pine cone-derived active carbon. *Adsorption Science and Technology*. 2014;32(10):791-806. doi:10.1260/0263-6174.32.10.791

8. SUPPLEMENTARY MATERIAL

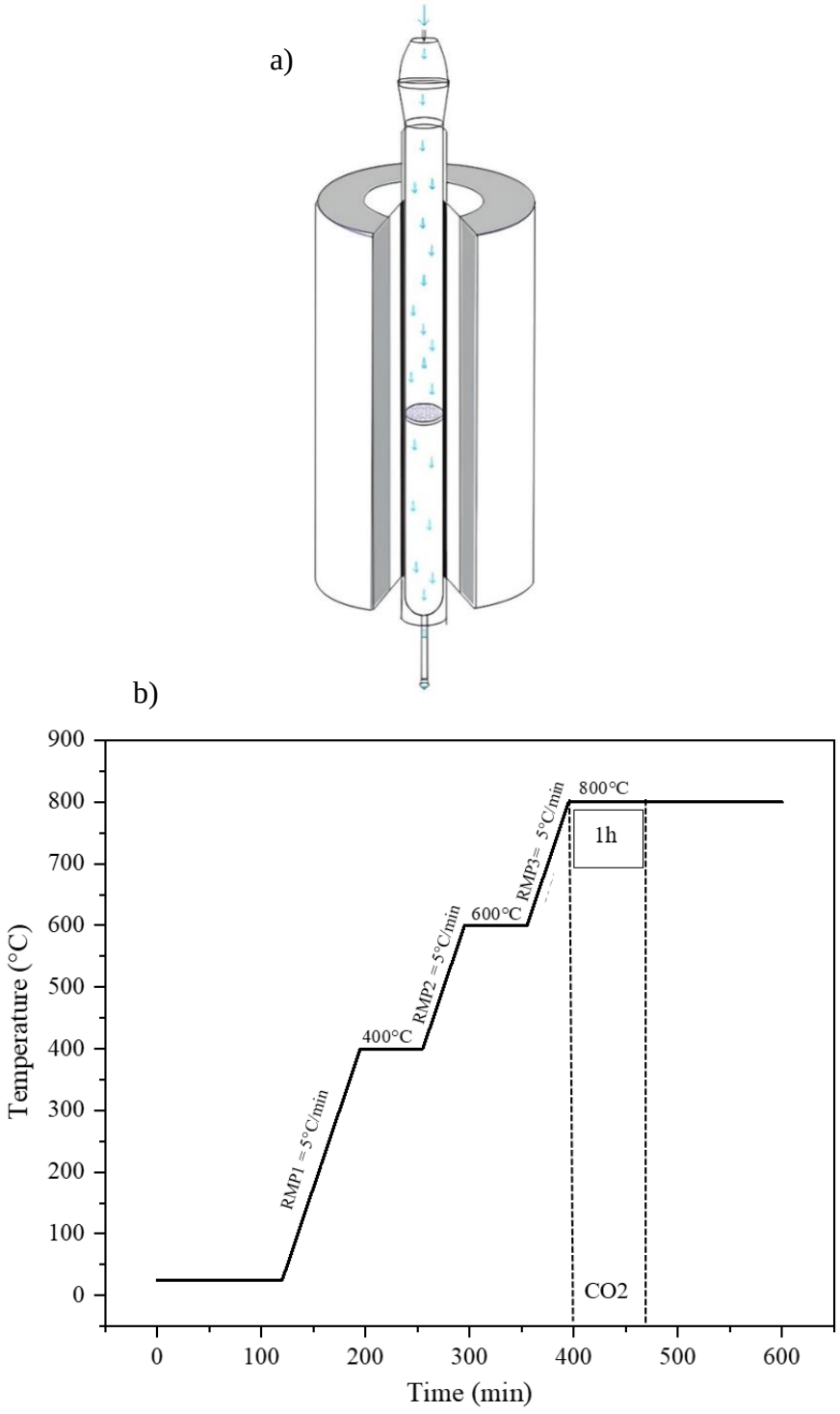

Figure S1: a) Pyrolysis oven for AC and b) Heating ramps and residence time for slow pyrolysis

Figure S2: Vertical oven for CNT

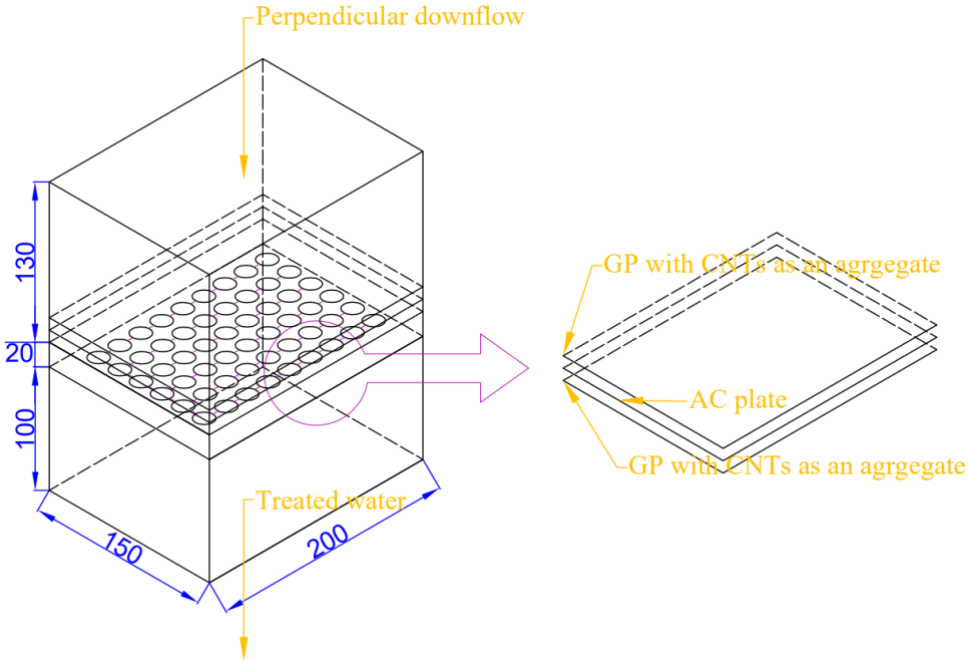

Figure S3: Permeable barrier preliminary version

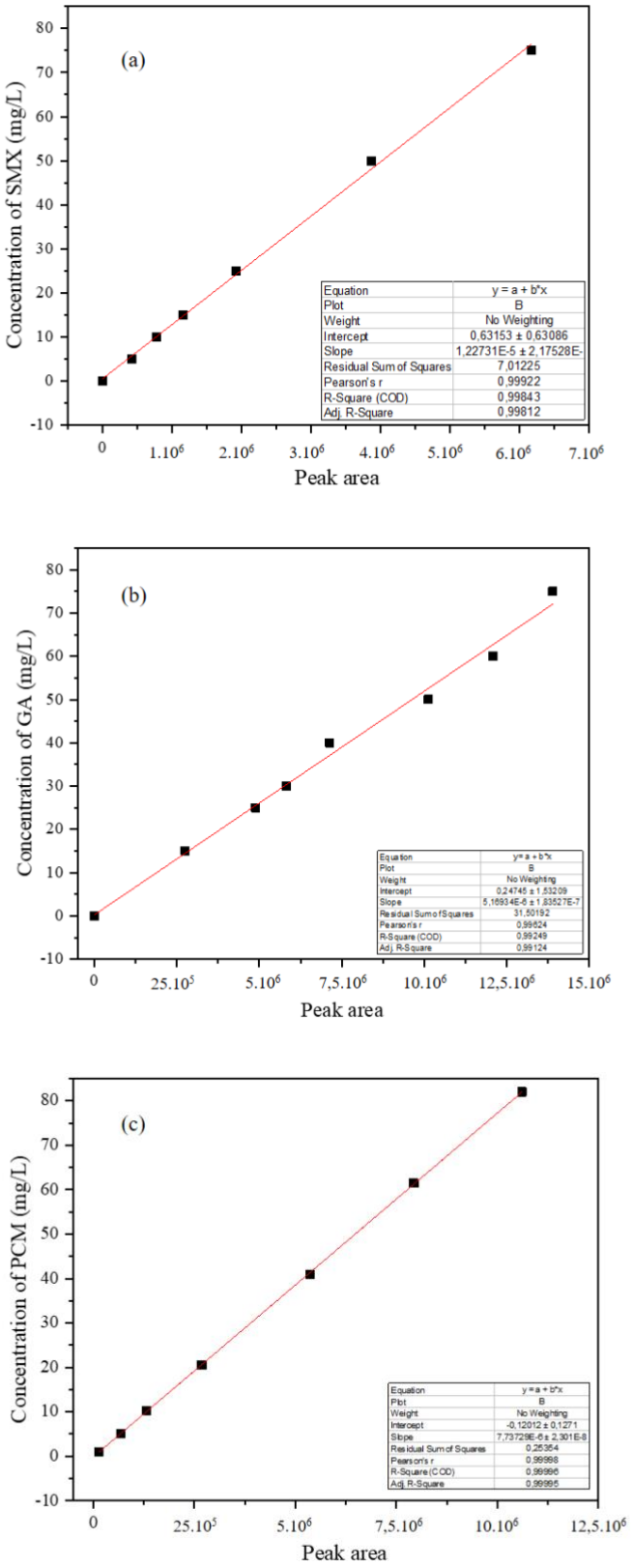

Figure S4: Calibration curve for a) SMX; b) GA; c) PCM

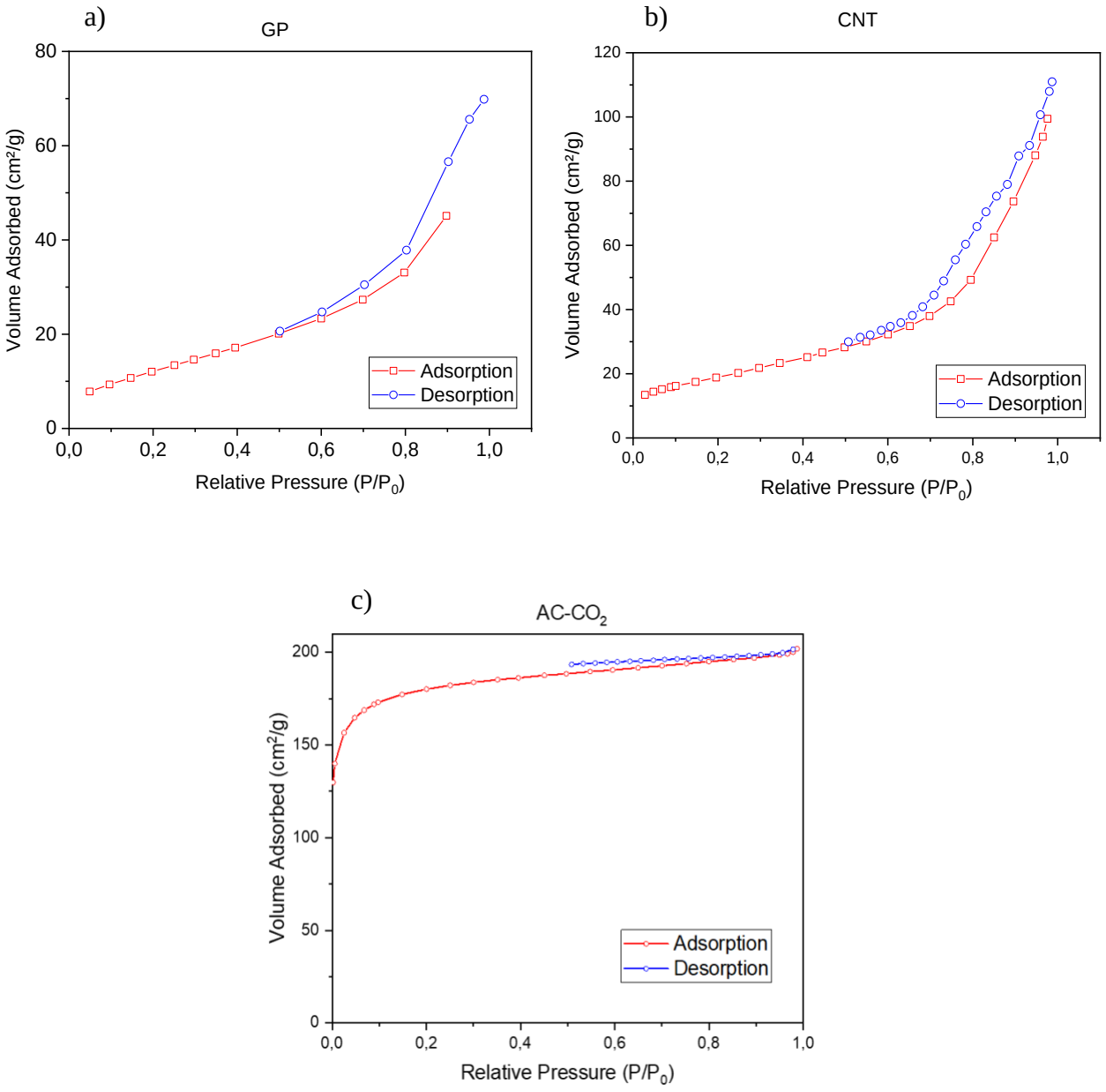

Figure S5: Isotherm N_2 adsorptions for B.E.T analysis for a) GP; b) CNT; c) AC